THE INTERACTION OF SOUND AND SHOCK WAVES WITH FLEXIBLE POROUS MATERIALS

by

JAMES FULLER ABBOTT

Submitted to the Department of Physics in
partial fulfillment of the requirements
for the degree of

DOCTOR OF PHILOSOPHY

at the

MASSACHUSETTS INSTITUTE OF TECHNOLOGY

June, 1991

Signature of Author _____

Department of Physics

Certified by _____

Karl Uno Ingard
Professor of Physics
Thesis Supervisor

Accepted by _____

George F. Koster
Professor of Physics
Chairman, Department Committee

THE INTERACTION OF SOUND AND SHOCK WAVES WITH FLEXIBLE POROUS MATERIALS

by

James Fuller Abbott

Submitted to the Department of Physics on May 1, 1991
in partial fulfillment of the requirements for the
Degree of Doctor of Philosophy in Physics

ABSTRACT

Several topics are studied which illustrate the role of flexibility in determining the acoustical properties of flexible porous materials. Characteristic lengths and times of the acoustic problem of the flexible porous material are discussed, the equations of mass balance, momentum balance, and compressibility definitions are then written, then expressions for the propagation constants are derived. A power balance relation is obtained for the flexible porous material which explicitly identifies two loss mechanisms for sound absorption: the losses due to the irreversible deformation of the structure, and those attributed to the viscous drag between the fluid and the structure. The finite flexible porous layer backed by a rigid wall is then considered. We derive normal incidence and angle averaged absorption coefficients for the layer with and without an impervious skin covering the free surface. The loss integrals derived previously and the ratio of structure to fluid velocity are then calculated for a number of cases, and then used to study mechanisms of sound absorption in open layers. Irreversible deformation of the structure is shown to be the dominant loss mechanism for closed layers. Transmission matrices are derived for a layer of flexible porous material for the two cases where the layer is, or is not, covered with an impervious skin on both boundaries.

Three departures from the basic model – a porous layer with anisotropic flow resistance and structure factor, periodic structures consisting of porous layers separated by air gaps, and the porous medium in bulk with mean fluid flow – are considered. An anisotropic material, treated as isotropic in the laboratory because of its high flow resistance, is shown to exhibit very anisotropic behavior at some frequencies where structural resonances reduce the relative motion between the fluid and structure and therefore reduce the effective flow resistance. Another demonstrated consequence of flexibility is shown for the periodic structure, in particular the multiple layer attenuator. Here the dips in the absorption coefficient due to structural layer resonances can coincide with peaks or dips due to fluid resonances in the air gaps; the absorption coefficient which results from this overlap is shown to be made more or less smooth over frequency compared to the corresponding rigid case. Mean flow is then shown to introduce a spatial gradient in the equilibrium porosity (and other field variables)

of a flexible porous material, an effect which could have important consequences for the design of a porous baffle with a graded wave impedance.

The reflection of shock waves is also studied, and a quasi-linear theory is developed which reproduces the principal features of experimental results obtained previously by Ingard. The theory assumes that the propagating pulses in the air and structure are linear and the gross, zeroth order motion of the porous layer is modeled by including its energy and momentum in the conservation equations; these equations compare the system just before and just after the reflection of the incident shock from the front surface of the layer. The substantial motion of the layer and its dragging against a constraining boundary (in this case the walls of the shock tube) are found to introduce a dependence of the front reflection coefficient and maximal layer deformation on the peak pressure of the incident shock.

Lastly, we address the question of measurement of the complex compressibility K, a key parameter used to describe the dynamics of a given flexible porous material. The standard long-wavelength assumption used to determine K from experimental measurements of the frequency dependent velocity transfer function across a sample is shown to often introduce significant errors into the subsequent estimate of K. We then provide a computer algorithm which makes the long-wavelength assumption unnecessary.

Thesis Supervisor: Prof. K. U. Ingard

Title: Professor of Physics

To the memory of my friend,

Thomas J. Cianciolo III

Acknowledgments

I would like to thank my family for their support and encouragement. Rich, in particular, I thank for his frequent visits to Cambridge and sharing my love of nature and mathematics. To Mom, I am especially grateful for the use of her car on those many occasions when my sanity depended on a speedy break from school. Mild allergic reactions notwithstanding, Maxine is credited with making my thesis writing a more pleasant experience.

In the department, Peggy must be recognized for her never ending words of wisdom and Kim I thank for making working with undergraduates a more positive and meaningful experience. Teaching while a graduate student had a positive effect on my research and opened my eyes to the importance of good physics instruction - for this vision I am forever indebted to Dr. Edwin Taylor, Prof. A. P. French, and Prof. George Koster.

No words of thanks adequately describe my appreciation for the many years of guidance provided by my teacher and friend Prof. K. U. Ingard. I truly hope his respect for careful, intuitive physical analysis will serve as a model for me for years to come.

Contents

List of Figures

Chapter 1

Historical Introduction

1.1 Motivation

The history of investigations relating to the acoustical properties of porous materials dates back more than one hundred years. The ability to predict the performance of a given porous material, however, based on knowledge of a small number of measurable macroscopic parameters, remains a difficult and unsolved problem. In addition, the ability to consistently measure the performance of a given material, using different laboratories and experimental techniques, often falls short of desired reproducibility. This is not to say that the last century has not brought great progress in this field. For certain material types or frequency ranges, the agreement between theory and experiment is very good. Great advances have also been made in the instruments and techniques of the modern acoustical laboratory. In some cases, the difficulties seem to stem from a faulty assumption that a given flexible material can be treated as limp or rigid, or that a particular consequence of the flexibility may be ignored. Techniques for determining certain material properties using laboratory measurements can also be flawed by such erroneous assumptions.

For this reason, this study examines the particular role of flexibility in determining the measurable acoustical properties of porous materials. By doing this we hope to shed some light on the problem of limited performance predictability and inadequate reproducibility of laboratory measurements.

1.2 A Brief History

Lord Rayleigh treated the problem of the porous wall in "The Theory of Sound" [1]. This was the first extensive discussion of how the acoustical properties of a porous layer might be related to measurable, macroscopic parameters. He considered an infinitely extended half-space of porous material which contained parallel narrow tubes running normal to the free surface. The medium was taken to be rigid, and the analysis of the propagation of sound in narrow tubes, when viscosity and thermal conduction are included, was used to derive an absorption coefficient for normally incident sound. Included in his analysis was a porosity-like parameter and the necessary boundary condition for an open surface (no impervious covering).

Monna [2], some forty years later, examined the problem of the rigid porous layer of infinite depth using the flow resistance of the material and considering oblique angles of incidence. He computed absorption coefficients for normal and angle averaged (diffuse field) incident sound. He briefly referred to the layer of finite thickness.

Some of the first considerations of flexibility of the porous material are found in Rettinger's work [3]. He reviewed progress in the field to date and introduced the effective mass density and effective flow resistance; these quantities are meant to include the effects of the motion of the material.

The following decade then brought a great increase in the research of this problem. Morse and Bolt [4] and Scott [5] continued to view the problem in terms of effective mass density and effective flow resistance. These parameters are meant to include the important effects of the motion of the structure without explicitly modeling the wave in the porous structure. Scott also discussed the significance of isothermal versus isentropic thermodynamic changes of the fluid.

Perhaps the most significant advance to date came with the work of Zwikker and Kosten [6]. Their analysis was based on a two fluid model for the fluid saturated porous material. Flexibility of the structure was included as well as a complex compressibility for the structure which accounted for the losses due to the irreversible nature of the deformation of the structure with the passage of the sound wave. Their

approach was used in the work of Beranek [7], who studied this theory in the domains of very high and very low compressibility of the structure.

Biot [8, 9] later extended this coupled wave analysis to include shear as well as dilatational waves in the structure. His work laid out a complete theoretical framework for the coupled problem. The complexity of his model is formidable and, for a medium where the shear wave speed is much less than the dilatational wave speed, the method of Zwikker and Kosten is more appealing for its relative simplicity.

Soon after, Attenborough [10] and Zarek [11] presented reviews of the field and discussed the microscopic details of how certain macroscopic parameters of a porous material are determined.

More recently, Lambert [12], using a model analogous to that of Zwikker and Kosten, compared theoretical predictions with experiments with some success, and Ingard [13] pointed out the pitfalls of a faulty assumption of local reaction in flexible porous layers in certain cases.

1.3 Thesis Summary

Our analysis here uses the model of Zwikker and Kosten [6] as a starting point. In chapter 2 the characteristic lengths and times of the problem are discussed, then the equations of mass balance, momentum balance and defined compressibility are written down for both the fluid and the porous material. A power balance relation is then derived which explicitly identifies the physical mechanisms responsible for the absorption of sound. Propagation constants are then derived and discussed.

In chapter 3 the finite layer of flexible porous material is studied. Pressure and velocity fields, and the normal incidence and angle averaged (diffuse field) absorption coefficients are calculated for the layer backed by a rigid wall, with or without an impervious skin covering the free surface. The power balance results from chapter 2 are combined with calculated structure/fluid velocity ratios to reveal the mechanisms of sound absorption, and their relationship to the flexibility of the material, in more detail. Viscous drag between the fluid and structure is shown to be the dominant

loss mechanism for the open porous layer, whereas irreversible deformations of the structure are found to be chiefly responsible for absorption in closed layers. Transmission matrices are then derived for an isolated flexible porous layer with and without impervious coverings.

In chapter 4 three departures from the basic model of chapters 2 and 3 – a porous layer with anisotropic flow resistance and structure factor, periodic structures consisting of porous layers separated by air gaps, and the porous medium in bulk with mean fluid flow – are considered. An anisotropic material, treated as isotropic in the laboratory because of its high flow resistance, will be shown to exhibit very anisotropic behavior at some frequencies where structural resonances reduce the relative motion between the fluid and structure and therefore reduce the effective flow resistance. An example of a periodic structure, the multiple layer attenuator, is also studied. In particular we consider how fluid layer resonances and structural layer resonances conspire to affect the overall absorption coefficient of the attenuator backed by a rigid wall. The influence of mean flow on the propagation of sound in a porous material is considered; then mean flow is shown to induce a spatial gradient in the equilibrium porosity (and other field variables) of a flexible porous material.

In chapter 5 we study the reflection of shock waves from a flexible porous layer, and formulate a quasi-linear theory to explain key features in experimental data obtained previously by Ingard [14]. The theory predicts significant maximum fractional deformation of the layer, and demonstrates how the front reflection coefficient (defined in chapter 5) depends on the pressure of the incident shock because of dragging of the layer against a constraining surface.

Chapter 6 addresses questions of the measurement of the complex compressibility of a flexible porous material, and the errors introduced by the popular long-wavelength assumption in shaker experiments. An algorithm which makes this assumption unnecessary is then provided.

Lastly, in chapter 7, we review and summarize the conclusions reached in the previous chapters which demonstrate how flexibility can influence the acoustical properties of flexible porous materials.

Chapter 2

Basic Theory

2.1 Characterizing the Flexible Porous Material

The flexible porous material is modeled by a two-fluid system, in a manner similar to that presented by Zwikker and Kosten [6]. One of the fluids is the air which occupies the interconnected voids of the structure, the other is the material of the structure. In using the model we assume that shear and surface waves may be neglected in the dynamics of the structure, and we associate a pressure with the negative of the diagonal components of the material's stress tensor. Although both the fluid in the pores and the material are modeled as isotropic fluids in this analysis, we adopt the convention of referring to the fluid in the pores as the "fluid", the material of the structure as the "material", and the frame of the material composed of the open pores bounded by structural material as the "structure".

The porous material is assumed to consist exclusively of interconnected "open" cells. To treat a partially open cell structure where some fraction of the cells are closed, we would consider only the open cells in the measure of the porosity, and the closed cells would affect the density and compressibility of the structural material. In many cases closed cells in the structure lead to a medium which is inhomogeneous and anisotropic; questions of anisotropy will be discussed in chapter 4.

Although this chapter presents a basic model which is already widely known, we add a new discussion of power balance and mechanisms of sound absorption in a

flexible porous material. In addition, the idea of the porosity variation being treated as an acoustic field variable which was proposed by Ingard [15] is an addition to the widely used model of Zwikker and Kosten.

The basic theory of this chapter makes a number of simplifying assumptions about the porous medium. In later chapters most of these assumptions will be relaxed, one at a time, in more complex models. The medium is assumed to be isotropic and homogeneous. We assume no mean flow is present, and we initially consider the medium in bulk without the influence of boundaries. The changes of the field variables associated with waves in the porous material are assumed sufficiently small to justify linearization of the basic equations.

2.2 Physical Parameters

For the fluid, material, and structure we define, respectively, densities ρ, ρ', and $M = H'\rho'$ and compressibilities κ, κ', and K. Both κ' and K are complex; more will be said about their definitions in the next section. The experimental determination of the complex compressibility K is discussed in chapter 6.

The volume fraction of the open or inter-connected voids in the porous material is the porosity H and we define $H' = 1 - H$ as the corresponding volume fraction of the material.

The induced mass factor G is a dimensionless, empirically determined factor which accounts for tortuosity of the interconnected pores in the porous medium; it appears in the momentum balance relations for both the fluid and material (see section 2.4.3). It accounts for components of the total fluid velocity which contribute to the kinetic energy density but are averaged out in forming the average fluid velocity u. This will be shown explicitly in the section on power balance in the porous material.

The flow resistance per unit length is r. This is empirically determined by measuring the steady average flow velocity resulting from a constant pressure drop across a layer of porous material. This is obtained using the relation

$$Hru_x = -\frac{\partial p}{\partial x} \tag{2.1}$$

The inclusion of H above means u_x is the average flow velocity inside the porous layer.

2.3 Characteristic Physical Scales

The simplifying assumptions stated earlier correspond to certain magnitudes of characteristic length and time scales of waves in the porous material; these parameters and there acceptable magnitudes are discussed below.

2.3.1 Length Scales

The two-fluid model of waves in a flexible porous material has two distinct solutions, one for each of the modes of wave motion. Two length scales of the problem are the wavelengths of these two modes, labeled here as λ_1 and λ_2. At higher frequencies, the two modes are readily associated with a wave in the structure and a wave in the fluid; for an arbitrary frequency, such a distinction is not possible. The characteristic fiber or pore size of the frame δ_S is also important, and our assumption of homogeneity assumes

$$\lambda_1, \lambda_2 \gg \delta_S \tag{2.2}$$

The finite layer with a rigid backing is discussed in chapter 3; the layer thickness is d. In this case, for low values of flow resistance ($r \ll \rho\omega$), effects of the dominant layer resonance for the fluid wave are seen when

$$\nu_1 \approx \frac{1}{4d\sqrt{H\rho\kappa}} \tag{2.3}$$

and for the structure layer resonance when

$$\nu_2 \approx \frac{1}{4d\sqrt{H'\rho' K_r}} \tag{2.4}$$

In particular, the frequency ν_1 may correspond to a peak in the absorption coefficient due to significant relative motion between the fluid and the structure. Frequencies near ν_2, however, may correspond to a dip in the absorption coefficient due to the reduction in the relative motion. These effects are discussed in more detail in chapter 3.

For the case of high flow resistance, the fluid and structure move together and layer resonances are found when

$$\nu_3 \approx \frac{1}{4d\sqrt{\tilde{\rho}\tilde{\kappa}}} \tag{2.5}$$

where $\tilde{\rho} = H\rho + H'\rho'$ and $1/\tilde{\kappa} = 1/(H\kappa) + 1/K_r$.

As the fluid flows through the pores there is a characteristic thermal boundary layer thickness δ_T. In this analysis we assume that the thermodynamic changes in the fluid within the pores are isothermal so

$$\delta_T \sim \delta_S \tag{2.6}$$

For higher frequencies this may not be valid, but the analysis can be corrected by using an empirically determined complex compressibility for the fluid. Because of the isothermal assumption, the fluid compressibility κ is taken to be real.

The relative sizes of the viscous boundary layer and the pores influence the the flow resistance r, but this does not concern us here; we assume that the flow resistance has been determined experimentally and will not discuss the microscopic details of its origin here.

2.3.2 Time Scales

The acoustic angular frequency is ω with corresponding period $T = 2\pi/\omega$. Three important characteristic times or frequencies can be identified in the context of the

flexible porous material.

The first corresponds to the characteristic thermodynamic relaxation time for the structure and material. Unlike our isothermal assumption for the fluid, we cannot assume that either isothermal or isentropic changes apply for the structure and the material, because their relaxation times are unknown relative to the acoustic period. For this reason the compressibilities for the structure and material are taken to be complex, to be measured by experiment. In most materials, the magnitude of the complex compressibility of the material is much smaller than that of the structure.

Next we consider the relative roles of flow resistance r and inertial mass density of the fluid ρ in the pores which leads to the characteristic frequency

$$\omega_F = \frac{r}{\rho} \tag{2.7}$$

For acoustic frequencies such that $\omega \ll \omega_F$, the ...ction force dominates and the dynamics of the fluid wave is described by the approximately diffusive equation

$$\frac{\partial p}{\partial t} \simeq (\frac{\rho c^2}{r})\nabla^2 p \tag{2.8}$$

where p is the fluid pressure and the fluid sound speed, outside the porous material, is c.

For frequencies such that $\omega \gg \omega_F$, the inertial forces in the fluid dominate and the wave propagates much as it would in free space but with attenuation proportional to the flow resistance r.

Lastly we can define

$$\omega_S = \frac{r}{M} = \frac{\rho'}{M}\omega_F \tag{2.9}$$

where $M = H'\rho'$ is the bulk mass density of the porous frame, equal to the product of H', the volume fraction of the structure occupied by structure material, and ρ', the mass density of the structural material. This frequency is related to the ratio of the flow resistance force and the inertial forces in the porous frame and, for a material with small stiffness, the motion of the structure can be substantial for frequencies

such that $\omega \ll \omega_S$. For the domain $\omega \gg \omega_S$, the porous frame is essentially rigid.

2.4 Basic Equations

2.4.1 Physical Assumptions

The flexible porous material in bulk, assumed isotropic, homogeneous, and with no mean flow present, is considered here; in chapter 4 we examine the effects of anisotropy and mean flow.

The basic equations are linearized; we keep only terms to first order in the field variables. We will discuss this approximation in more detail below; for now we point out that linearization is consistent with the assumptions

$$\frac{|u|}{c}, \frac{|u'|}{c'}, \frac{\delta\rho}{\rho}, \frac{\delta\rho'}{\rho'}, \frac{\delta H}{H} \ll 1 \tag{2.10}$$

2.4.2 Acoustic Field Variables

The velocities for the fluid and structure, $\vec{u}$ and $\vec{u}'$ respectively, are average velocities. The actual velocities for both the fluid and the material can vary greatly over small distances in the porous medium because of the tortuous nature of the interconnected pores in the structure. For this reason, the velocity vectors $\vec{u}$ and $\vec{u}'$ result from an average of all the velocity vectors found in the medium over a region of characteristic dimension δ_V where

$$\lambda \gg \delta_V \gg \delta_S \tag{2.11}$$

where λ is the acoustic wavelength and δ_S is the size of the pores or channels in the frame.

The acoustic pressure in the fluid is denoted by p. In general the stresses in the structure of the porous material must be modeled by a three-dimensional, second rank stress tensor which is a function of position and time. We assume here that only dilatational waves propagate in the structure and that the medium is isotropic;

these assumptions allow us to replace the stress tensor with an acoustic pressure for the structure which is equal to the negative of the diagonal components of the stress tensor. Although on physical scales much larger than the pore size this is reasonable, on the length scale of the pores the shear deformations of the material are more responsible for the larger scale bulk deformations of the structure; this fact is central to our distinction between the material itself and the structure consisting of the material fibers.

The density of the fluid is ρ and the density of the structural material is ρ'. Because of the porous nature of the medium, the mass of the fluid per unit volume of the structure is $H\rho$ and correspondingly for the structure itself, $M = H'\rho'$.

These velocities, pressures, densities, and porosity form a set of eleven acoustic variables which will be determined by eleven equations below. They consist of eight equations of mass and momentum balance for the structure and fluid, and three compressibility definitions. A compressibility definition is equivalent to a statement of energy balance and equation of state.

2.4.3 Mass Balance

The fact that fluid or structure mass is neither created or destroyed leads to statements of continuity or mass conservation for the fluid and the material. After linearization of the field variables we have

$$H\frac{\partial \rho}{\partial t} + \rho\frac{\partial H}{\partial t} + H\rho \operatorname{div} \vec{u} = 0 \tag{2.12}$$

and

$$H'\frac{\partial \rho'}{\partial t} + \rho'\frac{\partial H'}{\partial t} + H'\rho' \operatorname{div} \vec{u}' = 0 \tag{2.13}$$

The linearization leads to the exclusion of terms like $u\rho\frac{\partial H}{\partial x}$, $uH\frac{\partial \rho}{\partial x}$, and $u'H'\frac{\partial \rho'}{\partial x}$ which, for a plane wave, corresponds to the physical assumptions:

$$\frac{\left|u\rho\frac{\partial H}{\partial x}\right|}{\left|H\rho\frac{\partial u}{\partial x}\right|} \sim \frac{\delta H}{H} \ll 1 \tag{2.14}$$

$$\frac{\left|uH\frac{\partial \rho}{\partial x}\right|}{\left|H\rho\frac{\partial u}{\partial x}\right|} \sim \frac{\delta \rho}{\rho} \ll 1 \tag{2.15}$$

and

$$\frac{\left|u'H'\frac{\partial \rho'}{\partial x}\right|}{\left|H'\rho'\frac{\partial u'}{\partial x}\right|} \sim \frac{\delta \rho'}{\rho'} \ll 1 \tag{2.16}$$

where δH, $\delta\rho$, and $\delta\rho'$ correspond to the first order fractional acoustic variations of the equilibrium values.

2.4.4 Momentum Balance

In the absence of any external volume forces on the flexible porous material, the linearized equations of momentum balance are

$$H\rho\frac{\partial \vec{u}}{\partial t} + H\rho G\frac{\partial}{\partial t}(\vec{u} - \vec{u}') = -Hr(\vec{u} - \vec{u}') - \operatorname{grad} p \tag{2.17}$$

and

$$H'\rho'\frac{\partial \vec{u}'}{\partial t} - H\rho G\frac{\partial}{\partial t}(\vec{u} - \vec{u}') = +Hr(\vec{u} - \vec{u}') - \operatorname{grad} p' \tag{2.18}$$

Here linearization causes the exclusion of terms containing factors like $u\frac{\partial u}{\partial x}$ which for a plane wave of speed c correspond to the physical assumptions

$$\frac{\left|u\frac{\partial u}{\partial x}\right|}{\left|\frac{\partial u}{\partial t}\right|} \sim \frac{|u|}{c} \ll 1 \tag{2.19}$$

and

$$\frac{\left|u'\frac{\partial u'}{\partial x}\right|}{\left|\frac{\partial u'}{\partial t}\right|} \sim \frac{|u'|}{c'} \ll 1 \tag{2.20}$$

where c' is the speed of a plane wave in the structure of the porous material.

The second terms on the left hand sides of equations 2.17 and 2.18 correct the momentum equations to account for the fact that, by averaging over all directions to obtain the velocities, contributions to the kinetic energy arising from components transverse to the resulting $\vec{u}$ and $\vec{u}'$ vectors are not accounted for. These induced mass factor terms account for the tortuosity of the pores in the porous material and are written so that any resulting forces exerted on the material by the fluid are equal and opposite to those applied to the fluid by the material.

The first terms of the right hand sides of 2.17 and 2.18 are the result of the mutual viscous drag between the fluid and the structure.

2.4.5 Compressibilities

We define three compressibilities for the flexible porous material; in each case the definition serves as a combined statement of energy balance and equation of state.

$$\kappa = \frac{1}{\rho}\frac{\partial \rho}{\partial p},\ \kappa' = \frac{1}{\rho'}\frac{\partial \rho'}{\partial p},\ K = \frac{1}{H'}\frac{\partial H'}{\partial p'} \tag{2.21}$$

The fluid compressibility κ is assumed real and will be taken to be the isothermal value. True, for sufficiently high frequencies an isentropic value would be more correct and in the intervening frequency range κ would be complex, but for our purposes here the impact of these considerations on the overall acoustic properties is small.

The compressibilities for the structure and the material are taken to be complex. The structure's bulk compressibility κ' is typically very small and here we have defined it with the assumption that deformation of the material itself is due largely to the the pressure in the fluid. Its compliance under shear deformations can be much larger. These shear deformations are largely responsible for the bulk deformations of the structure. As a result, the structure compressibility K can be quite important in the interactions we will examine; its magnitude is usually much larger than κ'. Here we assume that the pressure in the structure is responsible for the deformations associated with the compressibility K.

2.4.6 Power Balance

We now derive a equation which relates the acoustic energy density and intensity in the porous material to the losses due to viscous drag and irreversible changes which occur as the structure deforms.

For our purposes here, we take κ' to be sufficiently small that we can neglect the first term in equation 2.13 and take K as real, and account for the losses due to deformation of the structure by introducing a bulk viscosity term into equation 2.18 which gives us a momentum equation for the structure

$$H'\rho'\frac{\partial \vec{u}'}{\partial t} - H\rho G\frac{\partial}{\partial t}(\vec{u}-\vec{u}') = +Hr(\vec{u}-\vec{u}') - \operatorname{grad} p' + \beta\nabla^2\vec{u}' \tag{2.22}$$

Combining equations 2.12, 2.13, and 2.21 we can write

$$\kappa\frac{\partial p}{\partial t} - \frac{H'}{H}K\frac{\partial p'}{\partial t} + \operatorname{div}\vec{u} = 0 \tag{2.23}$$

$$\kappa'\frac{\partial p}{\partial t} + K\frac{\partial p'}{\partial t} + \operatorname{div}\vec{u}' = 0 \tag{2.24}$$

then, taking the dot product of $\vec{u}$ with equation 2.17 and $\vec{u}'$ with equation 2.18 and adding the results we obtain

$$\begin{aligned}\frac{\partial}{\partial t}\left[\frac{1}{2}H\rho(\vec{u}\cdot\vec{u}) + \frac{1}{2}H'\rho'(\vec{u}'\cdot\vec{u}') + \frac{1}{2}H\rho G(\vec{u}-\vec{u}')\cdot(\vec{u}-\vec{u}')\right] = \\ -Hr(\vec{u}-\vec{u}')\cdot(\vec{u}-\vec{u}') - \vec{u}\cdot\operatorname{grad} p - \vec{u}'\cdot\operatorname{grad} p' + \vec{u}'\cdot\beta\nabla^2\vec{u}'\end{aligned} \tag{2.25}$$

Also, multiplying equation 2.23 by p and equation 2.24 by p' and adding we have

$$\begin{aligned}\frac{\partial}{\partial t}\left[\frac{1}{2}\kappa p^2 + \frac{1}{2}Kp'^2\right] - \frac{H}{H'}Kp\frac{\partial p'}{\partial t} + \kappa' p'\frac{\partial p}{\partial t} = \\ -p\operatorname{div}\vec{u} - p'\operatorname{div}\vec{u}'\end{aligned} \tag{2.26}$$

It is interesting to note that the above equation 2.26 is actually a definition of

the total potential energy density. If we were to slowly compress a chunk of porous material we note that the time rate of change of the internal energy per unit volume would be given by

$$\frac{\partial \mathcal{PE}}{\partial t} = -p \operatorname{div} \vec{u} - p' \operatorname{div} \vec{u}' \tag{2.27}$$

so that the quantity on the left hand side of equation 2.26 is the time derivative of the potential energy density.

Adding equations 2.25 and 2.26 then leads to a power balance relation

$$\frac{\partial}{\partial t}(\mathcal{KE} + \mathcal{PE}) + \operatorname{div} \vec{\mathcal{I}} = -(\mathcal{L}1 + \mathcal{L}2) \tag{2.28}$$

where the kinetic energy density is

$$\mathcal{KE} = \frac{1}{2} H \rho |\vec{u}|^2 + \frac{1}{2} H' \rho' |\vec{u}'|^2 + \frac{1}{2} H \rho G |\vec{u} - \vec{u}'|^2 \tag{2.29}$$

the potential energy density is

$$\mathcal{PE} = \frac{1}{2} \kappa p^2 + \frac{1}{2} K p'^2 + \int (\kappa' p' \frac{\partial p}{\partial t} - \frac{H}{H'} K p \frac{\partial p'}{\partial t}) dt \tag{2.30}$$

the total intensity is given by

$$\vec{\mathcal{I}} = \frac{1}{2} Re(p\vec{u} + p'\vec{u}') \tag{2.31}$$

and the terms $\mathcal{L}1$ and $\mathcal{L}2$, defined below, correspond to power dissipated.

Equation 2.29 shows explicitly how the induced mass factor G accounts for the kinetic energy components in the frame of reference of the tortuous structure.

On the right hand side of equation 2.28 we see two terms which correspond to dissipation in the porous material. $\mathcal{L}1$, due to the resistive drag between the fluid and the structure is

$$\mathcal{L}1 = Hr |\vec{u} - \vec{u}'|^2 \tag{2.32}$$

As the structure deforms, irreversible changes occur, causing losses associated with $\mathcal{L}2$ where

$$\mathcal{L}2 = \vec{u}' \cdot \beta \nabla^2 \vec{u}' \tag{2.33}$$

In steady state the sum of the kinetic and potential energy densities is constant so the time derivative term in equation 2.28 is zero. Then, using the vector identity

$$\vec{\nabla} \cdot (\vec{u}' \cdot (\vec{\nabla} \cdot \vec{u}')) = \vec{u}' \cdot \nabla^2 \vec{u}' + (\vec{\nabla} \cdot \vec{u}')^2 \tag{2.34}$$

and equation 2.13 and taking a time average over an acoustic period we obtain:

$$\text{div}\,\langle \vec{\mathcal{I}} \rangle = -\frac{1}{2} Hr |\vec{u} - \vec{u}'|^2 - \frac{1}{2} \omega K_i |p'|^2 \tag{2.35}$$

where we have returned to the complex compressibility $K = K_r + iK_i$, and used the relationship between the bulk viscosity β and the real and imaginary parts of K as derived in appendix A which is

$$K_i = \beta \omega K_r^2 \tag{2.36}$$

and the fact that

$$\langle \vec{\nabla} \cdot (\vec{u}' \cdot (\vec{\nabla} \cdot \vec{u}')) \rangle = 0 \tag{2.37}$$

To complete our analysis of the power balance in the porous layer we now integrate equation 2.35 over the layer. The left hand side becomes

$$\int_V \text{div}\,\langle \vec{\mathcal{I}} \rangle dV = \int_A \langle \vec{\mathcal{I}} \cdot dA \rangle = \Pi_{in} \tag{2.38}$$

where the V integral is taken over the volume of the layer, the A integral is taken over the free surface of the layer, and Π_{in} is the power per unit area which flows into the layer. This leads to a power balance equation for the layer of the form

$$\Pi_{in} = \int_V (\frac{1}{2} Hr|\vec{u} - \vec{u}'|^2 + \frac{1}{2}\omega K_i |p'|^2) dV \tag{2.39}$$

The above result, divided by the incident intensity, is an absorption coefficient. The two terms of the integrand correspond to losses associated with viscous drag and deformation of the structure, respectively. This explicit identification of these sound absorption mechanisms will be used in chapter 3 to study their relative roles.

2.4.7 Propagation Constants

Propagation constants are now obtained for a plane wave in the porous material of frequency ω and wavenumber q. Using the compressibility definitions in 2.21 we can obtain complex amplitude equations for the field variables where now $p = p(\vec{r}, \omega)$ and $u = u(\vec{r}, \omega)$ with $\vec{r}$ a position vector.

The linearized equations 2.12,2.13,2.17,2.18 become

$$i(H'/H)\omega K p' - i\omega\kappa p = -\text{div}\,\vec{u} \tag{2.40}$$

$$-i\omega K p' - i\omega\kappa' p = -\text{div}\,\vec{u}' \tag{2.41}$$

$$-i\omega\tilde{\rho}\vec{u} = H\tilde{r}\vec{u}' - \vec{\nabla}p \tag{2.42}$$

$$-i\omega\tilde{M}\vec{u}' = H\tilde{r}\vec{u} - \vec{\nabla}p' \tag{2.43}$$

where we have defined

$$\tilde{r} \equiv r - i\omega G\rho \tag{2.44}$$

$$\tilde{\rho} \equiv H\rho(1 + \frac{i\tilde{r}}{\omega\rho}) \tag{2.45}$$

$$\tilde{M} \equiv M(1 + \frac{iH\tilde{r}}{\omega M}) \tag{2.46}$$

Equations 2.40 - 2.43 can then be combined to give two coupled wave equations in p and p'

$$\nabla^2 p + \omega^2 \tilde{\rho}\kappa(1 - iH\tilde{r}\kappa'/\omega\tilde{\rho}\kappa)p = iH\tilde{r}\omega K(1 - i\omega\tilde{\rho}H'/\tilde{r}H^2)p' \tag{2.47}$$

$$\nabla^2 p' + \omega^2 \tilde{M}K(1 + iH'\tilde{r}/\omega\tilde{M})p' = iH\tilde{r}\omega\kappa(1 + i\omega\tilde{M}\kappa'/\tilde{r}H\kappa)p \tag{2.48}$$

We now consider a plane traveling wave in the porous medium of propagation constant $\vec{q}$ for which the magnitude is written as q. The spatial dependence is $\exp(i\vec{q}\cdot\vec{r})$. Equations 2.47 and 2.48 can then be written as

$$[-q^2 + (\omega/c)^2\beta_f^2]p = (i\omega H\tilde{r}K)\delta_f p' \tag{2.49}$$

$$[-q^2 + (\omega/c)^2\beta_s^2]p' = (i\omega H\tilde{r}\kappa)\delta_s p \tag{2.50}$$

where we have used the definitions

$$\beta_f^2 \equiv \frac{\tilde{\rho}\kappa}{\rho\kappa_0}(1 - iH\tilde{r}\kappa'/\omega\tilde{\rho}\kappa) \tag{2.51}$$

$$\beta_s^2 \equiv \frac{\tilde{M}K}{\rho\kappa_0}(1 + iH'\tilde{r}/\omega\tilde{M}) \tag{2.52}$$

$$\delta_f \equiv 1 - iH'\omega\tilde{\rho}/H^2\tilde{r} \tag{2.53}$$

$$\delta_s \equiv 1 + i\omega\tilde{M}\kappa'/H\tilde{r}\kappa \tag{2.54}$$

$$\kappa_0 \equiv 1/\rho c^2 \tag{2.55}$$

Although we use these full expressions in our analysis here, in many cases of practical interest, where the "cross" terms in the mass balance equations 2.12 and 2.13 are very small, we would have

$$\delta_f \approx 1\ ,\ \ \delta_s \approx 1\ ,\ \ \beta_f^2 \approx \frac{\tilde{\rho}\kappa}{\rho\kappa_0}\ ,\ \ \beta_s^2 \approx \frac{\tilde{M}K}{\rho\kappa_0} \tag{2.56}$$

Now, by introducing the normalized propagation constant $\vec{Q} = \vec{q}/(\omega/c)$, we can use equations 2.49 and 2.50 to obtain the dispersion relation

$$Q^4 - (\beta_f^2 + \beta_s^2)Q^2 + \beta_f^2\beta_s^2 + \Lambda = 0 \tag{2.57}$$

where

$$\Lambda \equiv (H\tilde{\tau}/\omega\rho)^2(K/\kappa_0)(\kappa/\kappa_0)\delta_f\delta_s \tag{2.58}$$

The two solutions to this equation are

$$Q_1^2 = \frac{1}{2}(\beta_f^2 + \beta_s^2) + \frac{1}{2}\sqrt{(\beta_f^2 - \beta_s^2)^2 - 4\Lambda} \tag{2.59}$$

$$Q_2^2 = \frac{1}{2}(\beta_f^2 + \beta_s^2) - \frac{1}{2}\sqrt{(\beta_f^2 - \beta_s^2)^2 - 4\Lambda} \tag{2.60}$$

where the subscripts 1 and 2 refer to the two characteristic wave modes of the system.

We also obtain the ratio $\Gamma_{1,2}$ between the pressure in the structure and the pressure in the fluid using equations 2.49 and 2.50:

$$\Gamma_{1,2} \equiv \frac{p'}{p} = \frac{Q_{1,2}^2 - \beta_f^2}{(-iH\tilde{\tau}/\omega\rho)(K/\kappa_0)\delta_f} = \frac{(-iH\tilde{\tau}/\omega\rho)(\kappa/\kappa_0)\delta_s}{Q_{1,2}^2 - \beta_s^2} \tag{2.61}$$

where again, the subscripts refer to the two modes. Then using equations 2.40 and 2.41 we also obtain, for the ratio of the velocity magnitude in the structure to the velocity magnitude in the fluid

$$\gamma_{1,2} \equiv \frac{|\vec{u}'|}{|\vec{u}|} = \frac{K\Gamma_{1,2} + \kappa'}{\kappa - (H'/H)K\Gamma_{1,2}} \tag{2.62}$$

Figures 2-1 - 2-4 are plots of the real and imaginary parts of the propagation constants for the two modes for a set of four cases of decreasing compressibility. In each case, the imaginary part of the structure compressibility is taken to be 1/10th of the real part.

For high frequencies ($\omega \gg r/\rho, r/\rho'$), one mode can be associated with the wave in the fluid and the other with the wave in the structure. In this case we have for the limiting values of Q

$$Q_1 \rightarrow \sqrt{\frac{H\kappa}{\kappa_0}} = \sqrt{H\gamma} \tag{2.63}$$

using the isothermal fluid compressibility $\kappa = \gamma\kappa_0$, and

$$Q_2 \rightarrow \sqrt{\frac{H'\rho' K_r}{\rho\kappa_0}} \tag{2.64}$$

In the low frequency limit, the fluid and structure move together and there is only one mode of significance, the other is strongly damped. This mode's wavenumber is

$$Q \rightarrow \sqrt{\frac{\tilde{\rho}\tilde{\kappa}}{\rho\kappa_0}} \tag{2.65}$$

where $\tilde{\rho} = H\rho + H'\rho'$ and $1/\tilde{\kappa} = 1/(H\kappa) + 1/K_r$.

In the domain where $\omega \sim r/\rho, r/\rho'$, the porous medium is considered flexible and each of the two modes corresponds to a combination of structure and fluid motion.

2.4.8 Wave Propagation in an Unbounded Porous Medium

In circumstances where the influence of boundaries in negligible, the propagation constants obtained above can be used to describe the propagation of a plane wave in the porous material. If the angular frequency of such a wave is ω, we have for the phase speed

$$c = \frac{\omega}{q_r} = \frac{\omega}{Q_r k_0} = \frac{c_0}{Q_r} \tag{2.66}$$

where c_0 is the isentropic speed of sound in the fluid outside the porous material and the complex propagation constant is written as $Q = Q_r + iQ_i$. The decay rate of the plane wave in the porous medium is

$$X_{dBpercm} = -20 \log_{10} e^{-Q_i k_0} \simeq 8.69 Q_i k_0 = \frac{8.69 Q_i \omega}{c_0} \tag{2.67}$$

if ω/c_0 has units of inverse centimeters.

Figure 2-1: $K/\kappa_0 = (2,0.2)$, Real and imaginary parts of normalized propagation constants for modes 1 and 2 for $H = 0.95, G = 0.5, H'\rho' = 2lbs/ft^3, r = 10\rho c/inch$

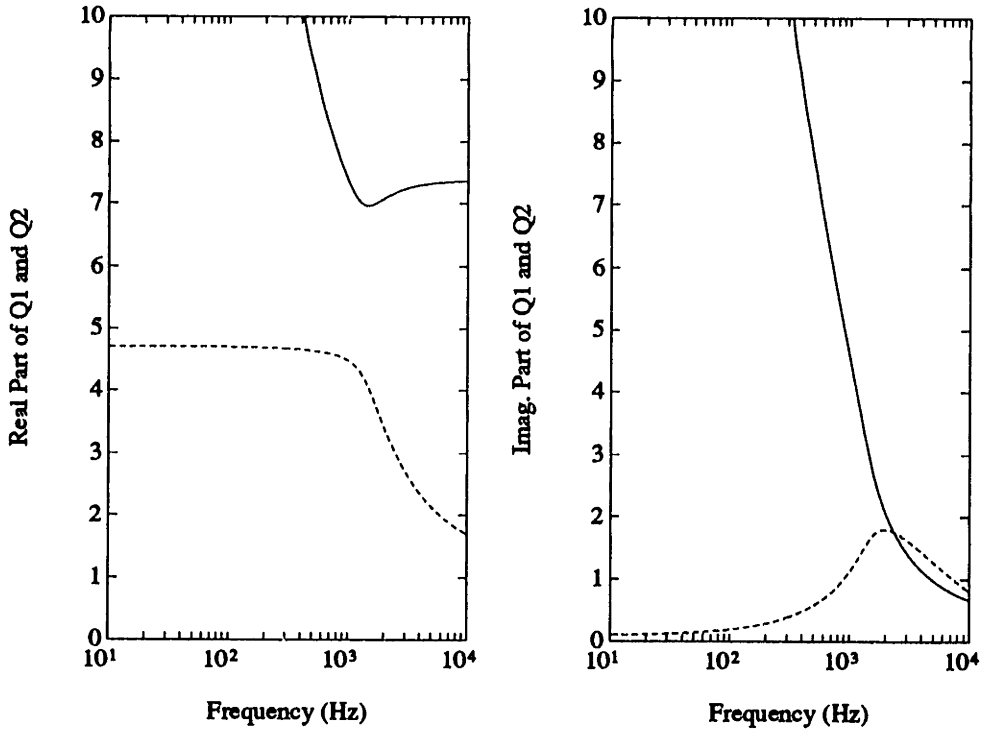

Figure 2-2: $K/\kappa_0 = (1.1,0.11)$, Real and imaginary parts of normalized propagation constants for modes 1 and 2 for $H = 0.95, G = 0.5, H'\rho' = 2lbs/ft^3, r = 10\rho c/inch$

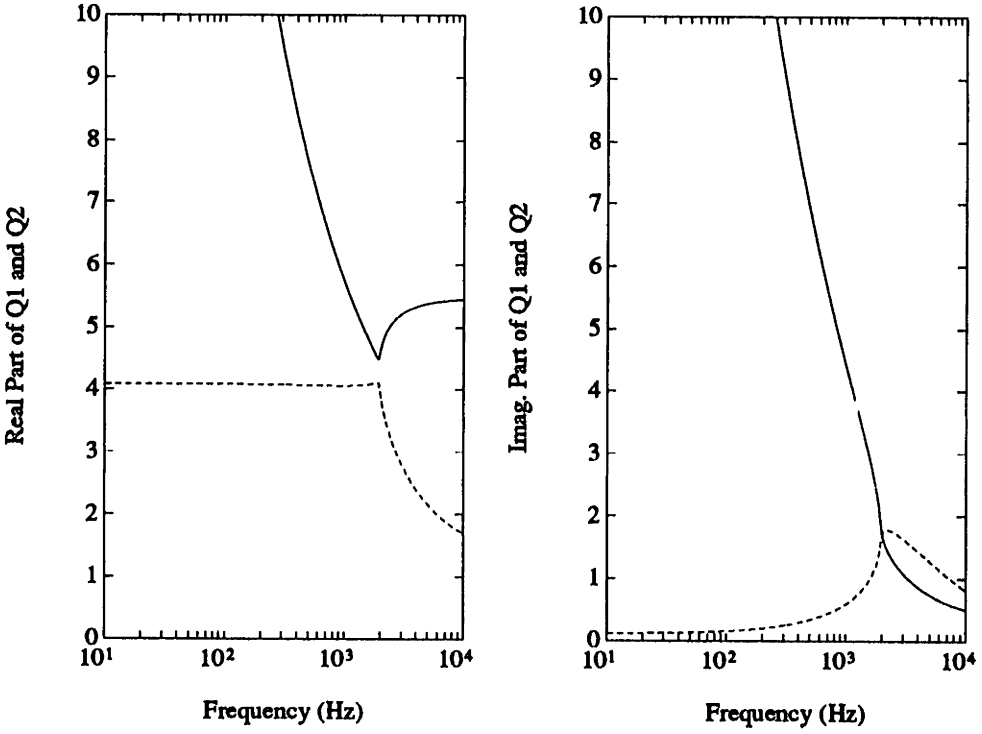

Figure 2-3: $K/\kappa_0 = (1.0,0.1)$, Real and imaginary parts of normalized propagation constants for modes 1 and 2 for $H = 0.95, G = 0.5, H'\rho' = 2lbs/ft^3, r = 10\rho c/inch$

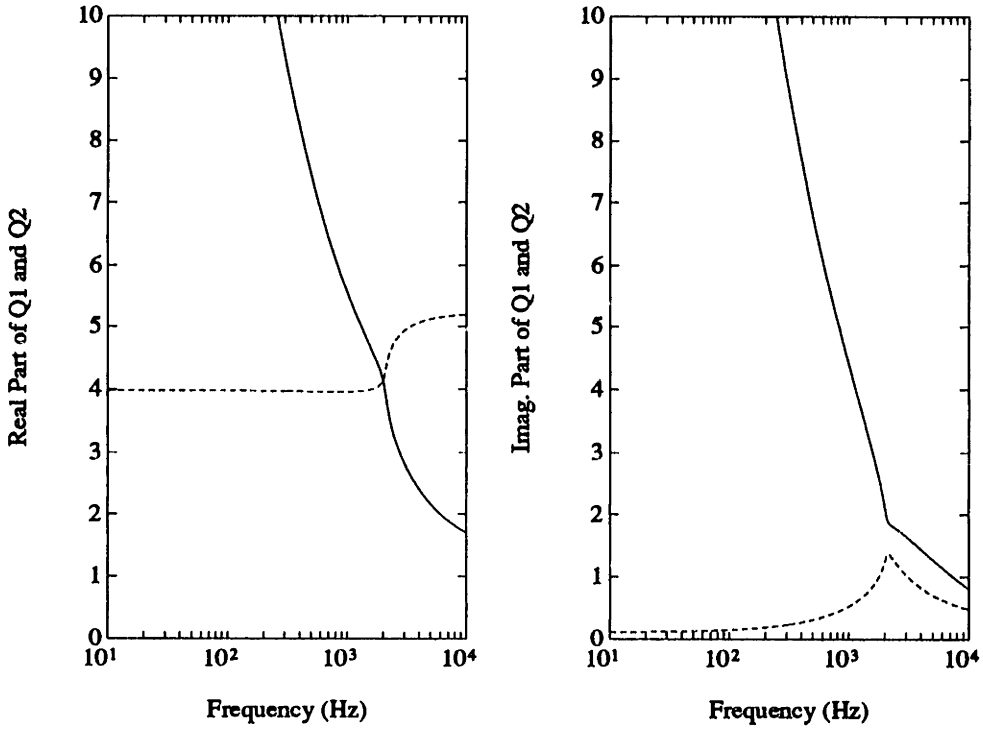

Figure 2-4: $K/\kappa_0 = (.5,0.05)$, Real and imaginary parts of normalized propagation constants for modes 1 and 2 for $H = 0.95, G = 0.5, H'\rho' = 2lbs/ft^3, r = 10\rho c/inch$

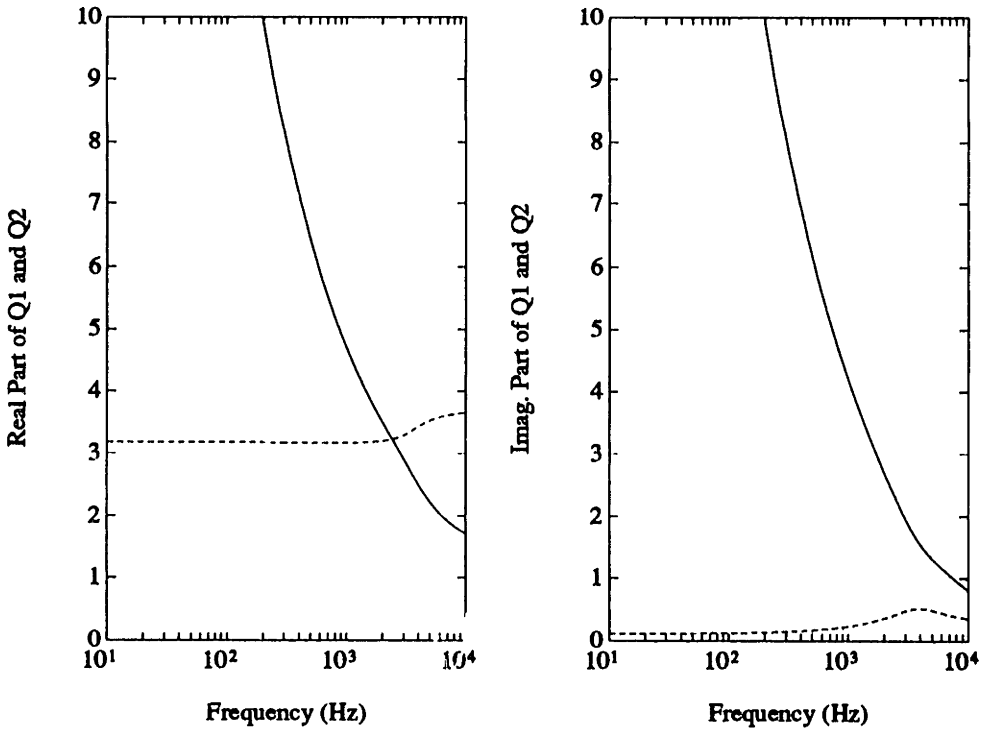

Chapter 3

The Finite Layer

3.1 Specific Configuration

We now consider a specific geometry, the layer of porous material backed by a rigid wall. Such a configuration is not only of considerable practical importance, it also serves to illustrate the many consequences of flexibility in a porous material. In this chapter, the absorption coefficient will be computed for an "open" and a "closed" layer in a manner following Ingard [15] with some additions. We then present a new discussion of the velocity ratio and mechanisms of sound absorption in the flexible porous material. In addition, we derive original expressions for the transmission matrices of open and closed flexible porous layers.

Figure 3-1 shows the coordinate system used. The layer, consisting of a homogeneous, isotropic, flexible porous material, is of uniform thickness d, of infinite extent in all directions parallel to its free surface, and backed by a rigid wall. We choose a coordinate system so that $\hat{x}$ is oriented normal to the free surface of the layer, with $x = -d$ coinciding with the free surface and $x = 0$ coinciding with the junction of the rigid wall and the back of the porous layer. The $\hat{y}$ and $\hat{z}$ directions are parallel to the free surface of the layer, and we will orient $\hat{y}$ so that the incident, reflected, and refracted waves all propagate in the xy plane.

We will examine two distinct types of surfaces at $x = -d$. The 'open' surface refers to the porous material terminating at $x = -d$ without any covering of impervious

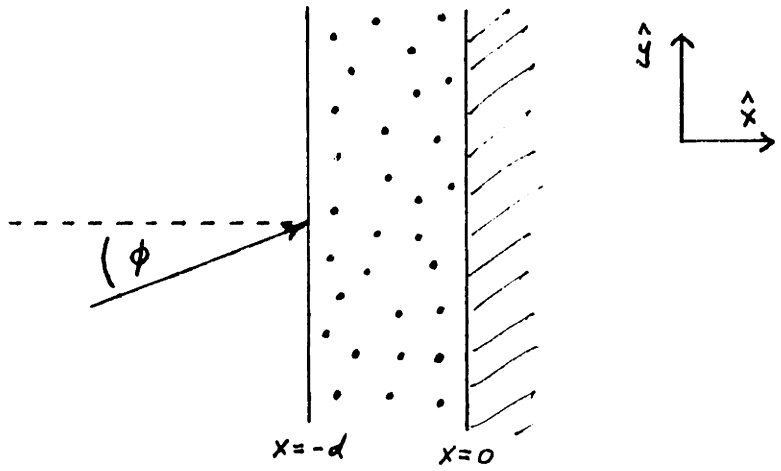

Figure 3-1: Geometry of Porous Layer and Defined Coordinate System

skin; the pores are open to the fluid at $x < -d$. The second, the 'closed' surface, corresponds to an impervious skin, of negligible thickness and mass per unit area, covering the porous layer at $x = -d$. For most of the results of this chapter, we will consider each of these two cases.

3.2 Boundary Conditions

As in chapter 2, we denote the pressure of the fluid p and that of the frame p', the velocity of the fluid is $\vec{u}$ and for the frame $\vec{u}'$. We denote components of the velocities using subscripts; for example, the $\hat{x}$ and $\hat{y}$ components of the fluid velocity would be written u_x and u_y respectively. The rigid wall backing the porous layer at $x = 0$ requires

$$u_x(x = 0) = u'_x(x = 0) = 0 \tag{3.1}$$

The open and closed layers have different boundary conditions at $x = -d$.

3.2.1 Open Layer

Continuity at the free surface of the open layer requires that

$$u_{0,x} = Hu_x(x = -d) + H'u'_x(x = -d) \tag{3.2}$$

where $u_{0,x}$ is the $\hat{x}$ component of the total fluid velocity just outside the layer at $x = -d$.

The fluid pressure p must be continuous since the layer is open, and the frame pressure p' must vanish at the free surface.

$$p_0 = p(x = -d) \ , \ p'(x = -d) = 0 \tag{3.3}$$

3.2.2 Closed Layer

The closed layer has an impervious skin at $x = -d$ which requires that the fluid just outside the layer, the fluid just inside the layer in the pores, and the edge of the frame must all have the same $\hat{x}$ velocity component.

$$u_{0,x} = u_x(x = -d) = u'_x(x = -d) \tag{3.4}$$

The covering is assumed to have negligible mass per unit area so the sum of the frame and fluid pressures just inside the cover must equal the fluid pressure just outside the cover.

$$p_0 = p(x = -d) + p'(x = -d) \tag{3.5}$$

3.3 Pressure and Velocity Fields

A plane wave of wavenumber k and angle of incidence ϕ (see figure 3-1) is incident on the free surface of the porous layer. Continuity of the trace velocity across the boundary at $x = -d$ requires

$$q_y = k \sin(\phi) \tag{3.6}$$

and

$$q_x = \sqrt{q^2 - q_y^2} = \sqrt{q^2 - k^2 \sin^2(\phi)} \tag{3.7}$$

Since there are two values of q (q_1 and q_2) for the two modes given in equations 2.59 and 2.60, there will be a corresponding q_{1x} and q_{2x}. In the $\hat{y}$ direction, $q_y = q_{1y} = q_{2y}$.

This means, in general, that each mode will have a different direction of travel in the porous material, although for a given mode the fluid and structure wave travel in the same direction. The pressure and velocity fields are in general a linear combination of the corresponding fields of each of the two modes.

Using the boundary condition in equation 3.1, the general form for the velocity components u_x and u'_x is

$$u_x = [U_1 \sin(q_{1x}x) + U_2 \sin(q_{2x}x)]e^{iq_y y} \tag{3.8}$$

$$u'_x = [\gamma_1 U_1 \sin(q_{1x}x) + \gamma_2 U_2 \sin(q_{2x}x)]e^{iq_y y} \tag{3.9}$$

where γ_1 and γ_2 are the ratios of structure to fluid speed in each of the modes.

Using these equations and the amplitude equations 2.42 and 2.43 , we can write for the pressure fields in the fluid and and frame

$$p = [P_1 \cos(q_{1x}x) + P_2 \cos(q_{2x}x)]e^{iq_y y} \tag{3.10}$$

$$p' = [\Gamma_1 P_1 \cos(q_{1x}x) + \Gamma_2 P_2 \cos(q_{2x}x)]e^{iq_y y} \tag{3.11}$$

where Γ_1 and Γ_2 are the ratios of structure to fluid speed in each of the modes and

$$P_1 = -i\rho c Z_1 U_1 \tag{3.12}$$

$$P_2 = -i\rho c Z_2 U_2 \tag{3.13}$$

with

$$Z_1 \equiv \frac{1}{Q_{1x}}(\tilde{\rho}/\rho - iH\tilde{r}\gamma_1/\omega\rho) \tag{3.14}$$

$$Z_2 \equiv \frac{1}{Q_{2x}}(\tilde{\rho}/\rho - iH\tilde{r}\gamma_2/\omega\rho) \tag{3.15}$$

3.4 Rigid, Limp, and Flexible Domains

Typically, a porous material is modeled as rigid, limp, or flexible based on the value of its structural compressibility. In fact any material is flexible, yet under certain conditions it may be essentially immobile or rigid, or in others it may comove with the fluid and be characterized as limp. For this reason, we instead refer to rigid, limp, or flexible *domains*; frequency ranges for which a given flexible porous material exhibits the corresponding behavior.

It is instructive to calculate the ratio of the structure and fluid velocities for some typical values of structure compressibility. This ratio allows us to define these rigid, limp, and flexible domains and sets the stage for a more complete discussion of mechanisms of sound absorption in section 3.8.

Figures 3-2 to 3-5 below show the magnitude Ψ_m and phase Ψ_p of the ratio

$$\Psi = \Psi_m e^{i\Psi_p} \equiv \frac{u'_x(x = -d/2)}{u_x(x = -d/2)} \tag{3.16}$$

taken in the middle of the layer at $x = -d/2$, using equations 3.8 and 3.9 .

In each of these cases, the *rigid* domain corresponds to the frequency range where $\Psi_m \to 0$ because $u' \to 0$; the structure does not move. The material behaves as *limp* when $\Psi_m \sim 1$ and $\Psi_p \sim 0$, this corresponds to comotion of the structure and fluid. It should be noted that, for materials of low compressibility, the low frequency limit gives $\vec{u} - \vec{u}' \to 0$ even though $\Psi_m \to 0$; this case would be regarded as limp. Note

that consistent with this definition, a material of low compressibility could exhibit limp behavior at some frequencies although the range of frequencies becomes smaller the lower the compressibility.

The *flexible* domain refers to intervening frequencies for which there is significant relative motion of the fluid and structure due at least partly to the motion of the structure.

Figure 3-2 shows Ψ for a material of very high compressibility which exhibits limp behavior at low frequencies and rigid behavior at high frequencies.

Figure 3-5 shows Ψ for a very stiff material, showing rigid behavior for most of the frequencies shown, except for some comotion resulting from structural layer resonances.

Figures 3-3 and 3-4 show Ψ for materials of moderate compressibility. The rigid domains are evident at the higher frequencies, and particularly interesting is the significant comotion occurring at intermediate frequencies. This type of limp behavior can result in a considerable reduction in the absorption coefficient as we shall see in later sections.

3.5 Input Admittance for the Open Layer

To compute the absorption coefficient for the open layer we use the normalized input admittance at $x = -d$ which has the form

$$\eta = \beta + i\sigma = \rho c \frac{u_x(x = -d)}{p(x = -d)} \tag{3.17}$$

Although input admittance is used here for the open layer, input impedance will be used for the closed layer in the following section. This is because the open layer boundary condition at $x = -d$ leads to an input admittance which is the sum of two terms, each of which correspond to one mode of the wave motion (see equation 3.20). The closed layer boundary condition at $x = -d$ leads to a more complicated form of the input admittance. The total input impedance for the closed layer, however, can be written as the sum of two terms, one for each of the modes, this will be evident in

Figure 3-2: $K/\kappa_0 = (2000,0.1)$, Limp limit of Magnitude and Phase angle of ratio between structure and fluid velocity in middle of layer. With $H = 0.95, G = 0.5, d = 1inch, H'\rho' = 2lbs/ft^3, r = 10\rho c/inch$

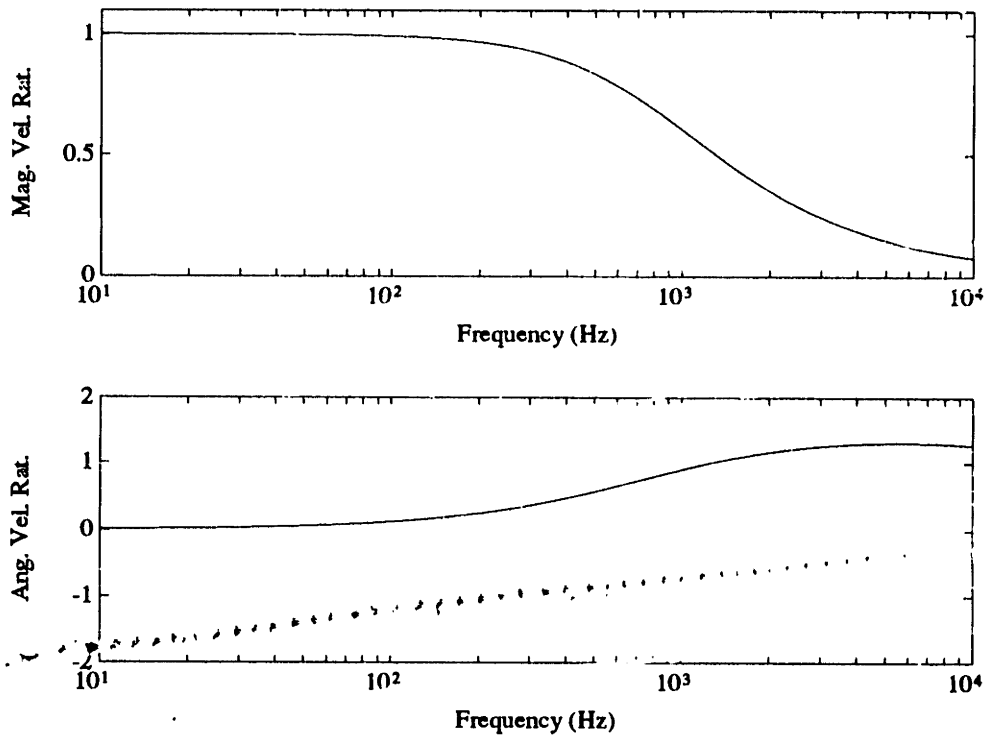

Figure 3-3: $K/\kappa_0 = (10,1)$, Magnitude and Phase angle of ratio between structure and fluid velocity in middle of layer. With $H = 0.95, G = 0.5, d = 1inch, H'\rho' = 2lbs/ft^3, r = 10\rho c/inch$

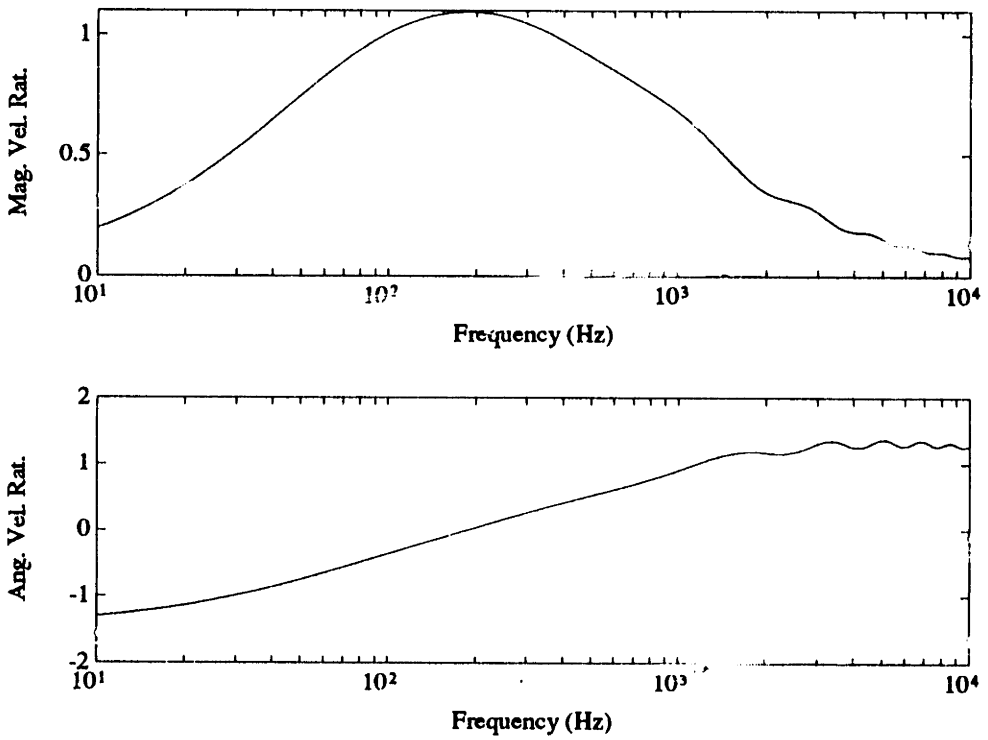

Figure 3-4: $K/\kappa_0 = (1,0.1)$, Magnitude and Phase angle of ratio between structure and fluid velocity in middle of layer. With $H = 0.95, G = 0.5, d = 1inch, H'\rho' = 2lbs/ft^3, r = 10\rho c/inch$

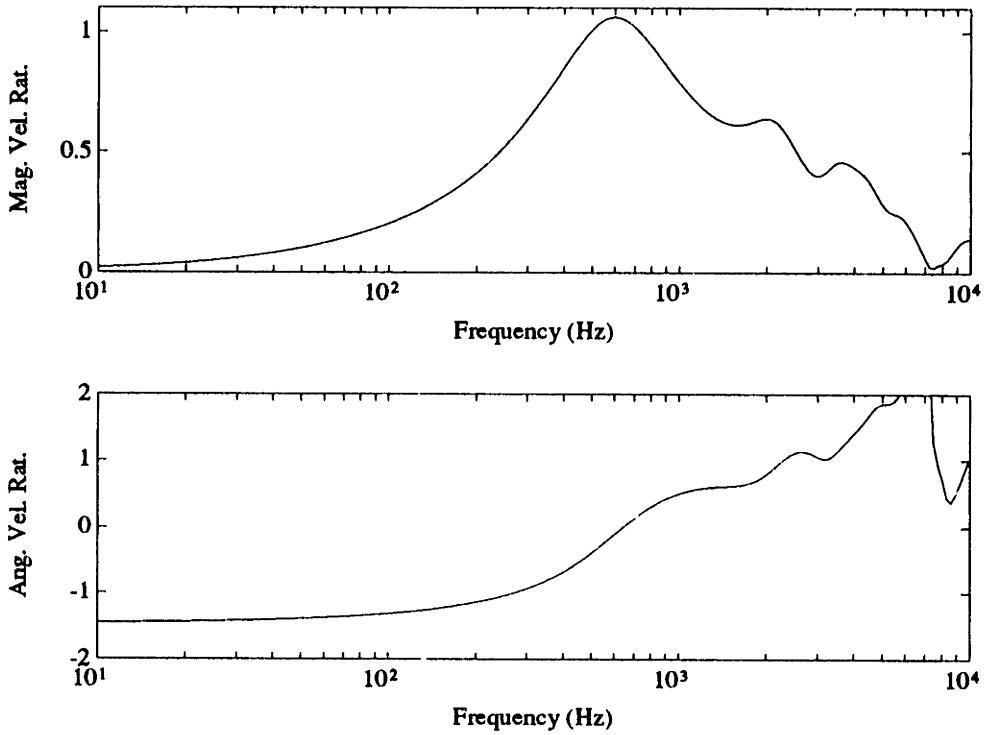

Figure 3-5: $K/\kappa_0 = (0.1,0.01)$, Magnitude and Phase angle of ratio between structure and fluid velocity in middle of layer. With $H = 0.95, G = 0.5, d = 1inch, H'\rho' = 2lbs/ft^3, r = 10\rho c/inch$

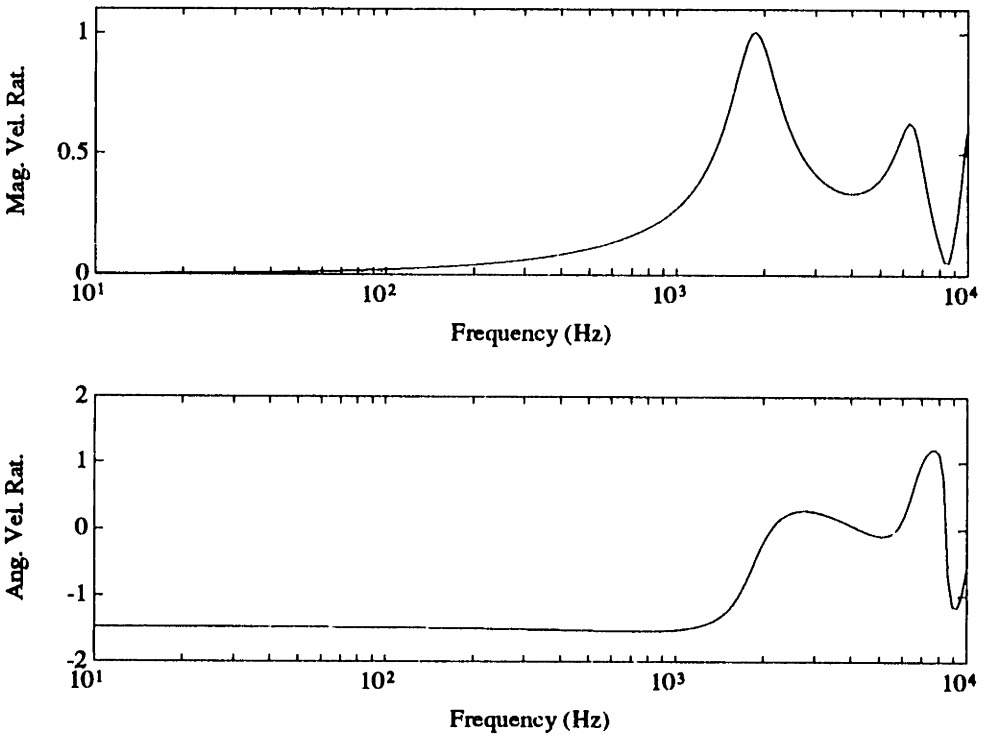

equation 3.26.

To obtain the input admittance for the open layer, we first obtain expressions for the amplitude of the fluid pressure and normal velocity just outside the layer. This is done by applying the boundary conditions 3.2 and 3.3 to the general expressions 3.8 - 3.11 which gives

$$p(x=-d) = (1-\frac{\Gamma_1}{\Gamma_2})P_1\cos(q_{1x}d)e^{iq_y y} = (1-\frac{\Gamma_2}{\Gamma_1})P_2\cos(q_{2x}d)e^{iq_y y} \tag{3.18}$$

$$u(x=-d) = [-U_1(H+H'\gamma_1)\sin(q_{1x}d) - U_2(H+H'\gamma_2)\sin(q_{2x}d)]e^{iq_y y} \tag{3.19}$$

The normalized input admittance at $x=-d$ is then

$$\eta_{open} = -i\eta_1\tan(q_{1x}d) - i\eta_2\tan(q_{2x}d) \tag{3.20}$$

where

$$\eta_1 \equiv \frac{(H+H'\gamma_1)}{Z_1}\left[\frac{\Gamma_2}{\Gamma_2-\Gamma_1}\right] \tag{3.21}$$

$$\eta_2 \equiv \frac{(H+H'\gamma_2)}{Z_2}\left[\frac{\Gamma_1}{\Gamma_1-\Gamma_2}\right] \tag{3.22}$$

3.6 Input Impedance for the Closed Layer

The normalized input impedance at $x=-d$ is defined as

$$\zeta = \theta + i\chi = \frac{1}{\rho c}\frac{p_(x=-d)}{u_x(x=-d)} \tag{3.23}$$

In a manner analogous to the previous section, we apply the boundary conditions 3.4 and 3.5 to the general expressions 3.8 - 3.11 to obtain

$$p(x=-d) = [(1+\Gamma_1)P_1\cos(q_{1x}d) + (1+\Gamma_2)P_2\cos(q_{2x}d)]e^{iq_y y} \tag{3.24}$$

$$u(x=-d) = (\gamma_1 - 1)U_1\sin(q_{1x}d)e^{iq_y y} = (1-\gamma_2)U_2\sin(q_{2x}d)e^{iq_y y} \tag{3.25}$$

The normalized input impedance at $x = -d$ is

$$\zeta_{closed} = i\zeta_1\cot(q_{1x}d) + i\zeta_2\cot(q_{2x}d) \tag{3.26}$$

where

$$\zeta_1 \equiv Z_1\left(\frac{\gamma_2 - 1}{\gamma_2 - \gamma_1}\right)(1+\Gamma_1) \tag{3.27}$$

$$\zeta_2 \equiv Z_2\left(\frac{1-\gamma_1}{\gamma_2 - \gamma_1}\right)(1+\Gamma_2) \tag{3.28}$$

3.7 Absorption Coefficients

The absorption coefficient, as a function of angle, is written for the open layer in terms of the real and imaginary parts of the normalized input admittance or, for the closed layer, is expressed in terms of the normalized input impedance. As explained in the previous section, this separate treatment of the open and closed cases results in more compact admittance and impedance expressions.

$$\alpha(\phi,\eta) = \frac{4\beta\cos\phi}{(\beta+\cos\phi)^2 + \sigma^2} \tag{3.29}$$

$$\alpha(\phi,\zeta) = \frac{4\theta\cos\phi}{(1+\theta\cos\phi)^2 + (\chi\cos\phi)^2} \tag{3.30}$$

The expression for the angle averaged absorption coefficient, which can also be computed for either case, is obtained by assuming that the sound incident on the layer

is the sum of plane waves in all possible angles of incidence with the total intensity per unit solid angle the same for all directions, a so called 'diffuse' sound field. (There are other aspects of the definition of a 'diffuse' sound field which do not concern us here.) This average takes the form

$$\bar{\alpha} = \frac{\int_0^{\pi/2} \alpha(\phi) \cos\phi \sin\phi \, d\phi}{\int_0^{\pi/2} \cos\phi \sin\phi \, d\phi} = 2 \int_0^{\pi/2} \alpha(\phi) \cos\phi \sin\phi \, d\phi \qquad (3.31)$$

Figures 3-6 to 3-9 show computed absorption coefficients, both for normal incidence and angle averaged, for a number of cases of increasing flow resistance.

The layer resonances discussed in section 2.3.1 are very apparent in most of these cases. For the open layer, peaks in absorption occur when the layer thickness is one-quarter of a wavelength for the fluid wave at higher frequencies. Dips are seen when the structure has a quarter-wave resonance. This is a consequence of reduced relative motion between the fluid and the structure and will be examined in more detail in the following section. For the closed layer the resonant peaks have more regular spacing and height due to the abrupt wave impedance changes at both $x = -d$ and $x = 0$. In the low frequency limit, all the cases show $\alpha \to 0$. For high frequencies the open layer approaches the absorption coefficient of a rigid layer and the closed layer can be modeled as a frequency independent characteristic impedance at $x = -d$ (see equations 3.14 and 3.15); thus α is constant for high frequencies.

The dotted lines represent the angle averaged absorption coefficient obtained using equation 3.31. These $\bar{\alpha}$'s are consistently higher than the normal incidence α's. This can be understood by taking a particular case and plotting $\alpha(\phi)$ where ϕ is the angle of incidence. Such a case in shown in figure 3-10.

We see a peak in the absorption coefficient for a particular angle which in general will be different from that for $\phi = 0$. This is a common result seen, for example, in the absorption of sound in a rigid porous sheet. For this reason, the angle averaged $\bar{\alpha}$ is usually greater than $\alpha(\phi = 0)$.

Figure 3-6: Absorption Coefficients for Open and Closed Layers; Normal Incidence (solid line) and Angle Averaged (dashed line); With $r = 1\rho c/inch, H = 0.95, G = 0.5, K/\kappa_0 = (1, 0.1), d = .25inches$ and $d = 1inch, H'\rho' = 2lbs/ft^3$

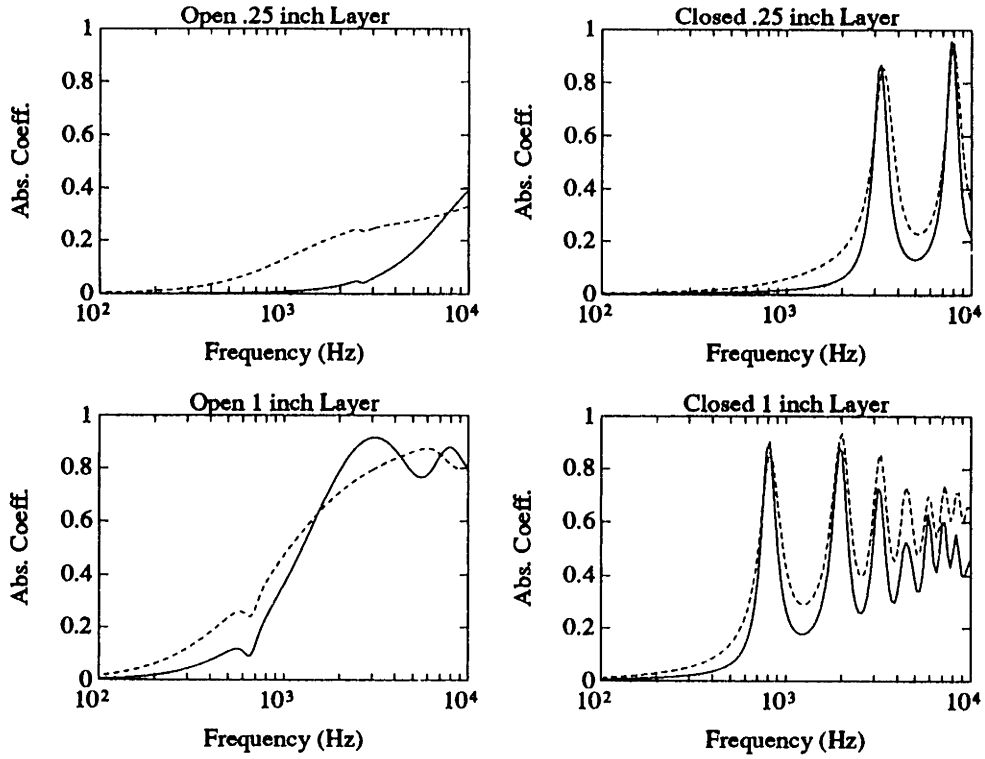

Figure 3-7: Absorption Coefficients for Open and Closed Layers; Normal Incidence (solid line) and Angle Averaged (dashed line); With $r = 4\rho c/inch, H = 0.95, G = 0.5, K/\kappa_0 = (1, 0.1), d = .25inches$ and $d = 1inch, H'\rho' = 2lbs/ft^3$

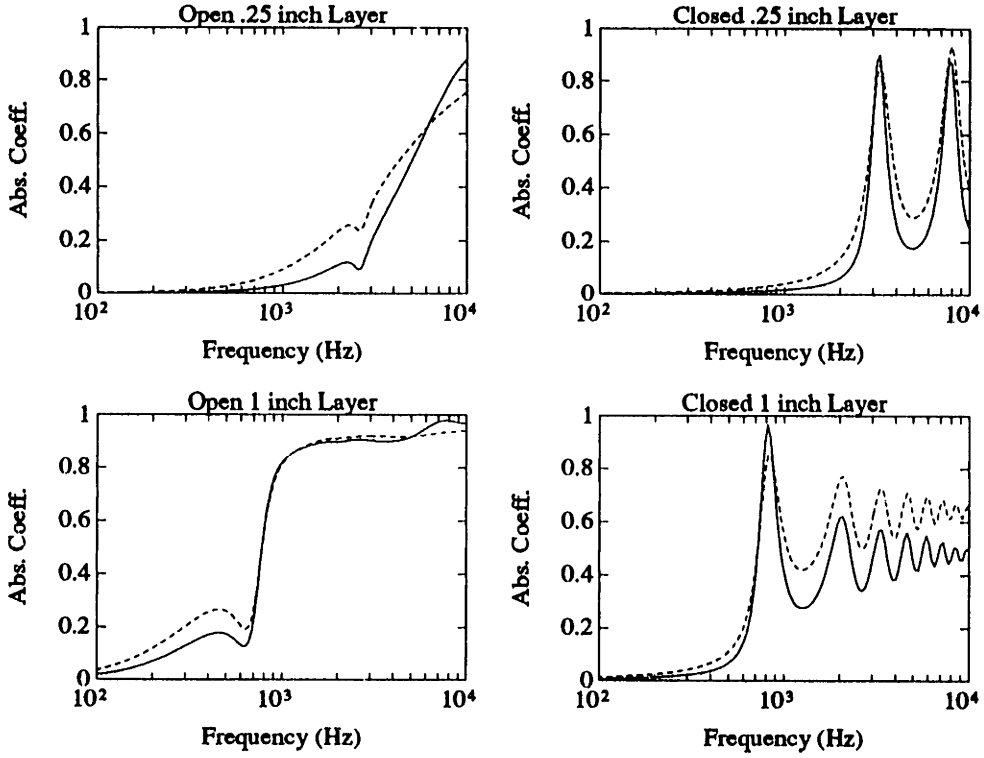

Figure 3-8: Absorption Coefficients for Open and Closed Layers; Normal Incidence (solid line) and Angle Averaged (dashed line); With $r = 16\rho c/inch, H = 0.95, G = 0.5, K/\kappa_0 = (1, 0.1), d = .25inches$ and $d = 1inch, H'\rho' = 2lbs/ft^3$

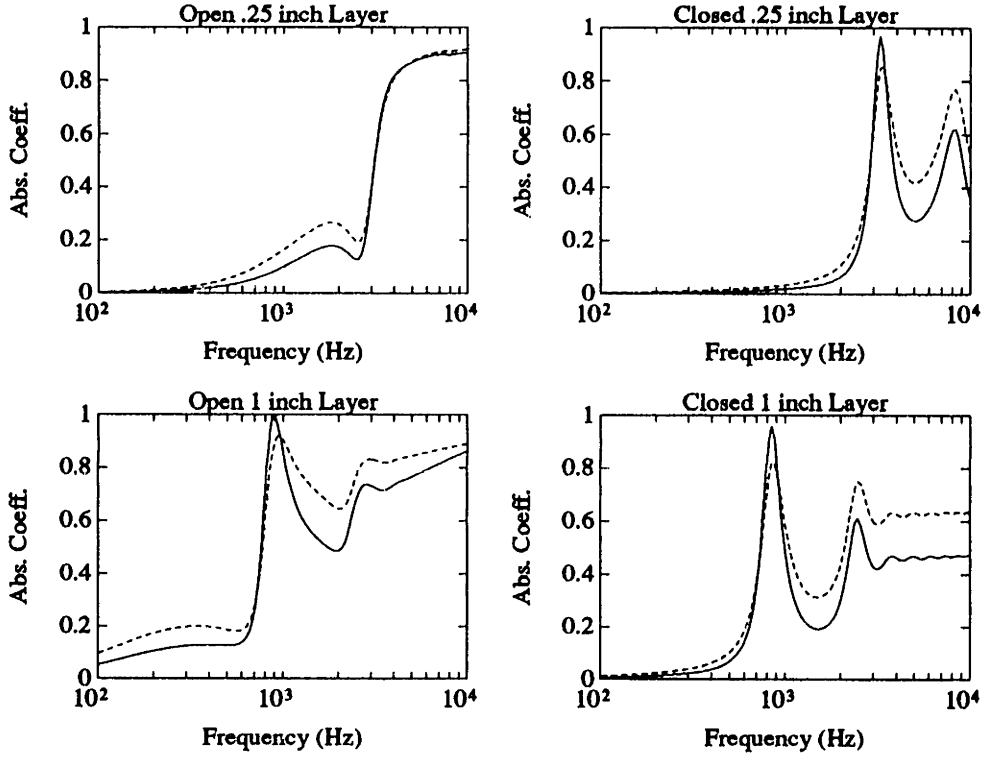

Figure 3-9: Absorption Coefficients for Open and Closed Layers; Normal Incidence (solid line) and Angle Averaged (dashed line); With $r = 32\rho c/inch, H = 0.95, G = 0.5, K/\kappa_0 = (1, 0.1), d = .25inches$ and $d = 1inch, H'\rho' = 2lbs/ft^3$

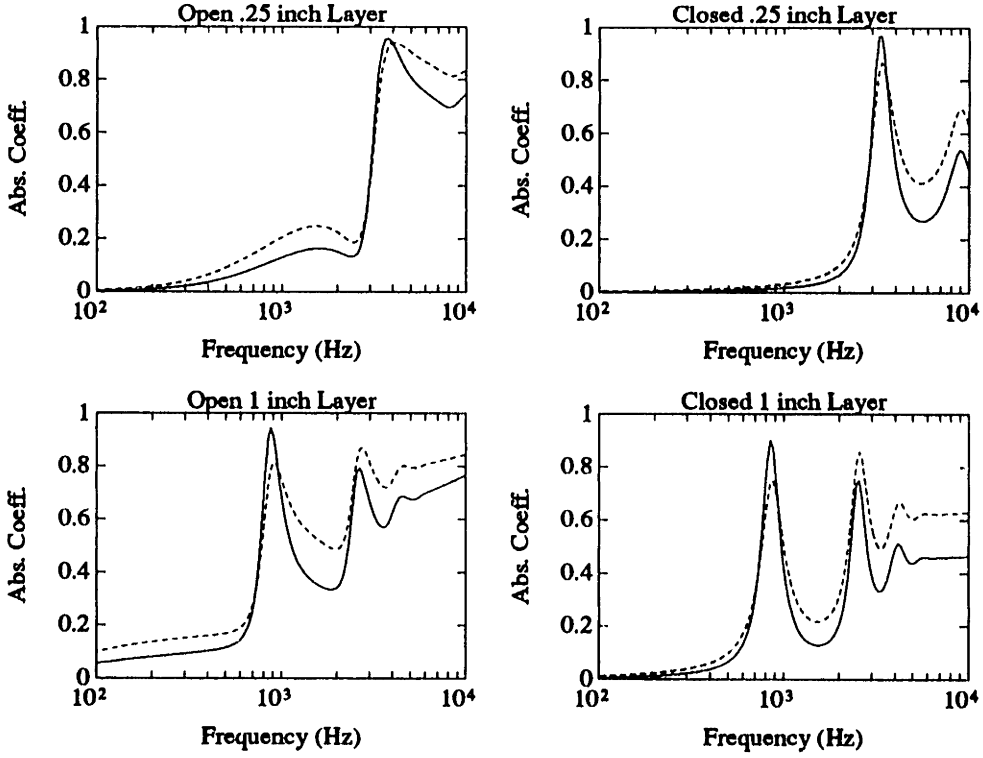

Figure 3-10: Absorption Coefficient as a Function of Angle for Open and Closed Layers, Frequency = 1000 Hz; all with $K = (1, 0.1), H = 0.95, G = 0.5, d = 1inch, H'\rho' = 2lbs/ft^3, r = 10\rho c/inch, \nu = 1000Hz$

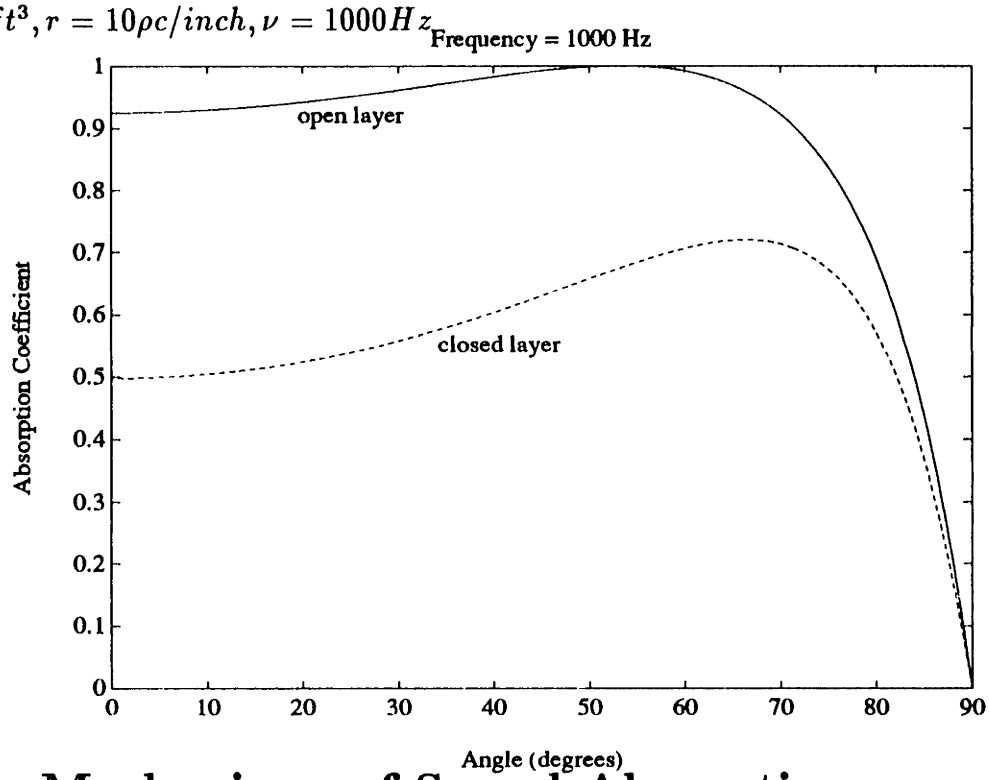

3.8 Mechanisms of Sound Absorption

If the goal is to design a sound absorbing material with certain acoustical characteristics, then it is important to more fully understand what underlying physical mechanisms are responsible for the conversion of acoustic energy into heat in the flexible porous layer. We will consider open and closed layers separately, and reveal fundamentally different loss mechanisms in the two cases.

For purposes of discussion of the open porous layer, we choose a typical set of material properties as a test case. Figure 3-11 shows the normal incidence (our discussion in this section will focus only on normally incident sound) absorption coefficient for a material with H=0.95, G=0.5, d = 1 inch, H'ρ' = 2 lbs/ft^3, $r = 10\rho c/inch$, and K = (1,0.1)κ_0 (κ_0 is the isentropic compressibility of air). Also shown in this figure are the corresponding curves for two other materials which have K/κ_0 = (2000,0.1) and $\sim$ (0,0). These two traces are labeled as 'limp' and 'rigid' respectively.

The inclusion of flexibility has significant consequences in this case. Compared to the rigid case, the mobility of the structure has greatly altered the absorption

coefficient. In addition, the stiffness of the structure has caused comotion of the fluid and structure which has resulted in reduction of the absorption coefficient at certain frequencies. The question still remains, however: what is the relative importance of losses due to viscous drag between the fluid and structure and losses due to deformation of the structure itself? As was shown in section 2.4.6, these two effects can be separated by computing the integrals

$$loss_r = \frac{1}{\Pi_0} \int_{x=-d}^{0} \frac{1}{2} Hr|u - u'|^2 \, dx \tag{3.32}$$

$$loss_k = \frac{1}{\Pi_0} \int_{x=-d}^{0} \frac{1}{2} \omega K_i |p'|^2 \, dx \tag{3.33}$$

$$\alpha = loss_r + loss_k \tag{3.34}$$

where Π_0 is the incident intensity, and since we are considering only normal incidence, $\vec{u} \parallel \vec{u}' \parallel \hat{x}$ and $u = |\vec{u}|, u' = |\vec{u}'|$.

The three quantities α, $loss_r$, and $loss_k$ are plotted for the open layer test case in figure 3-12. For most frequencies, the losses attributed to the deformation of the structure are much less than those due to viscous drag. In the vicinity of the structure's layer resonance, however, the deformation losses are actually larger. For higher flow resistances this effect can be greater still.

To compare these two loss mechanisms we plot the quantity $10\log(loss_k/loss_r)$ for a few materials: the test case and two others with slightly different imaginary parts of the structure compressibility K_i. For the lower $K_i = 0.01$, we see narrow frequency ranges where the losses are comparable. In this case the structure is more readily excited in a layer resonance, but the resulting losses are less. For the case of higher $K_i = 1$, the loss ratio has a broader peak and is due to a more highly damped structural resonance, but has higher losses for a given deformation.

We next consider a closed flexible porous layer; an impervious skin (with negligible mass per unit area) covers the free surface. To identify the mechanisms responsible for sound absorption in such a layer, we set $r = 0$, and associate any remaining

absorption with the losses due only to the irreversible deformation of the structure. For the open layer, this method cannot be used because setting $r = 0$ prevents the sound in the fluid from inducing any motion of the structure, and makes any losses due to viscous drag impossible; as a result there is no absorption in such a layer. The impervious cover of the closed layer, however, permits the sound wave outside the layer to couple directly the structure at the free surface. For this reason, even with $r = 0$, a closed porous layer can exhibit significant absorption, which is due only to losses caused by the deformation of the structure.

Figure 3-14 shows two cases: the solid line is the normal incidence absorption coefficient for a closed porous layer with $r = 1\rho c/inch$ and the dotted line shows the same case, but with $r = 0$. This comparison shows the dominant role of structural deformation losses in such a layer.

A significant distinction is evident between the mechanisms of sound absorption between the open versus the closed layer. In the open layer, the absorption is due almost exclusively to viscous drag except at frequencies corresponding to structural layer resonances, or cases of very high flow resistance, in which case the closed layer boundary condition is almost realized at the free surface.

This difference has consequences for the design of an absorptive porous layer. On one hand a open layer can provide relatively smooth performance over frequency but the flow resistance of the material must be carefully specified. The closed layer, on the other hand, has a much rougher performance over frequency, due to the sharpness of the structural layer resonances, yet it will deliver good performance over a wider range of flow resistance. The effect of flow resistance in the closed layer is to lower and broaden the peaks in the absorption coefficient; perhaps a composite closed layer system could further smooth the performance over frequency.

Figure 3-11: $K/\kappa_0 = (2000,0.1),(1,0.1),(1.0e\text{-}20,1.0e\text{-}6)$; Open layer, Absorption Coefficient, Normal Incidence, for Flexible, Limp, and Rigid cases, all with $H = 0.95, G = 0.5, d = 1inch, H'\rho' = 2lbs/ft^3, r = 10\rho c/inch$

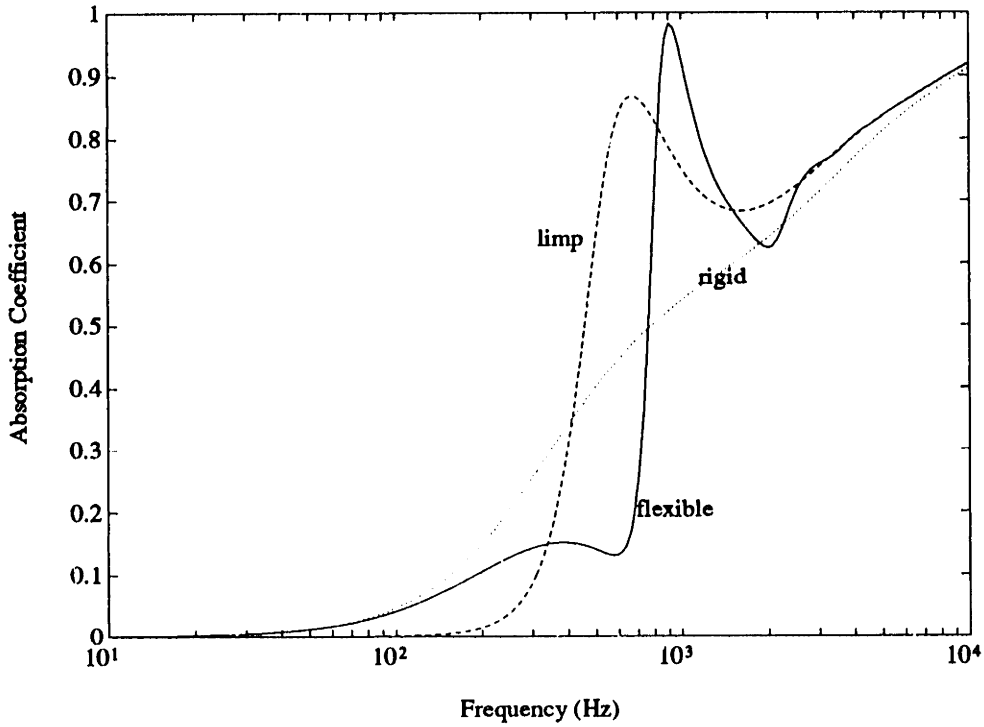

Figure 3-12: Open Layer, Absorption Coefficient, loss-r, loss-k (as defined in section 3.8); for a material with $H = 0.95, G = 0.5, d = 1inch, H'\rho' = 2lbs/ft^3, r = 10\rho c/inch$

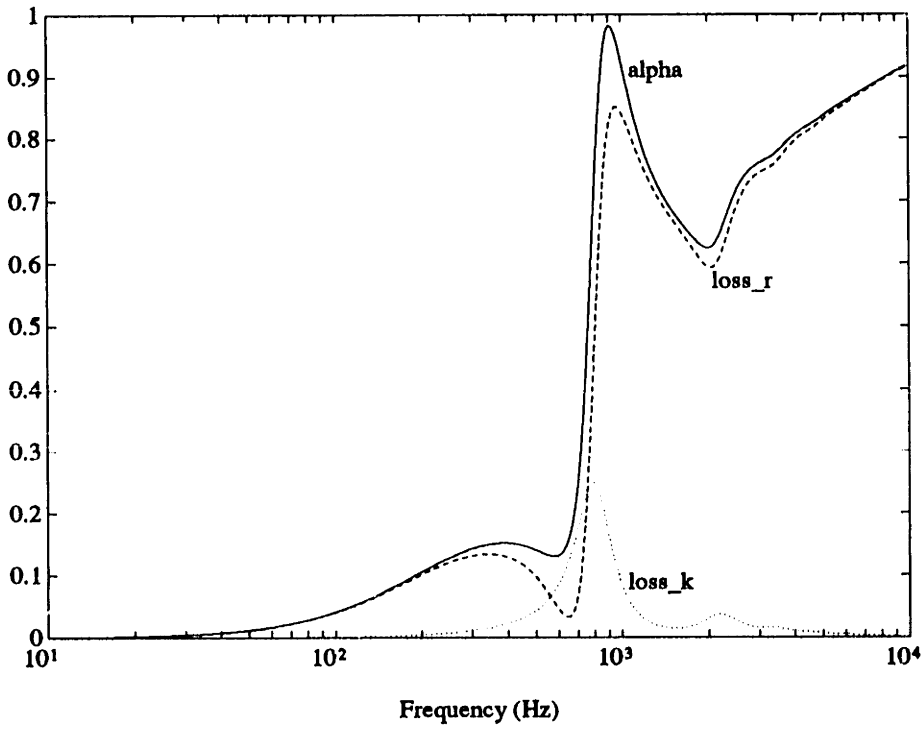

Figure 3-13: Open Layer, Ratio of Power Dissipated through Structure Deformation versus Resistive Drag; $10\log(loss_k/loss_r)$; 3 cases: $K = (1, 0.1)$, $K = (1, 1)$, $K = (1, 0.01)$, all with $H = 0.95, G = 0.5, d = 1inch, H'\rho' = 2lbs/ft^3, r = 10\rho c/inch$

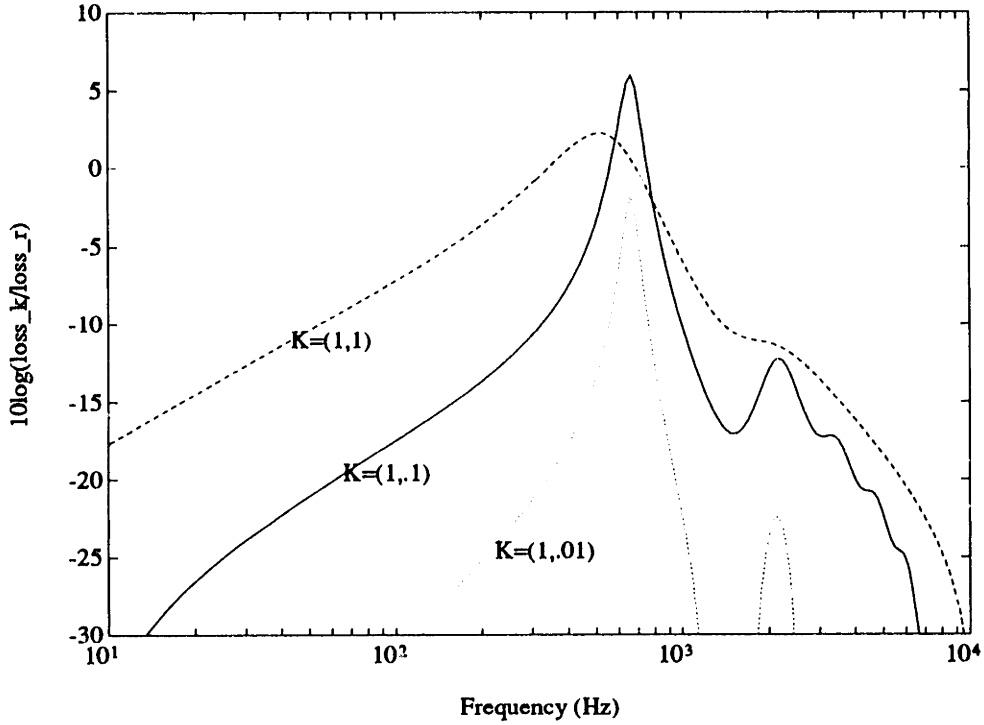

Figure 3-14: Closed Layer, Absorption Coefficient; for a material with $H = 0.95, G = 0.5, K = (1, 0.1), d = 1inch, H'\rho' = 2lbs/ft^3, r = 0$ or $1\rho c/inch$

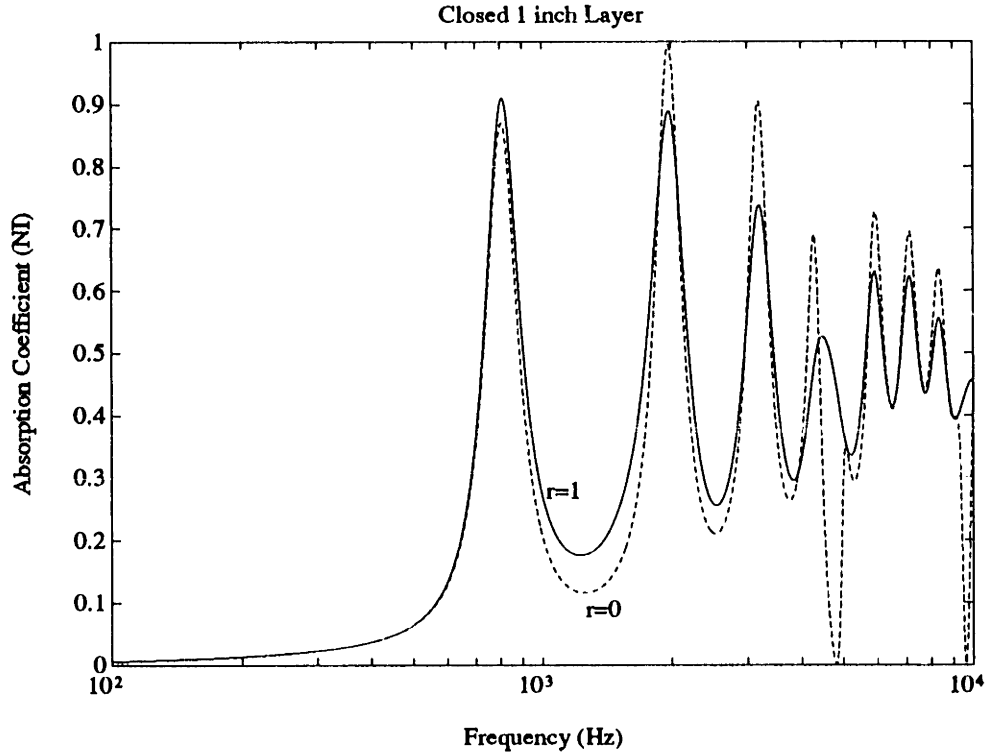

3.9 Transmission Matrices

A transmission matrix relates the pressure and normal velocity on one side of a finite layer to the pressure and normal velocity on the other side.

$$\begin{pmatrix} p_2 \\ u_2 \end{pmatrix} = \begin{pmatrix} T_{11} & T_{12} \\ T_{21} & T_{22} \end{pmatrix} \begin{pmatrix} p_1 \\ u_1 \end{pmatrix} \tag{3.35}$$

We define p_1, u_1 as the pressure and normal velocity at $x = 0$ and p_2, u_2 as the corresponding quantities at $x = l$. (Note: We are now placing the $\hat{x}$ coordinate so that the layer extends from $x = 0$ to $x = l$.)

In general we may write expressions for the field quantities at an arbitrary position in the layer as

$$p(x) = P_{1+}e^{iq_1x} + P_{1-}e^{-iq_1x} + P_{2+}e^{iq_2x} + P_{2-}e^{-iq_2x} \tag{3.36}$$

$$p'(x) = P_{1+}\Gamma_1 e^{iq_1x} + P_{1-}\Gamma_1 e^{-iq_1x} + P_{2+}\Gamma_2 e^{iq_2x} + P_{2-}\Gamma_2 e^{-iq_2x} \tag{3.37}$$

$$(\rho c)\, u(x) = \frac{P_{1+}}{Z_1}e^{iq_1x} - \frac{P_{1-}}{Z_1}e^{-iq_1x} + \frac{P_{2+}}{Z_2}e^{iq_2x} - \frac{P_{2-}}{Z_2}e^{-iq_2x} \tag{3.38}$$

$$(\rho c)\, u'(x) = \frac{\gamma_1 P_{1+}}{Z_1}e^{iq_1x} - \frac{\gamma_1 P_{1-}}{Z_1}e^{-iq_1x} + \frac{\gamma_2 P_{2+}}{Z_2}e^{iq_2x} - \frac{\gamma_2 P_{2-}}{Z_2}e^{-iq_2x} \tag{3.39}$$

where $P_{1+}, P_{1-}, P_{2+}, P_{2-}$ are amplitudes to be determined by the boundary conditions.

We now derive transmission matrices of the form shown in equation 3.35 for two distinct cases: that of the porous layer with open surface and that of a porous layer with an impervious skin on both sides.

3.9.1 Layer with Open Surface

For the porous layer with no coating of impervious skin, the boundary conditions at each free surface are of the form

$$p_1 = p(x=0) \ , \ p_2 = p(x=l) \ , \ p'(x=o) = p'(x=l) = 0 \tag{3.40}$$

$$u_1 = Hu(x=0) + (1-H)u'(x=0) \ , \ u_2 = Hu(x=l) + (1-H)u'(x=l) \tag{3.41}$$

Applying these boundary conditions to the field equations 3.36 - 3.39 we have, expressed in matrix form

$$\begin{pmatrix} p_1 \\ u_1 \\ 0 \\ 0 \end{pmatrix} = \mathcal{A}_{open} \begin{pmatrix} P_{1+} \\ P_{1-} \\ P_{2+} \\ P_{2-} \end{pmatrix} \tag{3.42}$$

where

$$\mathcal{A}_{open} = \begin{pmatrix} 1 & 1 & 1 & 1 \\ \left[\frac{H+(1-H)\gamma_1}{Z_1}\right] & -\left[\frac{H+(1-H)\gamma_1}{Z_1}\right] & \left[\frac{H+(1-H)\gamma_2}{Z_2}\right] & -\left[\frac{H+(1-H)\gamma_2}{Z_2}\right] \\ \Gamma_1 & \Gamma_1 & \Gamma_2 & \Gamma_2 \\ \Gamma_1 e^{iq_1 l} & \Gamma_1 e^{-iq_1 l} & \Gamma_2 e^{iq_2 l} & \Gamma_2 e^{-iq_2 l} \end{pmatrix} \tag{3.43}$$

And p_2 and u_2 can be expressed in matrix form as

$$\begin{pmatrix} p_2 \\ u_2 \end{pmatrix} = \mathcal{B}_{open} \begin{pmatrix} P_{1+} \\ P_{1-} \\ P_{2+} \\ P_{2-} \end{pmatrix} \tag{3.44}$$

where

$$\mathcal{B}_{open} = \begin{pmatrix} e^{iq_1 l} & e^{-iq_1 l} & e^{iq_2 l} & e^{-iq_2 l} \\ \left[\frac{H+(1-H)\gamma_1}{Z_1}\right] e^{iq_1 l} & -\left[\frac{H+(1-H)\gamma_1}{Z_1}\right] e^{-iq_1 l} & \left[\frac{H+(1-H)\gamma_2}{Z_2}\right] e^{iq_2 l} & -\left[\frac{H+(1-H)\gamma_2}{Z_2}\right] e^{-iq_2 l} \end{pmatrix} \tag{3.45}$$

Combining the matrix equations 3.42 and 3.44 we can then write a matrix equation for the transmission matrix which is:

$$\begin{pmatrix} T_{11} & T_{12} \\ T_{21} & T_{22} \end{pmatrix} = \mathcal{B}_{open} \, (\mathcal{A}_{open})^{-1} \begin{pmatrix} 1 & 0 \\ 0 & 1 \\ 0 & 0 \\ 0 & 0 \end{pmatrix} \tag{3.46}$$

where $(\mathcal{A}_{open})^{-1}$ denotes the matrix inverse of $\mathcal{A}_{open}$.

The resulting transmission matrix for the porous layer with open surfaces is:

$$\mathcal{T}_{open} = \begin{pmatrix} T_{11,open} & T_{12,open} \\ T_{21,open} & T_{22,open} \end{pmatrix} \tag{3.47}$$

where

$$T_{11,open} = \frac{\alpha_1\Gamma_2 \cos(q_1 l)\sin(q_2 l) - \alpha_2\Gamma_1 \sin(q_1 l)\cos(q_2 l)}{\alpha_1\Gamma_2 \sin(q_2 l) - \alpha_2\Gamma_1 \sin(q_1 l)} \tag{3.48}$$

$$T_{12,open} = i\left[\frac{(\Gamma_2 - \Gamma_1)\sin(q_1 l)\sin(q_2 l)}{\alpha_1\Gamma_2 \sin(q_2 l) - \alpha_2\Gamma_1 \sin(q_1 l)}\right] \tag{3.49}$$

$$T_{21,open} = i\left[\frac{((\alpha_1\Gamma_2)^2 + (\alpha_2\Gamma_1)^2)\sin(q_1 l)\sin(q_2 l) - 2\alpha_1\alpha_2\Gamma_1\Gamma_2(1 - \cos(q_1 l)\cos(q_2 l))}{(\Gamma_2 - \Gamma_1)(\alpha_1\Gamma_2 \sin(q_2 l) - \alpha_2\Gamma_1 \sin(q_1 l))}\right] \tag{3.50}$$

$$T_{22,open} = \frac{\alpha_1\Gamma_2 \cos(q_1 l)\sin(q_2 l) - \alpha_2\Gamma_1 \sin(q_1 l)\cos(q_2 l)}{\alpha_1\Gamma_2 \sin(q_2 l) - \alpha_2\Gamma_1 \sin(q_1 l)} \tag{3.51}$$

where

$$\alpha_1 \equiv \frac{H + H'\gamma_1}{\rho c Z_1} \quad , \quad \alpha_2 \equiv \frac{H + H'\gamma_2}{\rho c Z_2} \tag{3.52}$$

3.9.2 Layer with Closed Surface

The corresponding transmission matrix for the closed layer, where both surfaces are covered by an impervious skin of negligible mass per unit area, is obtained in a similar manner.

The boundary conditions at $x = 0$ and $x = l$ are

$$p_1 = p(x = 0) + p'(x = 0) \quad , \quad p_2 = p(x = l) + p'(x = l) \tag{3.53}$$

$$u_1 = u(x = 0) = u'(x = 0) \quad , \quad u_2 = u(x = l) = u'(x = l) \tag{3.54}$$

These boundary conditions applied to 3.36 - 3.39 give

$$\begin{pmatrix} p_1 \\ u_1 \\ 0 \\ 0 \end{pmatrix} = \mathcal{A}_{closed} \begin{pmatrix} P_{1+} \\ P_{1-} \\ P_{2+} \\ P_{2-} \end{pmatrix} \tag{3.55}$$

where

$$\mathcal{A}_{closed} = \begin{pmatrix} 1 + \Gamma_1 & 1 + \Gamma_1 & 1 + \Gamma_2 & 1 + \Gamma_2 \\ \frac{1}{Z_1} & \frac{1}{Z_1} & \frac{1}{Z_1} & \frac{1}{Z_1} \\ \frac{1-\gamma_1}{Z_1} & \frac{-(1-\gamma_1)}{Z_1} & \frac{1-\gamma_2}{Z_2} & \frac{-(1-\gamma_2)}{Z_2} \\ \frac{1-\gamma_1}{Z_1} e^{iq_1 l} & \frac{-(1-\gamma_1)}{Z_1} e^{-iq_1 l} & \frac{1-\gamma_2}{Z_2} e^{iq_2 l} & \frac{-(1-\gamma_2)}{Z_2} e^{-iq_2 l} \end{pmatrix} \tag{3.56}$$

And p_2 and u_2 can be expressed in matrix form as

$$\begin{pmatrix} p_2 \\ u_2 \end{pmatrix} = \mathcal{B}_{closed} \begin{pmatrix} P_{1+} \\ P_{1-} \\ P_{2+} \\ P_{2-} \end{pmatrix} \tag{3.57}$$

where

$$\mathcal{B}_{closed} = \begin{pmatrix} (1+\Gamma_1)e^{iq_1 l} & (1+\Gamma_1)e^{-iq_1 l} & (1+\Gamma_2)e^{iq_2 l} & (1+\Gamma_2)e^{-iq_2 l} \\ \frac{e^{iq_1 l}}{Z_1} & \frac{-e^{-iq_1 l}}{Z_1} & \frac{e^{iq_2 l}}{Z_2} & \frac{-e^{-iq_2 l}}{Z_2} \end{pmatrix} \tag{3.58}$$

Combining the matrix equations 3.55 and 3.57 we can then write a matrix equation for the transmission matrix which is:

$$\begin{pmatrix} T_{11} & T_{12} \\ T_{21} & T_{22} \end{pmatrix} = \mathcal{B}_{closed} \left(\mathcal{A}_{closed}\right)^{-1} \begin{pmatrix} 1 & 0 \\ 0 & 1 \\ 0 & 0 \\ 0 & 0 \end{pmatrix} \tag{3.59}$$

where $(\mathcal{A}_{closed})^{-1}$ denotes the matrix inverse of $\mathcal{A}_{closed}$.

The resulting transmission matrix for the porous layer with closed surfaces is:

$$\mathcal{T}_{closed} = \begin{pmatrix} T_{11,closed} & T_{12,closed} \\ T_{21,closed} & T_{22,closed} \end{pmatrix} \tag{3.60}$$

where

$$T_{11,closed} = \frac{\epsilon_1 \cos(q_1 l)\sin(q_2 l) - \epsilon_2 \sin(q_1 l)\cos(q_2 l)}{\epsilon_1 \sin(q_2 l) - \epsilon_2 \sin(q_1 l)} \tag{3.61}$$

$$T_{12,closed} = i\left[\frac{(\epsilon_1^2 + \epsilon_2^2)\sin(q_1 l)\sin(q_2 l) - 2\epsilon_1\epsilon_2(1 - \cos(q_1 l)\cos(q_2 l))}{(\gamma_1 - \gamma_2)(\epsilon_1 \sin(q_2 l) - \epsilon_2 \sin(q_1 l))}\right] \tag{3.62}$$

$$T_{21,closed} = i\left[\frac{(\gamma_1 - \gamma_2)\sin(q_1 l)\sin(q_2 l)}{\epsilon_1 \sin(q_2 l) - \epsilon_2 \sin(q_1 l)}\right] \tag{3.63}$$

$$T_{22,closed} = \frac{\epsilon_1 \cos(q_1 l)\sin(q_2 l) - \epsilon_2 \sin(q_1 l)\cos(q_2 l)}{\epsilon_1 \sin(q_2 l) - \epsilon_2 \sin(q_1 l)} \tag{3.64}$$

where

$$\epsilon_1 \equiv \rho c Z_1 (1+\Gamma_1)(1-\gamma_2) \ , \ \epsilon_2 \equiv \rho c Z_2 (1+\Gamma_2)(1-\gamma_1) \qquad (3.65)$$

Chapter 4

Departures from the Basic Model

We now consider three models, each of which represents some increase in complexity compared to the finite layer discussed in chapter 3. First we relax the assumption that the porous medium is isotropic, and consider a finite layer backed by a rigid wall which has different flow resistances and induced mass factors in the directions normal and parallel to the free surface of the layer. Second, we compute the absorption coefficient for a multiple layer attenuator, consisting of open flexible porous layers separated by air gaps, backed by a rigid wall. Here the method of characterizing wave propagation in periodic structures due to Brillouin [16] is used to simplify the calculation. Lastly, the consequences of mean fluid flow for sound propagation in a porous material in bulk are discussed, and the equilibrium problem for the flexible porous material is solved for the case of constant equilibrium fluid density.

4.1 Anisotropic Flexible Porous Layer

The motivation for studying the anisotropic porous layer is the following. In some cases, laboratory measurements are made of the flow resistance of such a layer in the direction normal to the free surface. This flow resistance is then used to predict the performance of such a layer backed by a rigid wall in a reverberation room where diffuse sound conditions are assumed. Only the normal flow resistance (which we call r_x) is used to predict the angle averaged (diffuse field) absorption coefficient; this

assumes that the layer is one of local reaction and that the wave speed in the normal direction is much greater than the wave speed in the parallel direction. In this case, the surface admittance of the layer is independent of angle of incidence, and a relation between the normal incidence and angle averaged absorption coefficient based on this approximation is used.

For sufficiently low frequencies the refracted wave in the porous layer travels almost normal to the surface for all angles of incidence. In this case, the assumption of local reaction will provide accurate results, and knowledge of the flow resistance normal to the surface is adequate to determine the angle averaged absorption coefficient.

For higher frequencies, as we shall show, the refracted wave can have a significant component parallel to the surface. This means that the layer must be treated as non-locally reacting, and the relation between the normal incidence and angle averaged absorption coefficients must assume a surface admittance which depends on angle of incidence. In particular, the flow resistance parallel to the layer's surface must be known to accurately predict the diffuse field absorption coefficient.

For this reason, we try to better understand the circumstances under which the assumption of local reaction is invalid and, given this, how anisotropy of the layer may lead to poor predictions of acoustic performance of the flexible porous material.

4.1.1 Changes to the Basic Theory given Anisotropy

An analysis, similar to that used for the isotropic layer found in chapters 2 and 3, is repeated with the new assumptions that both the flow resistance and the induced mass factor in the $\hat{x}$ and $\hat{y}$ directions can be different; we use the same $\hat{x}$ and $\hat{y}$ coordinates as in chapter 2. We define the flow resistance and induced mass factor in the $\hat{x}$ direction as r_x and G_x, and in the $\hat{y}$ direction, r_y and G_y.

The four mass and momentum balance amplitude equations 2.40 - 2.43 must now be replaced by two new amplitude equations for mass balance

$$i(H'/H)\omega K p' - i\omega\kappa p = -iq_x u_x - iq_y u_y \tag{4.1}$$

$$-i\omega Kp' - i\omega\kappa' p = -iq_x u'_x - iq_y u'_y \tag{4.2}$$

and four new amplitude equations for momentum balance

$$-i\omega\tilde{\rho}_x u_x = H\tilde{r}_x u'_x - iq_x p \tag{4.3}$$

$$-i\omega\tilde{\rho}_y u_y = H\tilde{r}_y u'_y - iq_y p \tag{4.4}$$

$$-i\omega\tilde{M}_x u'_x = H\tilde{r}_x u_x - iq_x p' \tag{4.5}$$

$$-i\omega\tilde{M}_y u'_y = H\tilde{r}_y u_y - iq_y p' \tag{4.6}$$

where we have defined

$$\tilde{r}_x \equiv r_x - i\omega G_x \rho \ \ , \tilde{r}_y \equiv r_y - i\omega G_y \rho \tag{4.7}$$

$$\tilde{\rho}_x \equiv H\rho(1 + \frac{i\tilde{r}_x}{\omega\rho}) \ \ , \tilde{\rho}_y \equiv H\rho(1 + \frac{i\tilde{r}_y}{\omega\rho}) \tag{4.8}$$

$$\tilde{M}_x \equiv M(1 + \frac{iH\tilde{r}_x}{\omega M}) \ \ , \tilde{M}_y \equiv M(1 + \frac{iH\tilde{r}_y}{\omega M}) \tag{4.9}$$

From these we obtain two expressions for the ratio between p' and p

$$\Gamma_I = \frac{p'}{p} = \frac{1}{\delta_x} \frac{Q_x^2 + \Lambda Q_y^2 - \frac{\kappa}{\kappa_0}\mu_x}{Q_x^2 + (\frac{\tilde{r}_y \tilde{M}_x}{\tilde{r}_x \tilde{M}_y})\Lambda Q_y^2 - (\frac{H'}{\mu_x H})\frac{K}{\kappa_0}\mu_x} \tag{4.10}$$

or

$$\Gamma_{II} = \frac{p'}{p} = \frac{\delta_x \tilde{M}_x}{\tilde{\rho}_x} \frac{Q_x^2 + (\frac{\tilde{r}_y \tilde{M}_x}{\tilde{r}_x \tilde{M}_y})\Lambda Q_y^2 + \frac{\kappa'}{\kappa_0}\frac{\mu_x}{\delta_x}}{Q_x^2 + (\frac{\tilde{\rho}_y \tilde{M}_x}{\tilde{\rho}_x \tilde{M}_y})\Lambda Q_y^2 - (\frac{\tilde{M}_x}{\tilde{\rho}_x})\frac{K}{\kappa_0}\mu_x} \tag{4.11}$$

where

$$\delta_x \equiv \frac{H\tilde{r}_x}{i\omega\tilde{M}_x} \tag{4.12}$$

$$\mu_x \equiv \frac{\tilde{\rho}_x}{\rho} - \delta_x^2 \frac{\tilde{M}_x}{\rho} \tag{4.13}$$

$$\Lambda \equiv \frac{\tilde{\rho}_x + (\frac{H}{\omega})^2(\frac{f_x^2}{\tilde{M}_x})}{\tilde{\rho}_y + (\frac{H}{\omega})^2(\frac{f_y^2}{\tilde{M}_y})} = \frac{\mu_x}{\mu_y} \tag{4.14}$$

By setting $\Gamma_I = \Gamma_{II}$ and substituting $Q_y^2 = \sin^2\phi$, we obtain two solutions for the $\hat{x}$ component of the propagation constant Q_x where, as in chapter 2 with the isotropic case, the two solutions correspond to the two modes of wave propagation in the flexible porous material.

The isotropic case corresponds to $\Lambda = 1$. It is interesting to compare how Q_x is determined for the isotropic versus the anisotropic case. For both cases, the incident wave with angle of incidence ϕ and open-air wavenumber k_0 determines the trace wavenumber and therefore Q_y in the porous medium. For the isotropic case, the dispersion relation then gives Q which is independent of direction of propagation in the medium, and Q_x is obtained using $Q_x = \sqrt{Q^2 - Q_y^2}$. For the anisotropic case, the dispersion relation gives Q_x in terms of Q_y and the propagation constant in the medium in dependent on the direction of propagation.

Another change from the isotropic case is the ratio of the velocities for a given mode, necessary for computation of the absorption coefficient. From the amplitude equations we obtain

$$\gamma_{x;1,2} \equiv \frac{u_x'}{u_x} = \frac{H\tilde{r}_x - i\omega\tilde{\rho}_x\Gamma_{1,2}}{-i\omega\tilde{M}_x + H\tilde{r}_x\Gamma_{1,2}} \tag{4.15}$$

With these results we proceed in a manner analogous to that used for the isotropic layer in chapter 3 and obtain normal incidence and angle averaged absorption coefficients for the open layer.

4.1.2 Consequences of Anisotropy

Figure 4-1 shows a comparison of an anisotropic and an isotropic layer. For each we have plotted the angle averaged absorption coefficient, then on the right is shown the refraction angle in the anisotropic layer of a plane wave which has angle of incidence of $\phi = 60$ degrees.

This case has a refracted angle which is greater than 40 degrees for most of the frequency range, and a corresponding significant disagreement between the absorption coefficients for the two material types.

Figure 4-2 shows the same comparison for an isotropic and anisotropic material with $r_x = 10\rho c/inch$, ten times the r_x value used previously. Here we see the increase in flow resistance has resulted in smaller refraction angles and a better agreement between the absorption coefficient curves for the two cases.

An interesting feature of the absorption coefficient for the isotropic material shown in Figure 4-2 is the significant disagreement with the anisotropic curve at 600 Hz. This is a result of a structural resonance in the material which, by reducing the relative motion between the fluid and structure, reduces the effective flow resistance and increases the disagreement between the isotropic and anisotropic cases.

This means that even in cases where a high flow resistance allows one to treat the anisotropic material as isotropic, the flexibility of the material, and in particular structural resonances, can result in poor predictions at certain frequencies.

Figure 4-1: Angle Averaged Absorption Coefficient for Anisotropic and Isotropic Layer, and Refraction Angles for both modes in Anisotropic layer for angle of incidence 60 degrees; all with $K = (1, 0.1), H = 0.95, G = (0.5, 0.1 \text{ or } 0.5), d = 1in., H'\rho' = 2lbs/ft^3, r = (1, 0.1 \text{ or } 1)\rho c$

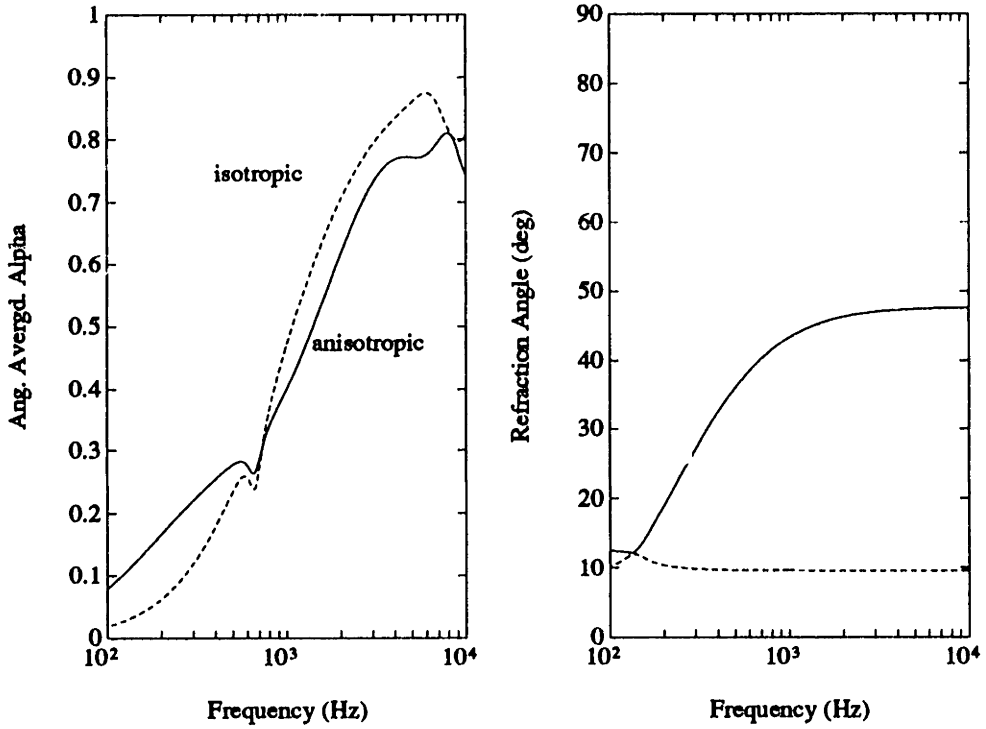

Figure 4-2: Angle Averaged Absorption Coefficient for Anisotropic and Isotropic Layer, and Refraction Angles for both modes in Anisotropic layer for angle of incidence 60 degrees; all with $K = (1, 0.1), H = 0.95, G = (0.5, 0.1 \text{ or } 0.5), d = 1in., H'\rho' = 2lbs/ft^3, r = (10, 1 \text{ or } 10)\rho c$

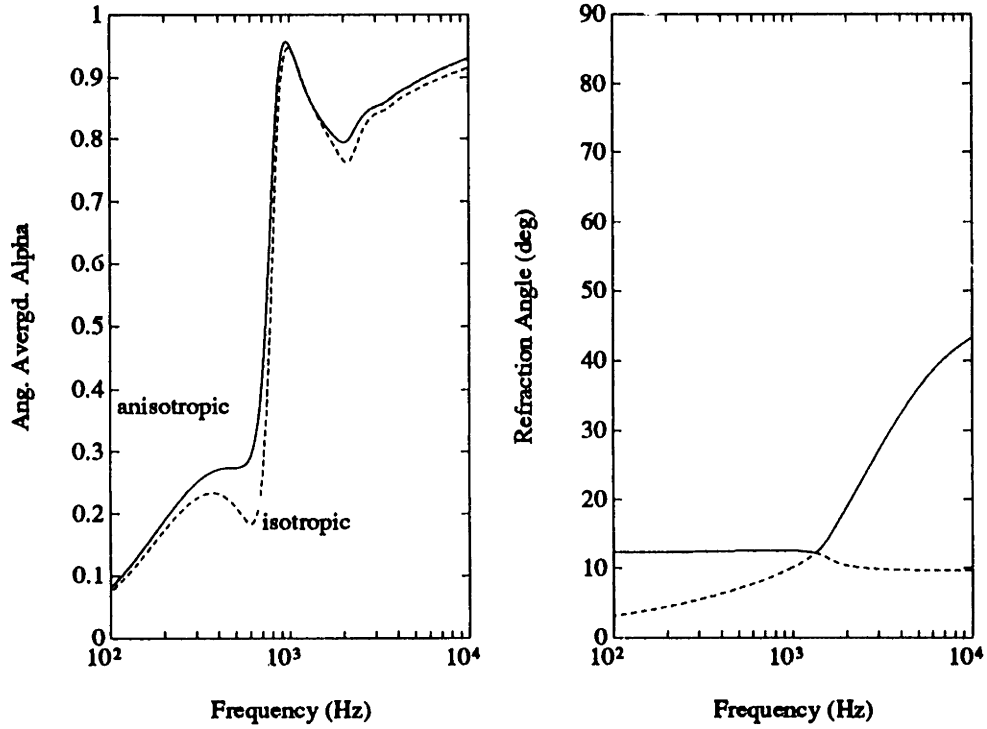

4.2 Periodic Structures

In some cases, acoustical attenuators consist of several porous layers separated by air gaps. A principal advantage of such a geometry is that the layer and air gap thicknesses can be 'tuned' so that the resulting absorption coefficient will be particularly high at certain frequencies or very uniform over a broad frequency range.

Using the transmission matrix for the open flexible layer derived in chapter 3 and the analytical methods for treating wave propagation in periodic structures provided by Brillouin [16] , we consider the problem of an attenuator consisting of a number of porous layers separated by air gaps. As with the finite layer studied in chapter 3, we back the attenuator with a rigid wall at $x = 0$. We consider the case of normal incidence for an attenuator consisting of N cells, each cell consisting of a porous layer of thickness d_l and an air gap of thickness d_a. The entire device extends from $x = -N(d_l + d_a)$ to $x = 0$ where it is terminated by a rigid wall. This configuration is shown in figure 4-3.

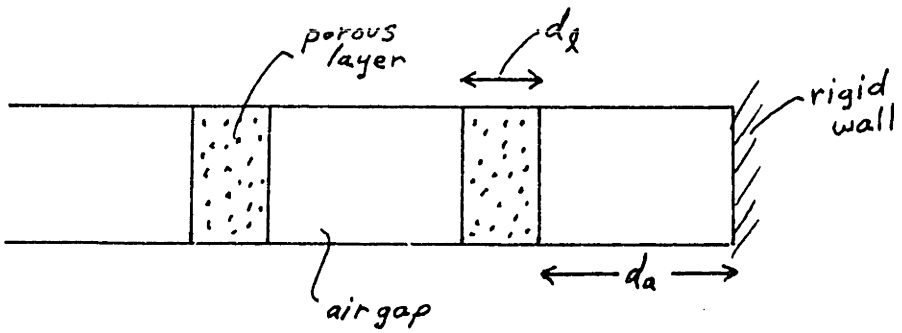

Figure 4-3: Geometry of the Multiple Layer Attenuator

4.2.1 The Multiple Layer Attenuator

The transmission matrix for a given cell of the attenuator can be used to relate the acoustic pressures and velocities on its two boundaries. Across a single cell we have

$$\begin{pmatrix} p_2 \\ u_2 \end{pmatrix} = \begin{pmatrix} C_{11} & C_{12} \\ C_{21} & C_{22} \end{pmatrix} \begin{pmatrix} p_1 \\ u_1 \end{pmatrix} \tag{4.16}$$

with

$$C = \begin{pmatrix} \cos(k_0 d_a) & i\rho c \sin(k_0 d_a) \\ (i/\rho c)\sin(k_0 d_a) & \cos(k_0 d_a) \end{pmatrix} \begin{pmatrix} T_{11} & T_{12} \\ T_{21} & T_{22} \end{pmatrix} \tag{4.17}$$

where the matrix **T** will be either the open or the closed transmission matrix provided in equations 3.47 - 3.51 or 3.60 - 3.64; in this study we will assume layers of the open type. In either case the layer thickness l in those expressions is set equal to d_l.

We associate a complex wavenumber S with the attenuator using

$$p_2 = \exp^{iS(d_a+d_l)} p_1 \ , \ u_2 = \exp^{iS(d_a+d_l)} u_1 \tag{4.18}$$

which means

$$e^{iS(d_a+d_l)} = \frac{C_{11}+C_{22}}{2} + \sqrt{\left(\frac{C_{11}+C_{22}}{2}\right)^2 - 1} \tag{4.19}$$

and define wave impedances Z_+ and Z_- (for waves propagating in the $+\hat{x}$ and $-\hat{x}$ directions respectively) using the two roots of the equation

$$Z_{+,-} = \left(\frac{p_1}{\rho c u_1}\right)_{+,-} = \left(\frac{p_2}{\rho c u_2}\right)_{+,-} \tag{4.20}$$

so

$$Z_{+,-} = \frac{1}{\rho c C_{21}} \left[\frac{C_{11}-C_{22}}{2} \pm \sqrt{\left(\frac{C_{11}+C_{22}}{2}\right)^2 - 1}\right] \tag{4.21}$$

In this derivation we have used the fact that, for a passive acoustic transmission element characterized by the transmission matrix **C** we have

$$C_{11}C_{22} - C_{12}C_{21} = 1 \tag{4.22}$$

The characteristic normal input admittance for the attenuator is

$$\eta(x=-d_t)=\rho c\frac{u(x=-d_t)}{p(x=-d_t)}=\frac{e^{-iSd_t}-e^{iSd_t}}{Z_+e^{-iSd_t}-Z_-e^{iSd_t}} \tag{4.23}$$

where

$$d_t=N(d_l+d_a) \tag{4.24}$$

With these results we compute the absorption coefficient for an attenuator of the open layer type and attempt to identify the specific consequences of layer flexibility for such a device.

4.2.2 Absorption Coefficient

We first consider how changing the size of the air gap between the open flexible porous layers affects the absorption coefficient of the attenuator. To do this we make the thickness of the porous layers very small, $d_l = 0.25$ in. In figure 4-4, four different cases are shown with progressively larger air gaps ranging from 1 to 8 inches. Dips in the absorption coefficient occur when the air gap equals an integral number of half wavelengths ($d_a = (2n\pi c)/\omega$; $n \rightarrow$ positive integer). This is because a fluid layer resonance occurs when the velocity nodes coincide with the locations of the porous layers, and the corresponding low fluid velocity in the layers results in a reduction in losses from the relative motion of the fluid and structure. This effect produces the 'comb-like' features seen at the higher frequencies, above 2000 Hz for the case $d_a = 2$ in. and above 400 Hz for the $d_a = 8$ in. case. At lower frequencies a sequence of peaks and dips is evident in all the plots of this section. These features are due to fluid layer resonances which span several air gaps. They are weaker than their high frequency counterparts because they must permit layers to coincide with non zero portions of the velocity resonance in the fluid and can be seen to extend progressively lower in frequency as the total length of the attenuator d_t is increased in the four cases of figure 4-4.

In order to focus on the effects of layer flexibility, we consider four cases with

Figure 4-4: Absorption Coefficients for Open Layer Multiple Baffle Attenuator. With $d_{air} = 1, 2, 4, 8in.; r = 10\rho c, H = 0.95, G = 0.5, K/\kappa_0 = (1, 0.1), d_{layer} = 0.25in., N = 8, H'\rho' = 2lbs/ft^3$

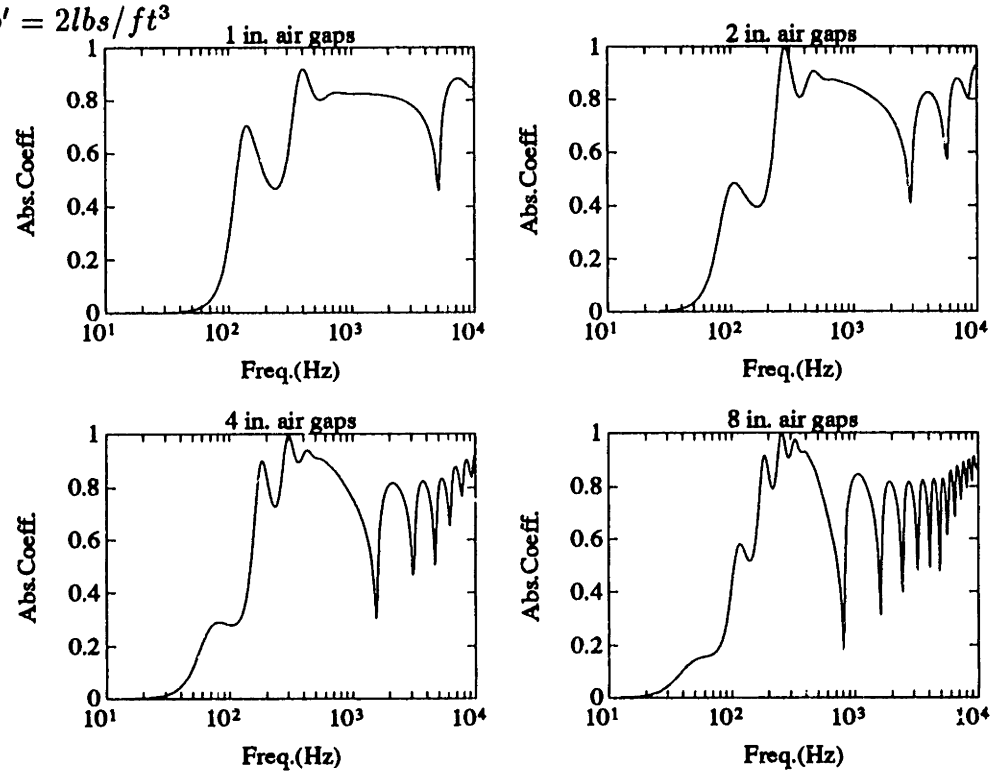

layer thickness $d_l = 1$ in. and air gap $d_a = 4$ in. This result, for a progression of increasing structure compressibilities, is shown in figure 4-5. The thicker layer prevents the strong fluid resonances seen in the previous cases; although the low frequency, multiple gap fluid resonances persist, they do not concern us here. The interesting result shown here is the appearance of a structural resonance in the layers of the attenuator as a consequence of their flexibility. First appearing around 2000 Hz for the $K/\kappa_0 = (0.5, 0.05)$ case, the resonance moves downward in frequency as the compressibility is increased. A resonance of this type corresponds to a structure wave whose half wavelength equals the thickness of the layer d_l.

We have seen that for an attenuator consisting of flexible porous layers, there can be significant impact on the absorption coefficient due to both fluid and structural resonances, an effect shared by the finite layer backed by the rigid wall. Lastly we consider a case where these two resonances occur at similar frequencies, this is shown in figure 4-6. Here a slow variation of the layer's thickness over the four cases shown causes the structural resonance to move through the frequencies of the fluid resonance.

Figure 4-5: Absorption Coefficients for Open Layer Multiple Baffle Attenuator. With $K/\kappa_0 = rigid, (0.5, 0.05), (1, 0.1), (2, 0.2); r = 10\rho c, H = 0.95, G = 0.5, d_{air} = 4in., d_{layer} = 1in., N = 4, H'\rho' = 2lbs/ft^3$

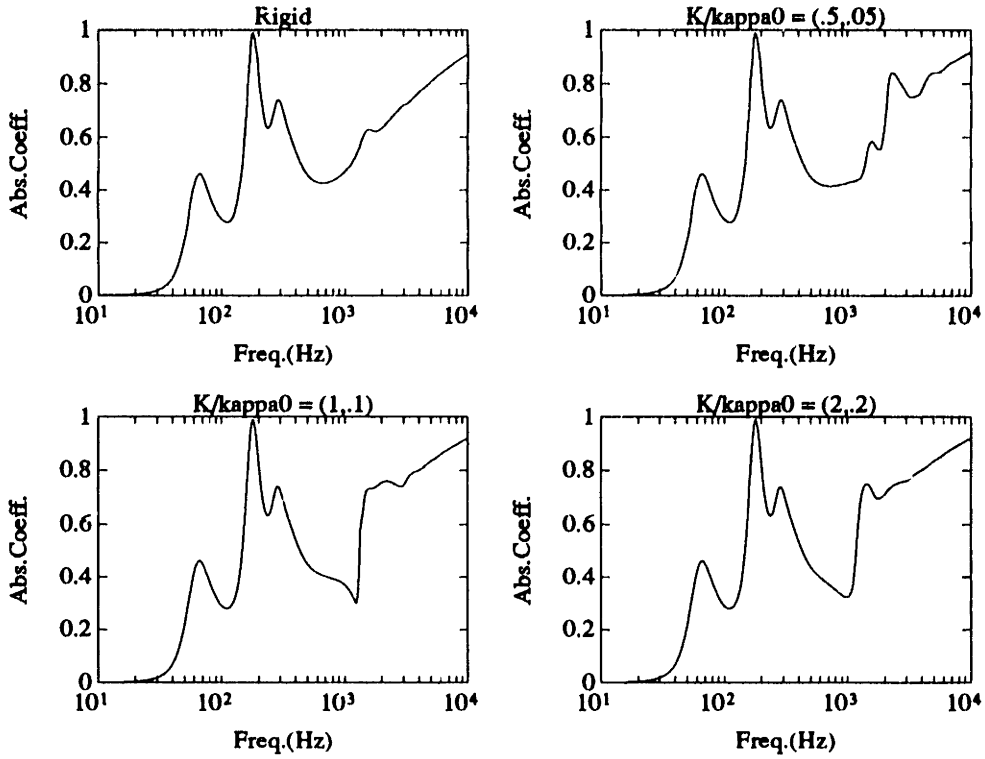

Figure 4-6: Absorption Coefficients for Open Layer Multiple Baffle Attenuator. With $d_{layer} = 0.5, 0.6, 0.7, 0.8in.; r = 10\rho c, H = 0.95, G = 0.5, K/\kappa_0 = (1, 0.1), d_{air} = 6in., N = 4, H'\rho' = 2lbs/ft^3$

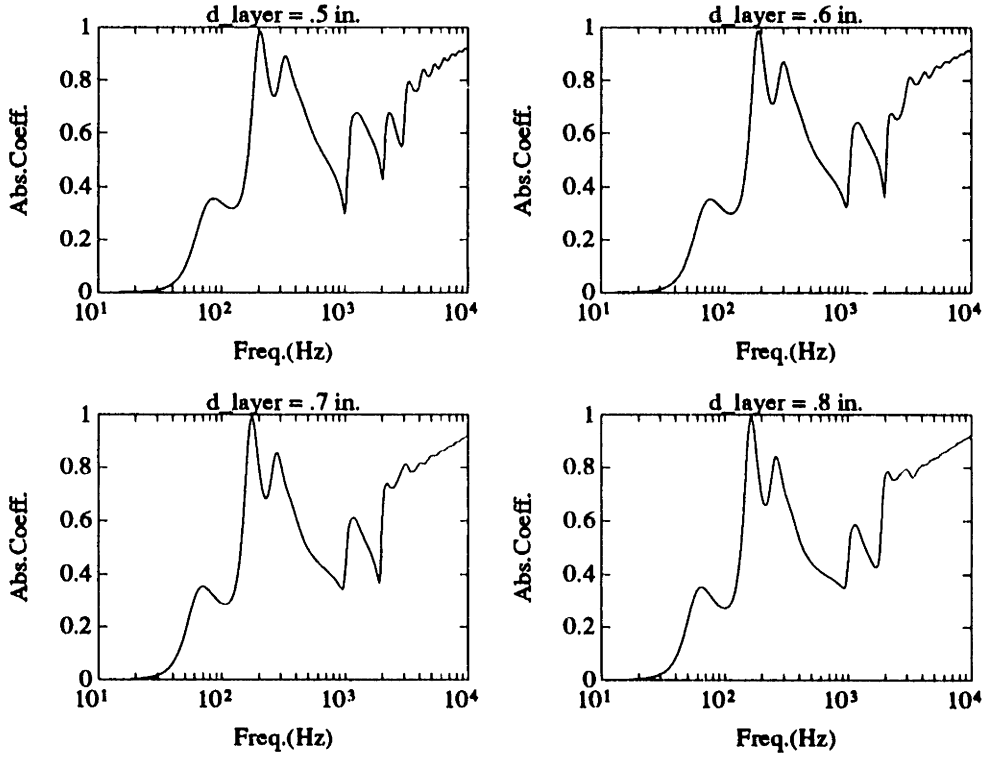

The consequence of this overlap is an absorption coefficient which is the result of both effects. In some cases the result is a smoothing of the absorption coefficient curve; in others the dips are deepened.

4.3 Mean Flow

In some cases a porous layer may cover the cross section of an air duct or the exit of such a duct into a room. The absorption characteristics of such a layer may then be altered due to the presence of a zeroth order, time independent fluid flow or 'mean' flow.

We focus here first on the problem of the rigid porous material in bulk with a mean flow present. In particular we will show the basic influence of the presence of mean flow on the phase speed and attenuation of plane waves traveling with and against the flow. Then we solve the equilibrium problem for the *flexible* porous material and show that the mean flow may induce, among other things, a spatial gradient of the equilibrium porosity.

4.3.1 The Rigid Porous Medium with Mean Flow

We start by deriving the general form of the equations of mass and momentum balance for the rigid porous material. Velocity, pressure, and density are initially assumed to consist of a zeroth order equilibrium value which has space dependence, and a first order acoustic part which depends on space and time. Using the subscript 't' to denote the total fields we have

$$\begin{aligned} H_t &= H \\ U_t &= U(x) + u(x,t) \\ P_t &= P(x) + p(x,t) \\ \rho_t &= \rho(x) + \delta(x,t) \end{aligned} \tag{4.25}$$

The mass balance relation

$$\frac{\partial H\rho_t}{\partial t} + \frac{\partial H\rho_t U_t}{\partial x} = 0 \tag{4.26}$$

becomes

$$\left(\frac{\partial}{\partial t} + U_t\frac{\partial}{\partial x}\right)\rho_t = -\rho_t\frac{\partial U_t}{\partial x} \tag{4.27}$$

and the momentum balance relation

$$\frac{\partial H\rho_t U_t}{\partial t} + \frac{\partial H\rho_t U_t^2}{\partial x} = -\frac{\partial P_t}{\partial x} - HrU_t \tag{4.28}$$

is written as

$$H\rho_t\left(\frac{\partial}{\partial t} + U_t\frac{\partial}{\partial x}\right)U_t = -\frac{\partial P_t}{\partial x} - HrU_t \tag{4.29}$$

We next focus on the equilibrium problem by assuming all field quantities to be time independent. The above equations for mass and momentum balance become

$$U\frac{\partial}{\partial x}\rho = -\rho\frac{\partial U}{\partial x} \tag{4.30}$$

and

$$H\rho U\frac{\partial}{\partial x}U = -\frac{\partial P}{\partial x} - HrU \tag{4.31}$$

The above two equations, combined with a compressibility definition for the fluid could, for example, predict 'choked' flow under certain conditions. In general, these equations lead to a rather complicated spatial dependence for the equilibrium field variables. For our purposes here we assume that the equilibrium fluid density is constant. This assumption gives

$$\frac{\partial U}{\partial x} = 0 \tag{4.32}$$

$$
\begin{aligned}
\Rightarrow \quad U &\neq U(x) \\
\Rightarrow \quad \frac{\partial P}{\partial x} &= -HrU \\
\Rightarrow \quad P(x) &= -HrU(x - x_0) + P(x_0)
\end{aligned}
$$

Given these equilibrium solutions we now write for the total values of the field variables, with plane wave solutions for the acoustic parts,

$$
\begin{aligned}
H_t &= H \\
U_t &= U + \mathrm{Re}[u(q,\omega)e^{i(qx-\omega t)}] \\
P_t &= P(x_0) - HrU(x - x_0) + \mathrm{Re}[p(q,\omega)e^{i(qx-\omega t)}] \\
\rho_t &= \rho + \mathrm{Re}[\delta(q,\omega)e^{i(qx-\omega t)}]
\end{aligned}
\tag{4.33}
$$

These expressions for the field variables can be substituted into the mass and momentum balance equations 4.27 and 4.29 to give

$$
(\omega - qU)\kappa\, p(q,\omega) = q\, u(q,\omega) \tag{4.34}
$$

where we used the fluid compressibility $\kappa = (1/\rho)(\partial\rho_t/\partial P_t)$, and

$$
H\rho(\omega + i\frac{r}{\rho} - qU)\, u(q,\omega) = q\, p(q,\omega) \tag{4.35}
$$

We can use these results to obtain a dispersion relation, propagation constants, and plane wave impedances. Writing the ratio of p and u we have the dispersion relation

$$
\frac{p(q,\omega)}{u(q,\omega)} = \frac{q}{\kappa(\omega - qU)} = \frac{H\rho(\omega + i(r/\rho) - qU)}{q} \tag{4.36}
$$

and the propagation constants

$$
q^2 = H(\frac{\omega}{c} - q\frac{U}{c})(\frac{\omega}{c} + i\frac{r}{\rho c} - q\frac{U}{c}) \tag{4.37}
$$

which, by defining

$$c = \frac{1}{\sqrt{\rho\kappa}} \ , \ M \equiv \frac{U}{c} \ , \ R \equiv \frac{r}{\rho\omega} \tag{4.38}$$

allows us to write, for the normalized propagation constants $Q = q/k_0$,

$$\begin{aligned} Q^2 &= H(1-MQ)((1+iR)-MQ) \\ &\Rightarrow (1-HM^2)Q^2 + HM(2+iR)Q - H(1+iR) = 0 \end{aligned} \tag{4.39}$$

which gives, for the normalized propagation constants Q_+ and Q_-, in the direction with the flow and against the flow respectively

$$Q_\pm = \frac{-HM(2+iR) \pm \sqrt{4H(1+iR) - (HMR)^2}}{2(1-HM^2)} \tag{4.40}$$

Using the assumption that $M \ll 1$, we write for an approximate value of $Q_\pm$

$$Q_\pm = -HM(1+iR/2) \pm \sqrt{H(1+iR)} \tag{4.41}$$

If we take $M = 0$ we recover the familiar, symmetric pair or propagation constants for the rigid porous material without mean flow (see appendix A)

$$Q_\pm = \pm\sqrt{H(1+i\frac{r}{\rho\omega})} \tag{4.42}$$

If we further consider $R = 0$ and $H = 1$, we get $Q_\pm = 1/(M \pm 1)$ which gives $c'_\pm = U \pm c$, the expected result that the phase speed of a open air wave includes the parallel component of the flow velocity.

4.3.2 The Equilibrium Problem for the Flexible Material

We now consider the equilibrium problem for a porous medium when its flexibility is accounted for. We will again assume that the equilibrium density of the fluid is constant, but now include the potential spatial dependence of the porosity and

pressure in the structure. We also assume that the fractional change in the equilibrium fluid pressure (and consequently the Mach number, as we shall show) is small.

For this problem, we take as field variables the equilibrium porosity, pressure in the fluid and structure, and the mean flow velocity, all of which will be assumed to have spatial dependence. By definition, none of these zeroth order equilibrium field variables have time dependence.

The field variables are

$U(x) \rightarrow$ Mean flow velocity

$P(x) \rightarrow$ Equilibrium fluid pressure

$P'(x) \rightarrow$ Equilibrium structure pressure

$H(x) \rightarrow$ Equilibrium porosity

$H'(x) = 1 - H(x)$

and

$\rho \rightarrow$ Equilibrium porosity ($\rho \neq \rho(x)$)

The mass balance for the fluid is

$$\frac{\partial H\rho U}{\partial x} = 0 \tag{4.43}$$

which, with ρ being constant leads to

$$H\frac{\partial U}{\partial x} + U\frac{\partial H}{\partial x} = 0 \tag{4.44}$$

The mass balance for the structure tells us nothing since the zeroth order velocity of the structure is zero.

Momentum balance for the fluid looks like

$$\frac{\partial H\rho U^2}{\partial x} = -\frac{\partial P}{\partial x} - HrU \tag{4.45}$$

which, after combining with 4.44 gives

$$H\rho U\frac{\partial U}{\partial x} = -\frac{\partial P}{\partial x} - HrU \tag{4.46}$$

For the structure the momentum balance looks like

$$\frac{\partial H'\rho' U'^2}{\partial x} = -\frac{\partial P'}{\partial x} + HrU \tag{4.47}$$

and since $U' = 0$ this is

$$HrU = \frac{\partial P'}{\partial x} \tag{4.48}$$

Also, using the compressibility

$$K = \frac{1}{H'}\frac{\partial H'}{\partial p'} \tag{4.49}$$

we have

$$\frac{\partial H'}{\partial x} = KH'\frac{\partial P'}{\partial x} \tag{4.50}$$

and lastly, the porosities are related by

$$H + H' = 1 \quad \Rightarrow \quad \frac{\partial H}{\partial x} + \frac{\partial H'}{\partial x} = 0 \tag{4.51}$$

These equations 4.44, 4.46, 4.48, 4.50, and 4.51 can be combined to give

$$\frac{\partial U}{\partial x} = H'KrU^2 \tag{4.52}$$

$$\frac{\partial P}{\partial x} = -HrU(1 - H'K\rho U^2) \tag{4.53}$$

$$\frac{\partial P'}{\partial x} = HrU \tag{4.54}$$

$$\frac{\partial H}{\partial x} = -HH'KrU \tag{4.55}$$

$$\frac{\partial H'}{\partial x} = HH'KrU \tag{4.56}$$

We pause for a moment to comment on the consequences of our assumption that the fractional change of the equilibrium pressure in the fluid is small. This fractional change can be written as

$$\frac{\triangle P}{P} \approx \frac{HrU(\triangle X)}{P} \approx \frac{HrU(\triangle X)}{\rho c^2} = \frac{Hr(\triangle X)}{\rho c} M \tag{4.57}$$

where $\triangle X$ is the characteristic distance of sound propagation through the porous material, and M is the Mach number of the mean flow. Since, for our purposes, we are assuming $Hr(\triangle X)/\rho c \approx 1$, we have

$$\frac{\triangle P}{P} \approx M \tag{4.58}$$

Therefore our assumption of a small fractional change of the equilibrium fluid pressure corresponds to $M \ll 1$.

In the above equation 4.53, the second term is of order M^2 and will be dropped. The U^2 term in equation 4.52 however, can be shown to be of order M and will be kept.

The equations can be easily solved by noting that the product HU is constant as specified by equation 4.44. If we define this product to be $\tilde{U} \equiv HU$, and refer to value of the field variables at $x = 0$ with the subscript 0, we have for the solutions

$$U(x) = \tilde{U}\left[1 - (1 - H_0)e^{x/\tilde{x}}\right]^{-1} \tag{4.59}$$

$$P(x) = P_0 - r\tilde{U}x \tag{4.60}$$

$$P'(x) = P'_0 + r\tilde{U}x \tag{4.61}$$

$$H(x) = (H_0 - 1)e^{x/\tilde{x}} + 1 \tag{4.62}$$

$$H'(x) = H'_0 e^{x/\tilde{x}} \tag{4.63}$$

where the characteristic distance in the layer is

$$\tilde{x} = \frac{1}{Kr\tilde{U}} \tag{4.64}$$

The exponential terms in equations 4.62 and 4.63 will never get very large because in this model we are assuming $x < \tilde{x}$.

A very interesting feature of these solutions is that they predict a spatial gradient of the equilibrium porosity in such a manner that the wave impedance will increase steadily in the direction of the mean flow. This effect may provide some interesting opportunities to create a graded impedance so as to enhance the absorptive performance of a flexible porous material.

The complete solution of the acoustic problem in the flexible porous medium is extremely complicated because, as we saw with the corresponding rigid problem, the local speed of sound varies with position in the layer. It may be possible, using techniques similar to the WKB approximation, to make some headway by assuming that this sound speed is a weak function of position. The flexible case, however, is further complicated by the fact that two modes of wave motion exist in two coupled media, with different spatial dependencies of their equilibrium properties.

Chapter 5

Reflection of Shock Waves

5.1 Introduction

Experimental measurements of the reflection of shock waves from flexible porous materials were made by Ingard in 1982 [14]. A 2 meter shock tube was employed with a driving section at one end and a changeable termination section at the other; figure 5-1 shows this configuration. This termination was prepared with an open surface porous plug which covered the cross section of the tube, was 2, 4 or 8 inches in length, and was backed by a rigid plate. Shock pulses were initiated from the driving end, recorded as they passed a pressure transducer half way down the tube (approximately 1 meter from the termination), then recorded again after reflection from the termination. The maximal deformation of the porous plug as a result of the reflection was measured by allowing an ink saturated edge of the layer to leave a permanent record of its compression on a small dowel placed through it, coaxially with the shock tube. A much more complete discussion of the experimental apparatus and techniques can be found in [14].

The experimental data shown on the following pages consist of a pressure trace obtained from the pressure transducer in the shock tube, a frequency spectrum of a typical incident shock wave, and a compilation of measured front reflection coefficients and maximum fractional deformations of the porous layer as a function of the incident shock's peak overpressure.

Figure 5-1: Shock Tube Experimental Configuration

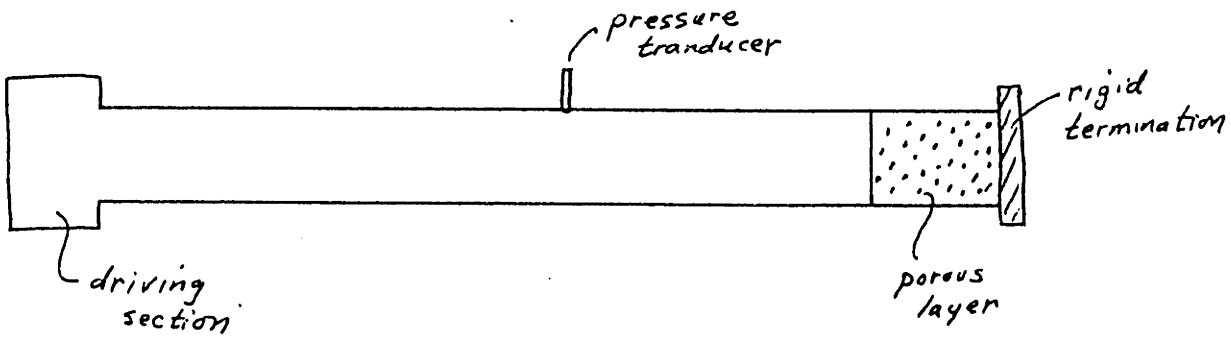

These results indicate that the role of the flexibility of the porous material and the zeroth order motion of the layer must be taken into consideration to accurately predict reflection coefficients for such a material.

Not only does the layer exhibit zeroth order motion and compression during the reflection, but the fluid in the pores and the free surface boundary does as well. In addition, the propagation of the shock through the shock tube and the porous layer is non-linear. This means that a complete model of the problem would require a computational, numerical model which, while offering significant predictive power, would probably obscure many of the central physical mechanisms responsible for the dependence of the reflection coefficient and maximum deformation on the incident shock's peak pressure. Such a numerical study is left for the future and referred to again in chapter 7.

The quasi-linear model presented here treats the shock waves as linear pulses but accounts for the gross (zeroth order) motion of the layer by including its kinetic energy and momentum in the conservation equations. The objective is to construct a simple theory which predicts the general dependence of the front reflection coefficient and maximal deformation on the incident shock's pressure, yet at the same time provides insight into the physical mechanisms responsible for this dependence. A more comprehensive model of the type provided here might offer considerable predictive value without requiring cumbersome numerical techniques.

5.2 Characteristic Times of the Problem

It is useful at the outset to estimate the characteristic times of the problem, namely the time during which the shock is reflected from the front surface, the time of the round trip of the transmitted pulse through the porous layer, and the time required for the layer to fully deform.

The first characteristic time t_1 is the time over which the incident shock wave is reflected from the front surface of the porous layer. This will be taken to be approximately the temporal length of the shock from its maximum height to half its maximum height. A typical experimental pressure trace of a shock wave and its frequency spectrum are shown in figures 5-2 and 5-3. As can be seen from the pressure trace, $t_1 \approx 1$ mS.

Next we estimate a characteristic time t_2 which corresponds to the round trip travel time of the transmitted portion of the incident shock at the front surface of the layer as it propagates through the layer, reflects off the rigid backing, then propagates out to the front surface of the layer, then propagates through air to the location where the free surface of the layer was originally. This time can be estimated by noting that most of the pressure traces of the reflected shocks show a double peaked form. The first peak results from reflection of the shock from the front of the layer, and the second peak comes from the wave which does the round trip through the layer as described above. We will put these claims on a firmer basis later in this chapter. Considering the time separation of the two peaks in the reflected pulse to then be approximately equal to t_2, we have for the 8 inch layer $t_2 \approx 3$ mS for a 0.3 atm overpressure incident pulse. For thinner layers or stronger pulses t_2 is less than this value; these effects will also be discussed below.

The third time of importance is the time t_3 required for the layer to fully deform. Unfortunately, this time cannot be read directly off the pressure traces as was done to obtain t_1 or t_2. The best we can do, in the context of the model employed here, is to treat the layer as a mass and spring system characterized by an effective mass $\tilde{m}$ and an effective spring constant $\tilde{k}$. The time t_3 would then be one quarter the

Figure 5-2: Overpressure as a function of time, measured at the pressure transducer, showing typical incident and reflected shocks

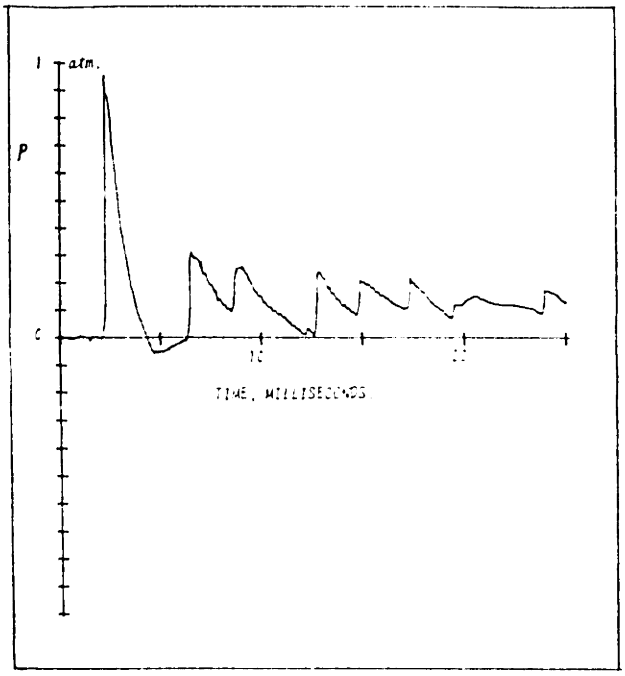

Figure 5-3: Frequency Spectrum of a typical Incident Shock Wave used in the experiments

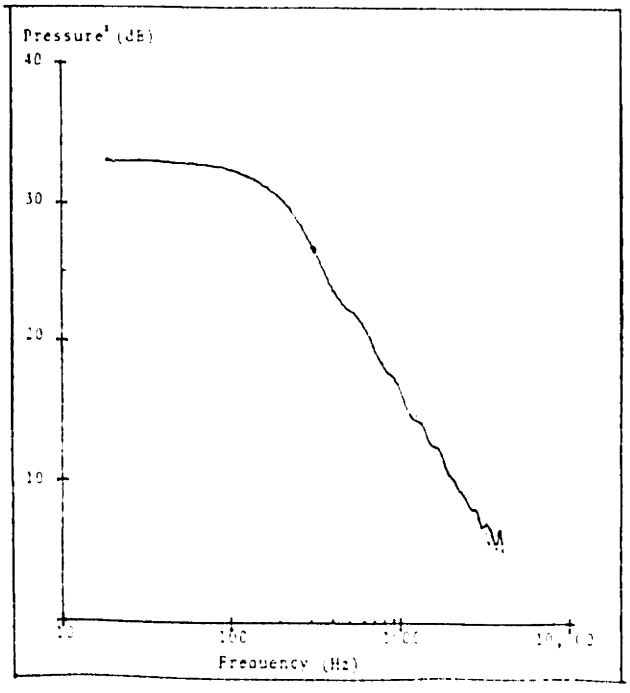

oscillation period of this mass spring system. We will demonstrate more conclusively the appropriateness of such a 'lumped' model in the next section.

Since the motion of the layer consists of free motion of one boundary and no motion of its other boundary (at the rigid termination), the effective mass of the layer can be shown to equal one third of its total mass for purposes of writing the kinetic energy of the layer as $KE_L = (1/2)\tilde{m}U_0^2$ or the natural frequency as $\omega_0^2 = \tilde{k}/\tilde{m}$. (For purposes of writing the total linear momentum of the layer in terms of its velocity at the free surface as $J_L = \tilde{m}'U_0$ we will use an effective mass which is one-half the total mass or $(3/2)\tilde{m}$.) Taking the layer to be of cross sectional area A and undeformed length d, we then have for the effective mass

$$\tilde{m} = \frac{M}{3} = \frac{1}{3}\tilde{\rho}Ad \tag{5.1}$$

The effective spring constant can be related to the effective compressibility of the layer material through

$$\frac{1}{\tilde{k}} = \frac{\partial d}{\partial F} = d\left(\frac{1}{d}\frac{\partial d}{\partial F}\right) = \frac{d}{A}\left(\frac{1}{d}\frac{\partial d}{\partial p}\right) = \frac{d}{A}\tilde{\kappa} \tag{5.2}$$

This gives us

$$t_3 \approx \frac{\pi}{2}\sqrt{\frac{\tilde{m}}{\tilde{k}}} \approx \frac{\pi d}{2\sqrt{3}}\sqrt{\tilde{\rho}\tilde{\kappa}} \approx \frac{\pi}{2\sqrt{3}}\frac{d}{c'} \approx \frac{\pi}{4\sqrt{3}}t_2 \approx \frac{t_2}{2} \approx 1.5\,\mathrm{mS} \tag{5.3}$$

The linear speed of sound in the layer is written here as c'. The fact that the actual propagation speed of the leading edge of a shock in the layer can be considerably greater than the linear speed means, for the stronger incident shocks, that we have under-predicted t_3's value. The quantity $\tilde{\rho}$ is the effective mass density of the layer and $\tilde{\kappa}$ is the effective longitudinal compressibility; both are discussed further in the following section.

The resulting times are

$$t_1 \approx 1\,\mathrm{mS} \; < \; t_3 \approx 1.5\,\mathrm{mS} < \; t_2 \approx 3\,\mathrm{mS} \tag{5.4}$$

We make three observations based on the relative magnitudes of these characteristic times. Since $t_1 < t_3$ we will assume that the free surface boundary does not move appreciably during the period of the reflection of the shock wave from its front surface, although we will allow for some motion to account for the dragging of the layer against the walls of the shock tube.

Secondly, the fact that $t_2 > t_3$ means that the so-called second peak in the reflected shock will be the result of a pulse which propagated through the layer while it was deforming (and deformed) appreciably. As a consequence, our model will attempt to make quantitative estimates of the front reflected pulse height and the maximum deformation of the layer and will not seek to predict the overpressure of the second reflected peak.

Since the time necessary for the transmitted wave to traverse the layer is $t_2/2 \approx 1.5$ mS, which is approximately the same as the reflection time t_1, the gross motion of the layer resulting from the front reflection will involve most of the layer, and in particular the portion with the greatest contribution to the kinetic energy and momentum of the layer as a whole. The errors introduced by this assumption may be significant and are discussed in section 5.5.

5.3 The Incident Shock Wave

We make a number of simplifying assumptions about the shock wave which propagates through the air in the shock tube as well as in the porous layer. We assume that the shock can be modeled as a pulse which is a solution to the linear equation of sound without dissipation, and therefore that the speed of the shock, in the air for example, is the linear speed of sound c. This approximation is clearly not valid for the shocks used here of 1 atm overpressure, since not only will they deform as they propagate, from non-linear effects and dissipation, but they can also have a leading-edge propagation speed which is significantly larger than c. It is our hope, however, that these approximations will not destroy our ability to reproduce the principal features in the experimental data.

The shape of the shock is taken to be approximately a triangle as shown in figure 5-4. The shock's overpressure is P, its spatial length is l, and its temporal length is τ, with $l = c\tau$. Over the extent of the shock wave the overpressure is taken to fall linearly from the peak overpressure P to 0 or atmospheric pressure over a distance l; this gives the triangular form. P will be written with the subscripts 'i', 'r', and 't' to correspond to the incident, reflected, and transmitted shocks respectively at the front surface of the layer.

Figure 5-4: Shock Wave Geometry

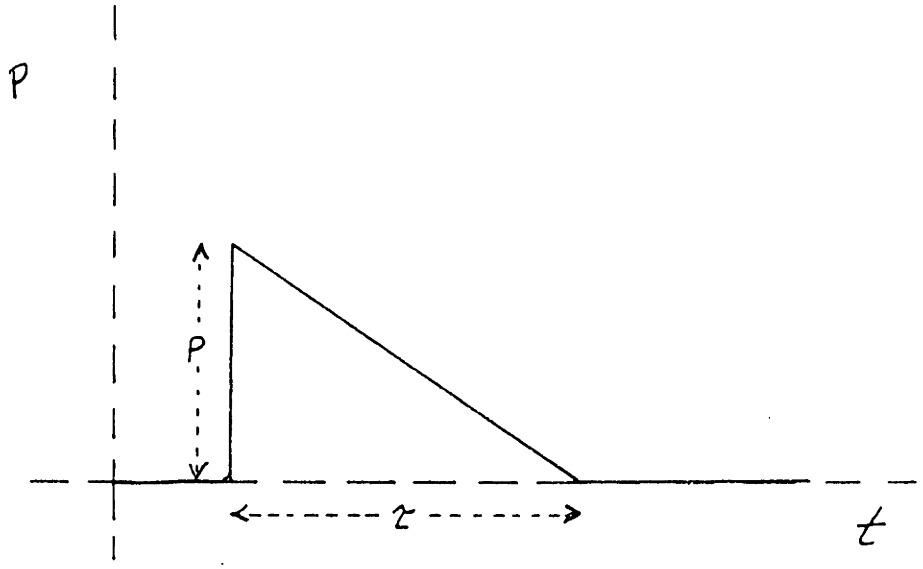

A computer program was used to determine the frequency spectrum of a typical incident shock; the result is shown in figure 5-3. The spectrum gives an indication of the energy content of the pulse as a function of frequency. We note that most of the energy of the pulse occurs for $\nu < 500\,\text{Hz}$. This suggests that we can use the low frequency limit of the flexible porous material described in chapter 2 and appendix D. In particular we found that for low frequencies the fluid and structure tend to move together, the structure can be treated as limp, and one can estimate the wavenumber in such a medium by referring to an effective density and compressibility. The normalized wavenumber in such a medium can be related to the wave speed in the medium and the open air wave speed using $Q = c/c'$.

This supports our claim that it is reasonable to treat the porous layer as consisting

of a homogeneous material of mass density $\tilde{\rho}$ and compressibility $\tilde{\kappa}$. Further support for this assumption comes from the results of Ingard's experiments [14]; he states that most of the measurements were repeated for a material of significantly different flow resistance with the same results. This further justifies our claim that relative motion of the fluid and the structure in the porous layer may be ignored.

5.4 Front Reflection and Compression

We define the *front reflection coefficient* as the peak pressure of the shock which has just reflected from the front surface of the layer divided by the peak pressure of the incident shock just before it reaches the layer. The 'second' peak evident in the complete reflected shock, therefore, does not figure into this reflection coefficient. The *maximal fractional deformation* of the layer is defined as the maximum distance the front surface of the porous layer moves as a result of the shock wave reflection divided by the layer length before the reflection.

Figures 5-5 and 5-6 summarize the experimental data by showing the front reflection coefficient and maximal fractional deformation as a function of incident shock overpressure for four separate cases. These figures have been corrected for the non-linear attenuation suffered by the shocks traveling between the pressure transducer and the layer front surface; as a result they better represent conditions at the layer surface. Both traces illustrate significant dependence on the incident shock's overpressure, indicating that non-linear effects are important. If the process were entirely linear, the front reflection coefficient would be constant and the maximal fractional deformation would be only a first order, acoustic perturbation.

Our goal is to develop a quasi-linear theory which is both simple yet sufficient to reveal the basic physical mechanisms responsible for the dependence of these two quantities on the incident shock pressure. To do this we focus for this calculation on the interval during which the incident shock is reflected from the front surface of the flexible porous layer. We will proceed by writing equations of energy and momentum balance which account for the incident, reflected, and transmitted shocks at the front

Figure 5-5: Front pressure reflection coefficient as a function of incident shock overpressure from the experiments

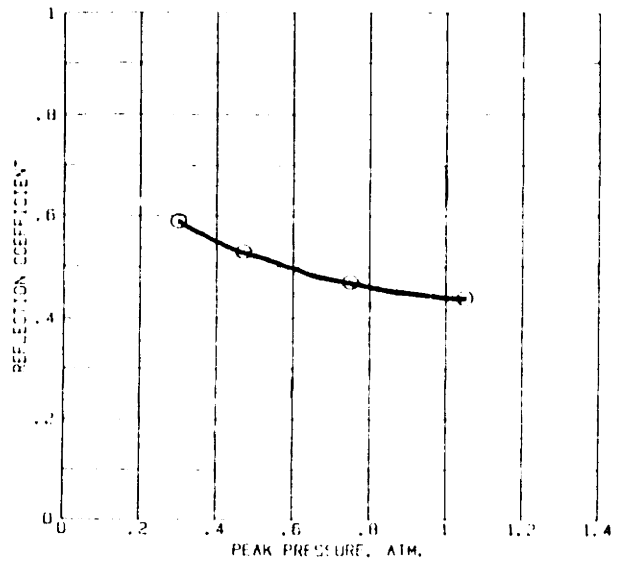

Figure 5-6: Maximum fraction deformation of porous layer as a function of incident shock overpressure from the experiments

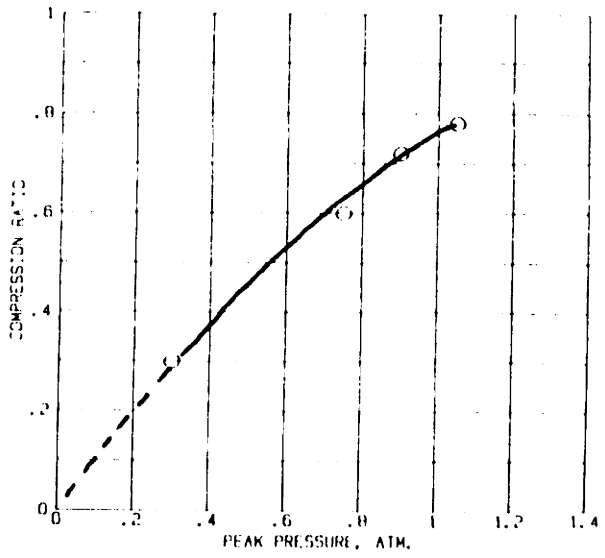

surface of the layer, as well as the layer's gross (zeroth order) motion. In addition we will attempt to account for the dragging of the porous layer against the walls of the shock tube during the interval of the front reflection by introducing an empirical, adjustable friction parameter which is described in more detail below.

Denoting the total shock energy as E (with the appropriate subscript), the kinetic energy of the gross motion of the layer as E_L, and the work done by the layer as it drags against the shock tube wall as W, we can write for the energy balance

$$E_i = E_r + E_t + E_L + W \tag{5.5}$$

For the incident and reflected shocks in the air the energy density is $\epsilon = P^2/\rho c^2$. Integrating this density over the triangle form of the shock gives

$$E_i = \frac{Al}{3\rho c^2} P_i^2 \quad , \quad E_r = \frac{Al}{3\rho c^2} P_r^2 \tag{5.6}$$

The transmitted shock in the layer requires a similar expression for the energy with l, ρ, and c replaced by their counterparts in the layer, namely l', $\tilde{\rho}$, and c'. We are further assuming that the layer's front surface has acquired a velocity U_0 during the period of the front surface reflection. This means that the approximate expression for the energy in the laboratory frame of the transmitted wave should utilize a wave speed $c'' = c' + U_0$. These assumptions lead to a transmitted wave energy of

$$E_t = \frac{Al'}{3\tilde{\rho}c''^2} P_t^2 = \frac{Al}{3c\tilde{\rho}c''} P_t^2 = \frac{Al}{3c\tilde{\rho}(c/Q + U_0)} P_t^2 = \frac{AlQ}{3\tilde{\rho}c^2(1 + QU_0/c)} P_t^2 \tag{5.7}$$

where we have used the fact that $l'/c'' = l/c$.

For the purposes of our calculations here we will neglect the U_0 dependent term in the denominator of the above expression so we write $1/(1 + QU_0/c) \approx 1$. This simplifies the calculation and, as can be demonstrated, the fact that $QU_0/c \sim 0.1$ justifies the approximation. In addition, the pressure amplitude of the transmitted pulse will ultimately be an adjustable parameter of our analysis.

The kinetic energy of the gross motion of the porous layer will be taken to be

$$E_L = \frac{1}{2}\tilde{m}U_0^2 \tag{5.8}$$

and the work done by the layer as it drags against the wall of the shock tube during the interval of the reflection from the front surface of the layer can be approximated by

$$W \approx F\frac{U_0}{2}\tau \approx F\frac{U_0}{2}\frac{l}{c} = \mathcal{F}(\tilde{\rho}gAd)\frac{U_0}{2}\frac{l}{c} \tag{5.9}$$

where we have introduced an average frictional force F, and then a *friction factor* $\mathcal{F}$ which is the force F normalized by the weight of the layer so $\mathcal{F} = F/(\tilde{\rho}gAd)$ with g being the acceleration of gravity.

These energy expressions can be substituted into equation 5.5 to give

$$\frac{Al}{3\rho c^2}P_i^2 = \frac{Al}{3\rho c^2}P_r^2 + \frac{AlQ}{3\tilde{\rho}c^2}P_t^2 + \frac{1}{2}\tilde{m}U_0^2 + \mathcal{F}(\tilde{\rho}gAd)\frac{U_0}{2}\frac{l}{c} \tag{5.10}$$

By defining

$$R \equiv \frac{P_r}{P_i}\ ,\ T \equiv \frac{P_t}{P_i}\ ,\ f \equiv \left(\frac{gl}{c^2}\right)\mathcal{F}\ ,\ \mathcal{P} \equiv \frac{d}{3l}\tilde{\rho}c^2 \tag{5.11}$$

we can write equation 5.10 as

$$1 = R^2 + Q\frac{\rho}{\tilde{\rho}}T^2 + \frac{9}{2}\frac{l}{d}\left(\frac{U_0}{c}\right)^2\left(\frac{\mathcal{P}}{P_i}\right)^2 + f\frac{l}{d}\frac{\rho}{\tilde{\rho}}\frac{U_0}{c}\left(\frac{\mathcal{P}}{P_i}\right)^2 \tag{5.12}$$

We then proceed to derive an equation of momentum balance in a similar manner. We denote the incident, reflected, and transmitted shock's momentum as J with the appropriate subscript, the momentum of the layer as a whole as J_L, and the impulse imparted to the shock tube walls by frictional dragging as I. In each case we are writing the component of momentum in the direction of propagation of the incident pulse (thus J_r is implicitly negative). The momentum balance relation is

$$J_i = J_r + J_t + J_L + I \tag{5.13}$$

For the incident and reflected shocks the magnitude of the momentum density is $j = P/c$. Integrating this over the volume of the shock gives

$$J_i = \frac{Al}{2c} P_i \quad , \quad J_r = -\frac{Al}{2c} P_r \tag{5.14}$$

The transmitted shock in the layer has momentum

$$J_t = \frac{Al'}{2c''} P_t = \frac{Al}{2c} P_t \tag{5.15}$$

The momentum associated with the gross motion of the layer will be taken to be

$$J_L = \frac{3}{2} \tilde{m} U_0 \tag{5.16}$$

and the impulse imparted to the walls of the shock tube during the interval of front reflection is approximately

$$I \approx F\tau = \mathcal{F}(\tilde{\rho} g A d) \frac{l}{c} \tag{5.17}$$

where we have again used the friction factor $\mathcal{F}$ as in equation 5.9.

These expressions can be substituted into equation 5.13 to give

$$\frac{Al}{2c} P_i = -\frac{Al}{2c} P_r + \frac{Al}{2c} P_t + \frac{3}{2} \tilde{m} U_0 + \mathcal{F}(\tilde{\rho} g A d) \frac{l}{c} \tag{5.18}$$

which becomes, after using the definitions given in 5.11

$$1 = -R + T + 3 \frac{U_0}{c} \frac{\mathcal{P}}{P_i} + 3f \frac{\mathcal{P}}{P_i} \tag{5.19}$$

Finally, if we assume that losses resulting from friction between the layer and the shock tube walls are of secondary importance in relating the initial front surface speed of the layer U_0 to its maximum fractional deformation $\delta \equiv (\triangle d)_{MAX}/d$, we can then assume that the initial kinetic energy of the layer just after the front reflection is entirely converted into the potential energy in the layer's maximum compression. This energy balance takes the form

$$\frac{1}{2}\tilde{m}U_0^2 \approx \frac{1}{2}\tilde{k}(\triangle d)^2_{MAX} = \frac{1}{2}\tilde{k}d^2\delta^2 \tag{5.20}$$

Equations 5.12, 5.19 and 5.20 can be solved simultaneously to determine R and δ as functions of the incident shock overpressure P_i, once the other parameters of the equations have been specified.

The parameters which must be specified in advance of solving this system of equations are:

d $\rightarrow$ Undeformed Layer Thickness

$\tilde{\rho}/\rho \rightarrow$ Ratio of effective layer density to air density

$\tau \rightarrow$ Incident shock's temporal length

$\tilde{\kappa}/\kappa \rightarrow$ Ratio of effective layer compressibility to air isothermal compressibility

$\mathcal{F} \rightarrow$ Average friction force during front reflection normalized by layer weight

$T \equiv P_t/P_i \rightarrow$ Transmitted (into free surface of layer during interval of front reflection) shock overpressure divided by incident shock overpressure.

Of these parameters, the first three may be readily specified in advance. The undeformed layer length is provided with the experimental data. The effective layer density, based on the low frequency limit of the flexible porous material (discussed in chapter 2), can be taken to be approximately $\tilde{\rho} \approx H\rho + (1 - H)\rho'$, where ρ and ρ' are the densities of the fluid and the layer's structural material (without voids) respectively and H the layer porosity. The incident shock's temporal length can be read directly off the pressure traces and will be assumed to be independent of the shock's overpressure in this analysis.

The fourth parameter, the normalized compressibility of the frame of the porous layer, is difficult to estimate accurately without a specific experiment (as described in chapter 6) designed to do it. We do have, however, an estimate of the speed of the sound wave in the layer by taking the time separation t_2 of the front and back reflected pulses for a case where the incident shock's overpressure is sufficiently small (for example, using the 0.3 atm overpressure case) in which case the round trip distance traversed during time t_2 can be assumed to be $2d$ and totally within the

layer. Taking the speed of sound in the layer to be c' we can estimate

$$\tilde{\kappa} \approx \frac{1}{\tilde{\rho}(c')^2} \approx \frac{1}{\tilde{\rho}} \left(\frac{t_2}{2d}\right)^2 \tag{5.21}$$

The last two parameters are very difficult to estimate in the absence of more experiments. Without knowing how tightly the porous layer was squeezed into the shock tube and lacking even an approximate estimate of the relevant friction coefficient, the friction factor is a purely empirical, adjustable parameter. The transmission coefficient T might be estimated by considering a weak incident pulse, obtaining the ratio of the transmitted pressure after a round trip through the layer to the incident pulse pressure from the data, then attempting to extract an estimate of T by accounting for the fact that the shock underwent two crossings of the layer's front surface, the trip through the layer, and the trip through the air back to the original location of the layer's free surface. This would probably introduce significant errors since our previous discussion of characteristic times indicated that the layer was significantly deformed, in varying degrees, during the time the transmitted pulse made its way to the rigid termination and back. We will therefore take T also to be an adjustable parameter of the calculation and infer its correct value by the value which brings our model's predictions in closest alignment with the experimental data.

5.5 Model Predictions and Conclusions

Figures 5-7 to 5-12 are the result of calculations using this model. For purposes of comparison with the experimental results summarized in figures 5-5 and 5-6, we have used the model to estimate the front reflection coefficient and fractional maximum deformation for a few combinations of values of the parameters T and $\mathcal{F}$.

Good correspondence is seen between experiment and theory for the front reflection coefficient. For parameter values $T = 0.4$ and $\mathcal{F} = 200$, the theoretical curves shown in figures 5-7 and 5-9 exhibit both the correct magnitude and downward slope seen in the experimental data. It is particularly interesting to note that, in the absence of the dragging of the layer against the shock tube walls, the front reflection

coefficient would be constant (see $\mathcal{F} = 0$). This means that a measurement of this type, designed to reveal an incident amplitude dependence in the reflection coefficient, must attempt to control or measure the effects of this dragging in order to understand the role of other physical mechanisms.

The maximum fractional deformation predictions in figures 5-8 and 5-10 show the correct upward trend and order of magnitude found in the experimental data. They do, however, come out consistently low. Figures 5-11 and 5-12 show the interesting result that, by halving the effective density of the layer, one can obtain much better agreement between theory and experiment. Even the reflection coefficient predictions can be subsequently corrected by using a larger T or $\mathcal{F}$ (these have a weak effect on the deformation predictions as seen in figures 5-8 and 5-10).

A possible explanation for this improvement with a half-density assumption is that, during the interval of front reflection, the stress wave propagating into the layer has involved much of the layer in the gross (zeroth order) motion, but it has not involved all of it. The resulting error might then be reduced by using the lower effective density. Then the lower effective mass of the layer would correspond to the fraction of the total mass participating in this gross motion.

Figure 5-7: Model prediction of Front Reflection Coefficient (pressure) vs. Incident shock pressure for 8 inch layer; $\tilde{\rho}/\rho = 17.5$; T=0.4; $\mathcal{F}$ =0,100,200,300;

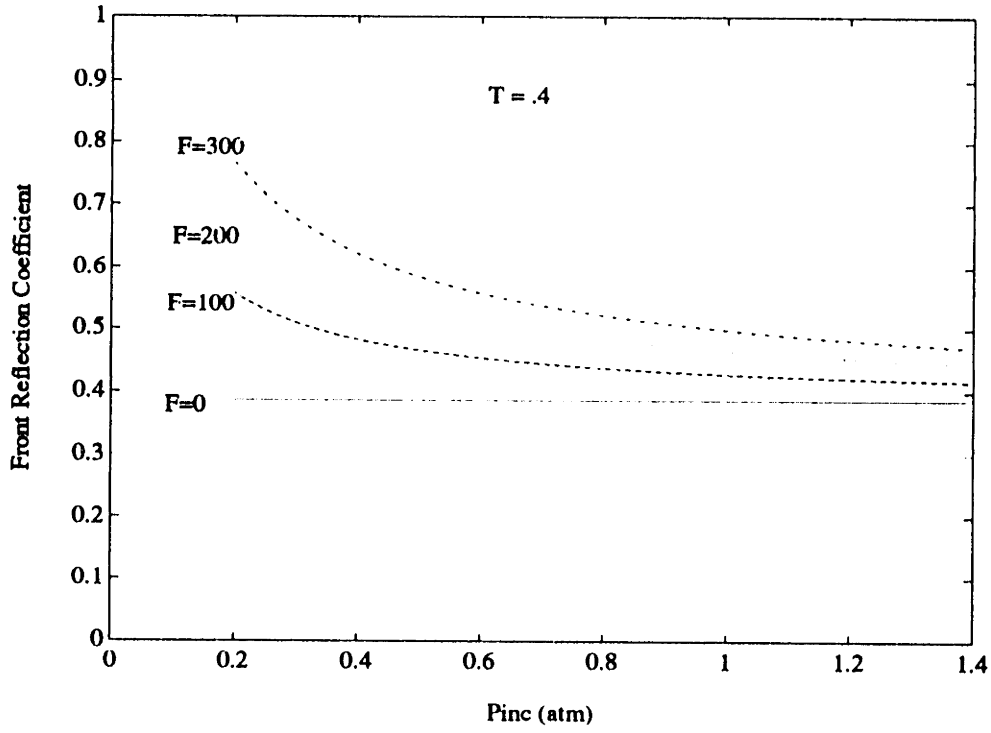

Figure 5-8: Model prediction of Maximum Fractional Deformation of Porous Layer vs. Incident shock pressure for 8 inch layer; $\tilde{\rho}/\rho = 17.5$; T=0.4; $\mathcal{F}$ =0,100,200,300;

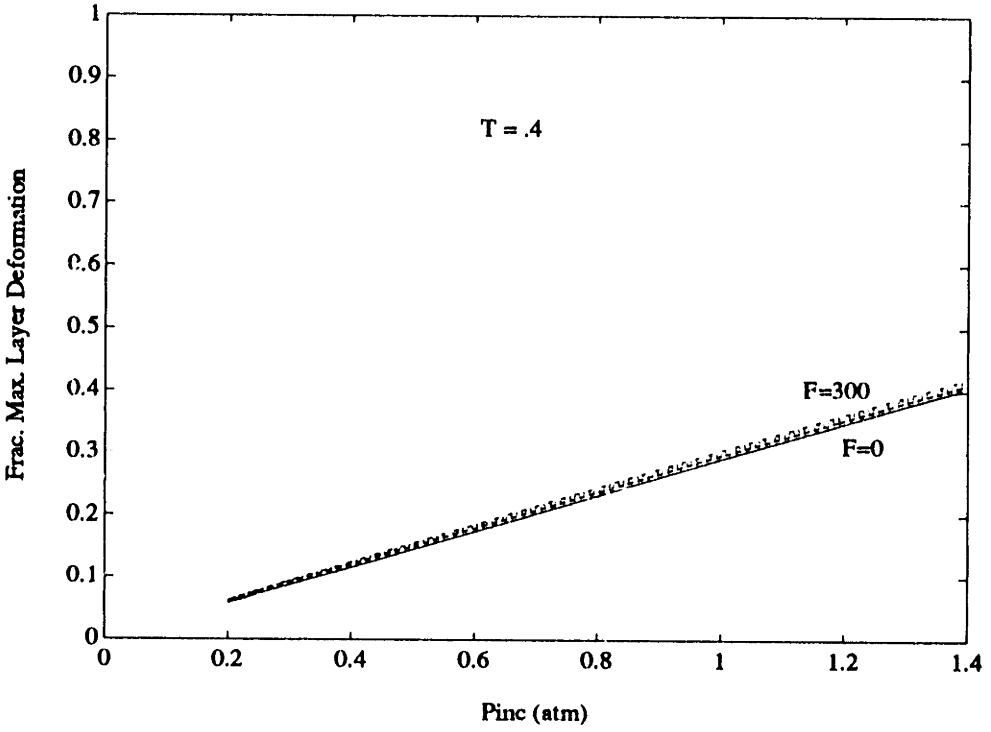

Figure 5-9: Model prediction of Front Reflection Coefficient (pressure) vs. Incident shock pressure for 8 inch layer; $\tilde{\rho}/\rho$ = 17.5; $\mathcal{F}$ =200; T=0.2,0.4,0.6;

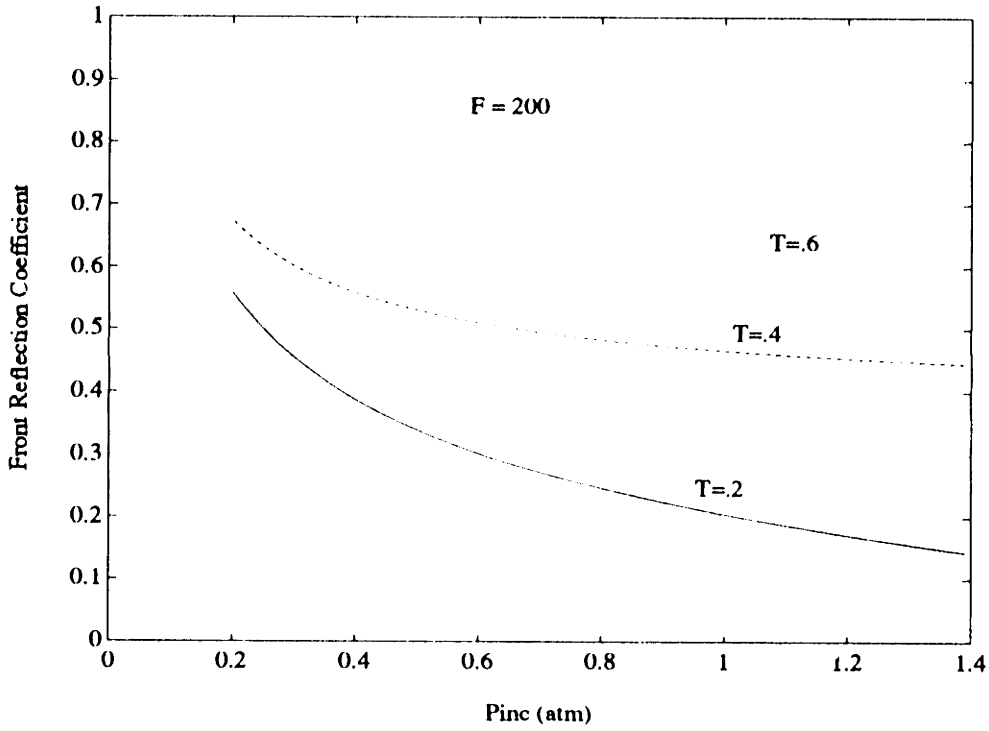

Figure 5-10: Model prediction of Maximum Fractional Deformation of Porous Layer vs. Incident shock pressure for 8 inch layer; $\tilde{\rho}/\rho$ = 17.5; $\mathcal{F}$ =200; T=0.2,0.4,0.6;

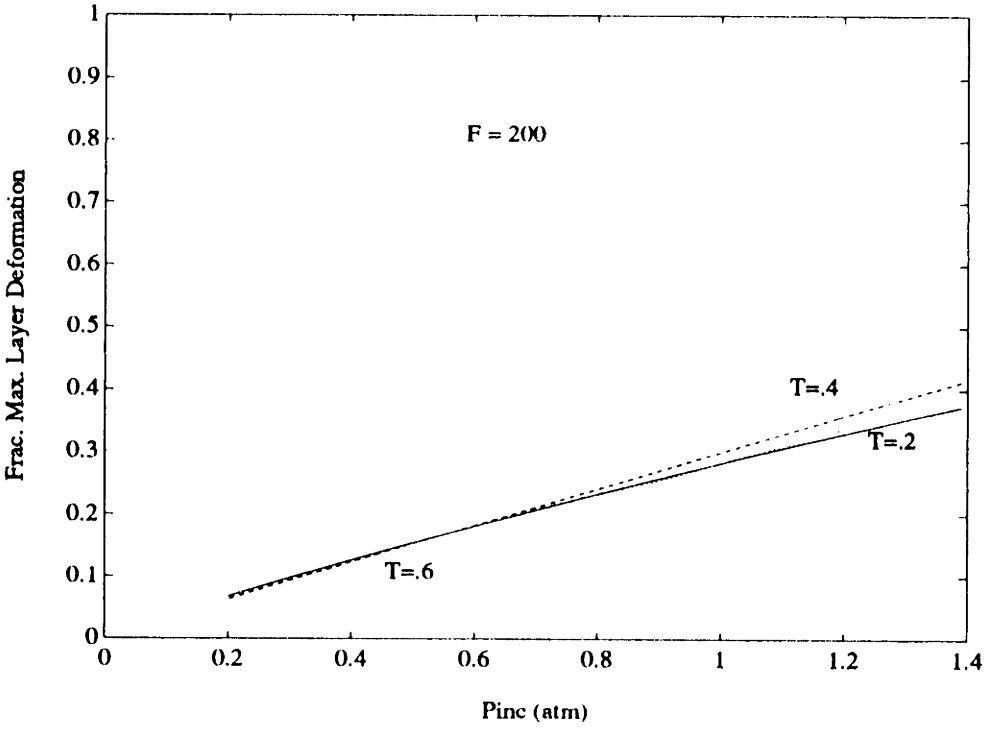

Figure 5-11: Model prediction of Front Reflection Coefficient (pressure) vs. Incident shock pressure for 8 inch layer; $\tilde{\rho}/\rho = 17.5$ or $(17.5)/2$; $\mathcal{F}$ =200; T=0.4;

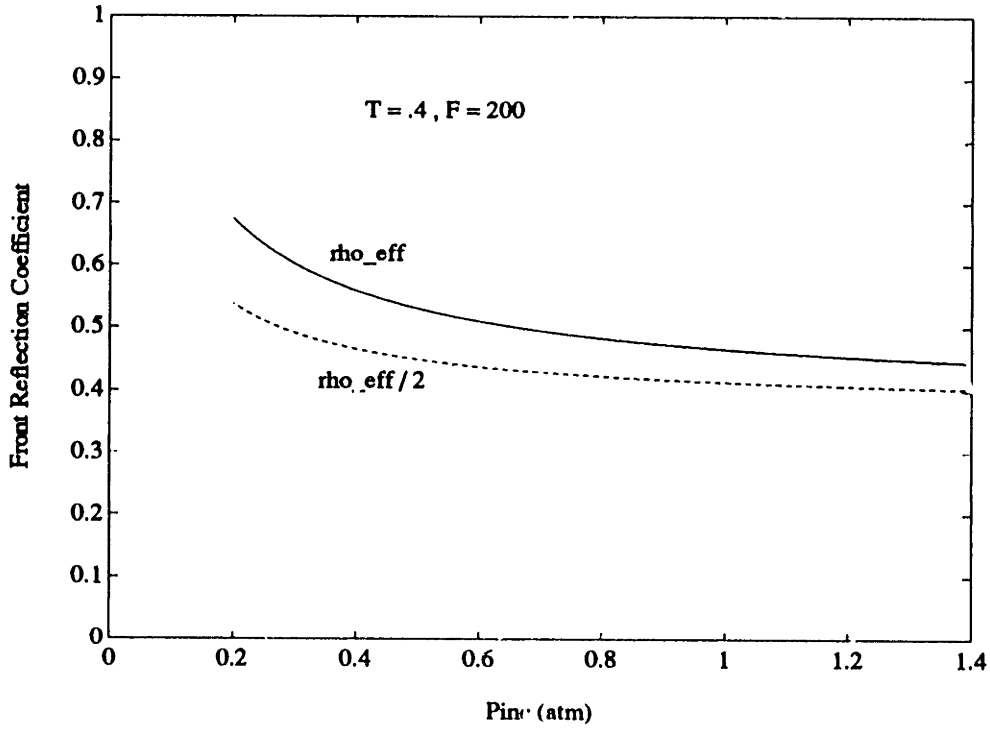

Figure 5-12: Model prediction of Maximum Fractional Deformation of Porous Layer vs. Incident shock pressure for 8 inch layer; $\tilde{\rho}/\rho = 17.5$ or $(17.5)/2$; $\mathcal{F}$ =200; T=0.4;

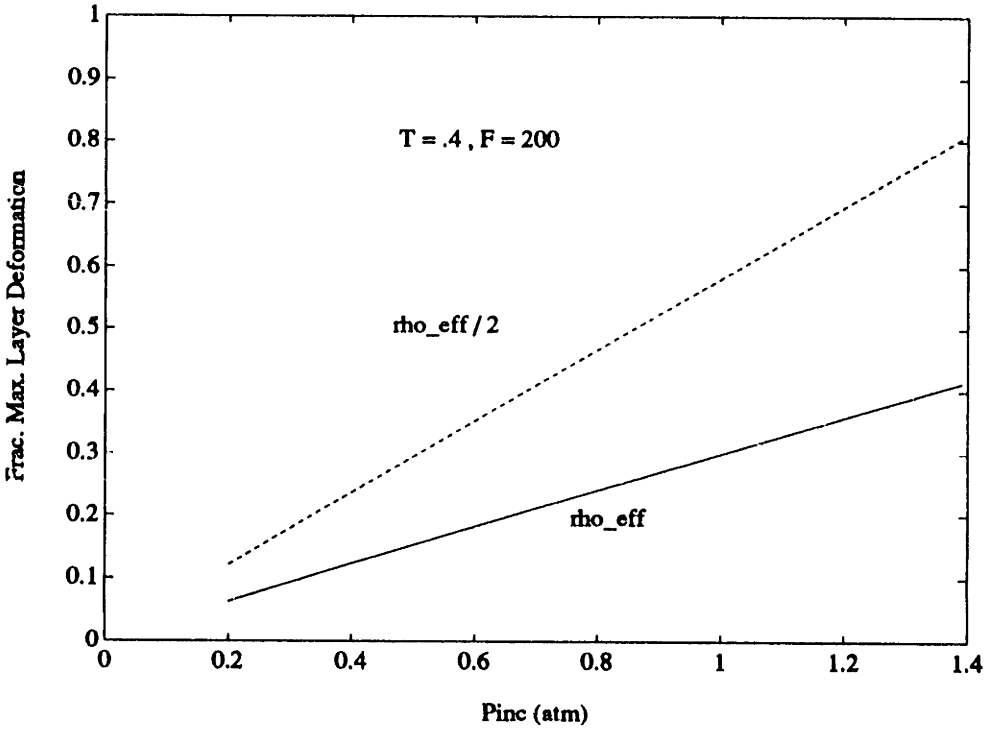

Chapter 6

Measurement of Complex Compressibility

The flexibility of a porous material, which has been shown to have important consequences for its acoustical properties, is specified by the complex compressibility K. The real part K_r accounts for the fractional density change in the structure resulting from a structural pressure change. The imaginary part K_i is related to the irreversible nature of the deformations of the structure. As discussed in chapter 2 (and explicitly shown in appendix A), K_i can be compared to a kind of bulk viscosity of the structure of the porous material since the pressure depends not only on the fractional deformation of the material, but also the time rate of change of the deformation.

The fact that K plays a central role in the theory of the flexible porous material means that its accurate measurement over the range of frequencies of interest is essential for the prediction of frequency dependent acoustical properties.

A diagram of a device which can be used to determine this compressibility is shown below. This particular design was proposed by Lugard and Koch [17].

The vessel is which the sample in placed is evacuated to remove the air from the voids of the porous sample. Although most of the analysis in previous chapters could be applied, with some minor modifications, to a semi-porous material in which some fraction of the voids are not interconnected, this experiment requires that no such voids exist. This is because as the vessel is evacuated these closed voids expand and

Figure 6-1: Experimental apparatus used for the measurement of the complex compressibility of a flexible porous material

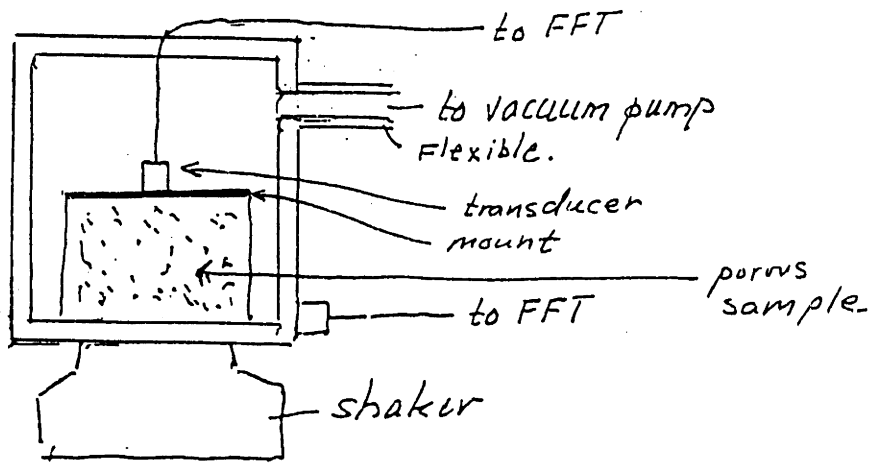

alter the relationship between the velocity transfer function across the sample and K; this makes the subsequent determination of K difficult, if not impossible.

The sample is set upon a shaker and driven with random vibrations. A Fast Fourier Transform program provides the magnitude of the velocity transfer function across the sample as a function of frequency. The location and height of the maximum of this curve can be used to determine K.

Typically a relationship between this curve and K is used which assumes that the wavelength in the sample is much larger than the sample length. In addition, the imaginary part of K is assumed to be much smaller than the real part. The resulting equations readily give the real and imaginary parts of K in terms of the location and height of the magnitude of the velocity transfer function, but significant errors can be introduced by the approximations. In the following discussion we calculate these errors and then describe a computer algorithm that allows K to be obtained from the data without these approximations; this is referred to as the *exact method.* A listing of a computer program based on this algorithm is provided in appendix E.

6.1 Relating K to the velocity transfer function

We can use the method of transmission matrices to derive a relationship between the peak of the velocity transfer function and the complex compressibility K. If we take as location 1 the base of the sample, location 2 at the top of the sample but beneath the transducer and mount, and location 3 on top of the transducer, the relevant transmission matrices are

$$\begin{pmatrix} p_2 \\ u_2 \end{pmatrix} = \begin{pmatrix} \cos ql & i\rho' c' \sin ql \\ (i/\rho' c') \sin ql & \cos ql \end{pmatrix} \begin{pmatrix} p_1 \\ u_1 \end{pmatrix} \tag{6.1}$$

and

$$\begin{pmatrix} p_3 \\ u_3 \end{pmatrix} = \begin{pmatrix} 1 & i\omega M/A \\ 0 & 1 \end{pmatrix} \begin{pmatrix} p_2 \\ u_2 \end{pmatrix} \tag{6.2}$$

where the length of the sample is l and its cross sectional area is A. In the sample, q is the propagation constant, ρ' is the effective density, and c' is the wave speed. M is the total mass of the transducer and mount on top of the sample.

Multiplying these matrices, and assuming $p_3 = 0$ at the free surface of the transducer, allows us to write for the ratio u_3/u_1

$$\frac{u_3}{u_1} = \frac{1}{\cos ql - \mu ql \sin ql} \tag{6.3}$$

where μ is defined as the ratio of the transducer and mount mass to the total mass of the sample

$$\mu \equiv \frac{M}{A\rho' l} = \frac{\omega M}{\rho' c' Aql} \tag{6.4}$$

and

$$c' = \frac{1}{\sqrt{\rho'(K_r + iK_i)}} \quad , \quad q = \frac{\omega}{c'} \tag{6.5}$$

An approximation typically used at this stage is $|ql| \ll 1$ which gives

$$\frac{u_3}{u_1} \approx \frac{1}{1-((1/2+\mu)(ql)^2)} = \frac{1}{1-((1/2+\mu)(\rho'/\rho)(\omega l/c)^2(K_r+iK_i))} \tag{6.6}$$

Making the additional assumption that $K_i \ll K_r$, knowledge of the frequency of the maximum of $|u_3/u_1|(\omega)$ determines K_r since

$$K_r \approx \frac{1}{(1/2+\mu)(\rho'/\rho)(\omega_{max}l/c)^2} \tag{6.7}$$

and the height of the maximum of $|u_3/u_1|(\omega)$ determines K_i using

$$K_i \approx \frac{K_r}{|u_3/u_1|_{max}} \tag{6.8}$$

where we have defined ω_{max} as the lowest frequency for which $|u_3/u_1|(\omega)$ has a maximum and $|u_3/u_1|_{max} \equiv |u_3/u_1|(\omega = \omega_{max})$.

The approximating assumptions therefore allow knowledge of the peak of the $|u_3/u_1|(\omega)$ curve to be easily converted to an estimate of K_r and K_i.

In many cases, however, these approximations introduce significant errors into the subsequent prediction of K. Even in some cases where $K_i \ll K_r$, the long-wavelength assumption alone is sufficient to cause errors.

These errors are calculated and plotted in figures 6-2 to 6-5. The exact value of K has been assumed in advance; then 6.3 is used to get an exact location of the frequency and height of the maximum of $|u_3/u_1|(\omega)$. This frequency and maximum height are put back in 6.7 and 6.8, and the compressibility estimate is obtained. This estimate, referred to as $\tilde{K} = \tilde{K}_r + i\tilde{K}_i$, is then compared with the actual K assumed at the start.

Figure 6-2 shows a comparison of $\tilde{K}$ and K for $K_r = 1$, plotted against the mass ratio μ. These results would be constant if plotted as a function of the density ratio ρ'/ρ or the sample length l. This is because they are each factors in the dimensionless parameter ql found in equations 6.3 and 6.6. Figure 6-2 shows $\tilde{K}_r$ differs significantly from K_r, even when $K_i = (1/10)K_r$. The error in this case is greatest

for the lower values of the mass ratio. One should be careful, however, when setting up an experimental apparatus, to keep the mass ratio μ small enough so that the peak frequency of $|u_3/u_1|(\omega)$ occurs within the operational frequency range of the apparatus. If $K_r \sim K_i$, then the error is greatest for the higher mass ratios. Figure 6-3 shows similar results when $K_i = 0.5$ is compared with $\tilde{K}_i$.

Figures 6-4 and 6-5 show the same cases as in figures 6-2 and 6-3 respectively, but instead we have plotted the *Percent Magnitude Error* (PME) which is defined as

$$PME \equiv \left| \frac{|K| - |\tilde{K}|}{|K|} \right| * 100 \tag{6.9}$$

For cases where $K_i = (1/10)K_r$, this error can be $\sim 10\%$ for a large range of mass ratios and goes to 0% as the mass ratio becomes large. For cases where $K_r \sim K_i$, errors of $\sim 50\%$ are found for a wide range of mass ratios.

6.2 The Exact Method

An algorithm is described here which allows one to obtain the complex compressibility K to essentially arbitrary precision once ω_{max} and $|u_3/u_1|_{max}$ have been specified. A flowchart outlining the algorithm and a sample run of a $c++$ program based on it are shown in figure 6-6. A source listing of the program is provided in appendix E.

After taking general parameters as input such as the mass ratio, density ratio, sample length, and the specifics of the search such as ω_{max} and $|u_3/u_1|_{max}$, the approximate method (using equations 6.7 and 6.8) is used to determine $\tilde{K}$, which is the starting location for the two dimensional search over the K_r, K_i plane.

Since K_r is determined by ω_{max} in equation 6.7, the first *bi-directional search* locates the K_r which corresponds to the best match to the target ω_{max} value input at the start. By *bi-directional search* we mean a search which begins at some starting point, then alternates looking upward or downward in the argument for a minimum in the function. After finding a minimum the search step size is reduced and the search is restarted. In this case, the function used is the absolute value of the difference between the local ω_{max} and the target ω_{max}. The resulting best K_r is called $K_{r,I}$.

The process is repeated by searching for the K_i which gives the best match to the target value of $|u_3/u_1|_{max}$; this K_i is called $K_{i,I}$.

Now using $(K_{r,I}, K_{i,I})$ as a starting point, the above two searches are repeated and the best compressibility obtained is called $(K_{r,II}, K_{i,II})$. If this value is good enough the algorithm is finished. If not, a new starting point is formed from the geometric mean of the two K's just obtained. Its value is $K_{new\ start} = (\sqrt{K_{r,I}K_{r,II}}, \sqrt{K_{i,I}K_{i,II}})$. The above four searches are then repeated.

As shown in figure 6-6 and found from extensive testing of the program, in many cases the program will zero in on K within a few iterations. This suggests the use of such a method in situations where the errors introduced using equations 6.7 and 6.8 are unacceptable.

Figure 6-2: Measurement of Complex Compressibility - $\tilde{K}_r$ versus Mass Ratio for the cases K/κ_0 = (1,0.1),(1,0.5),(1,1)

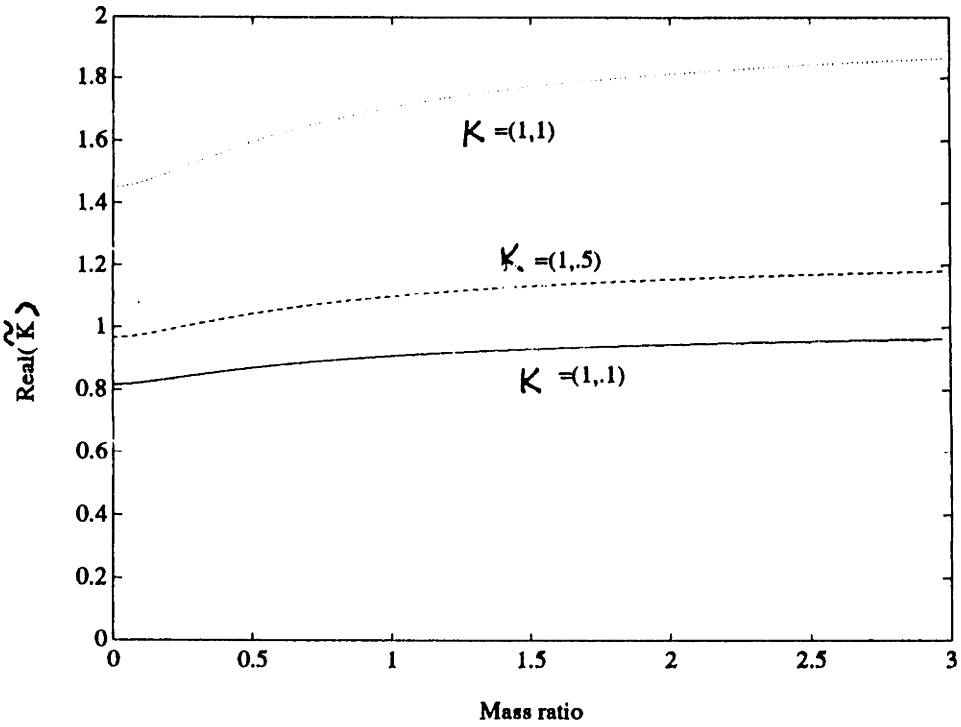

Figure 6-3: Measurement of Complex Compressibility - $\tilde{K}_i$ versus Mass Ratio for the cases K/κ_0 = (0.5,0.5),(1,0.5),(2,0.5)

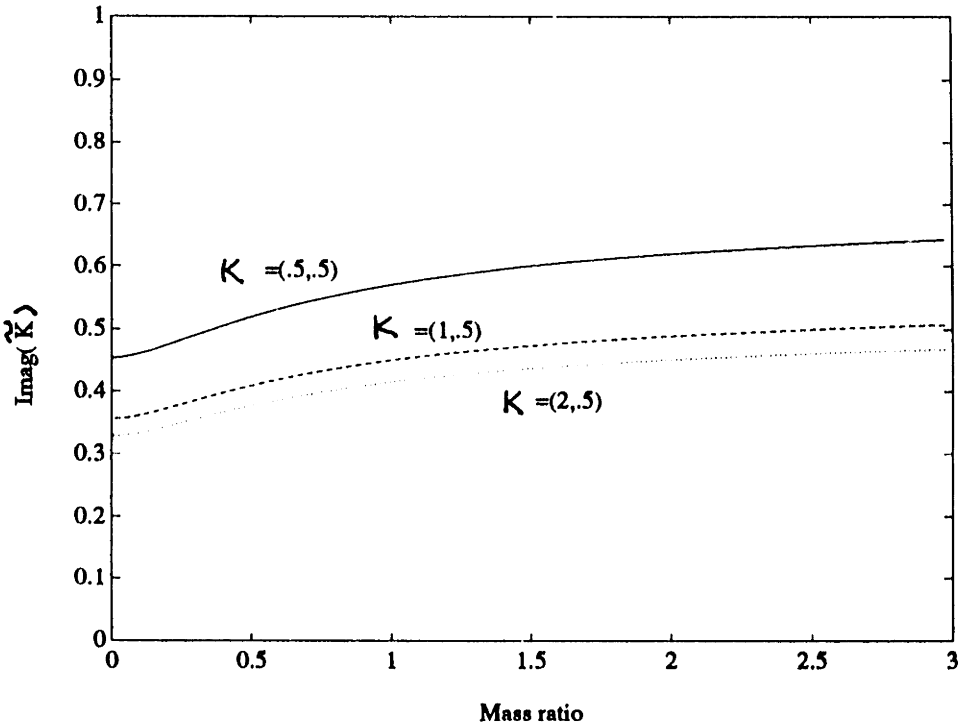

Figure 6-4: Measurement of Complex Compressibility - Per Cent Magnitude Error versus Mass Ratio for the cases K/κ_0 = (1,0.1),(1,0.5),(1,1)

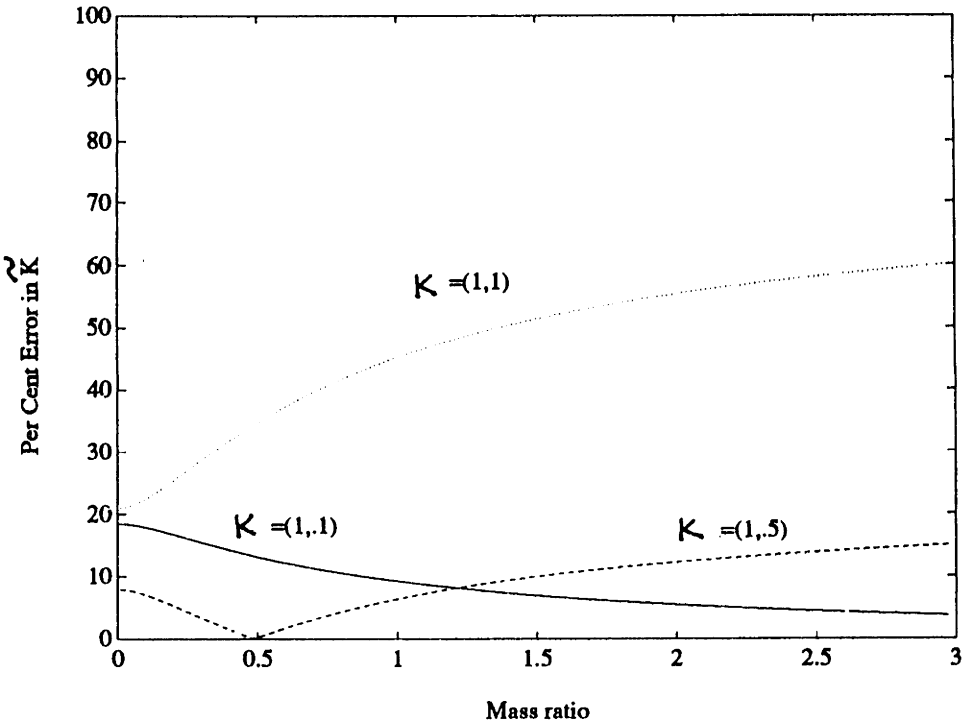

Figure 6-5: Measurement of Complex Compressibility - Per Cent Magnitude Error versus Mass Ratio for the cases K/κ_0 = (0.5,0.5),(1,0.5),(2,0.5)

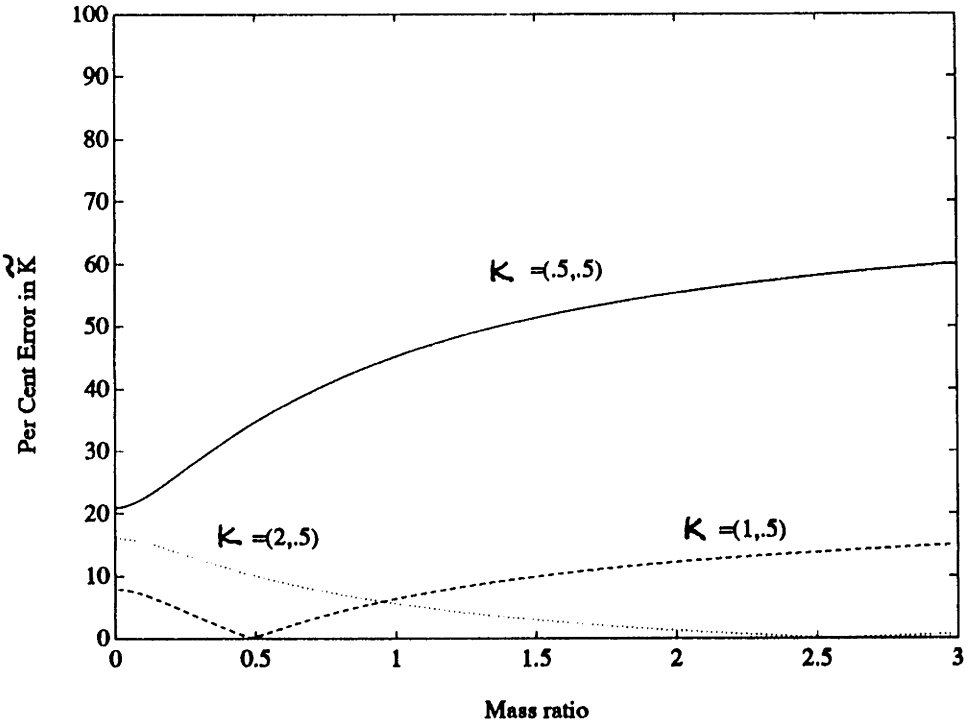

Figure 6-6: Flowchart and Sample Run for Exact Method Algorithm

Flowchart

Compare.C

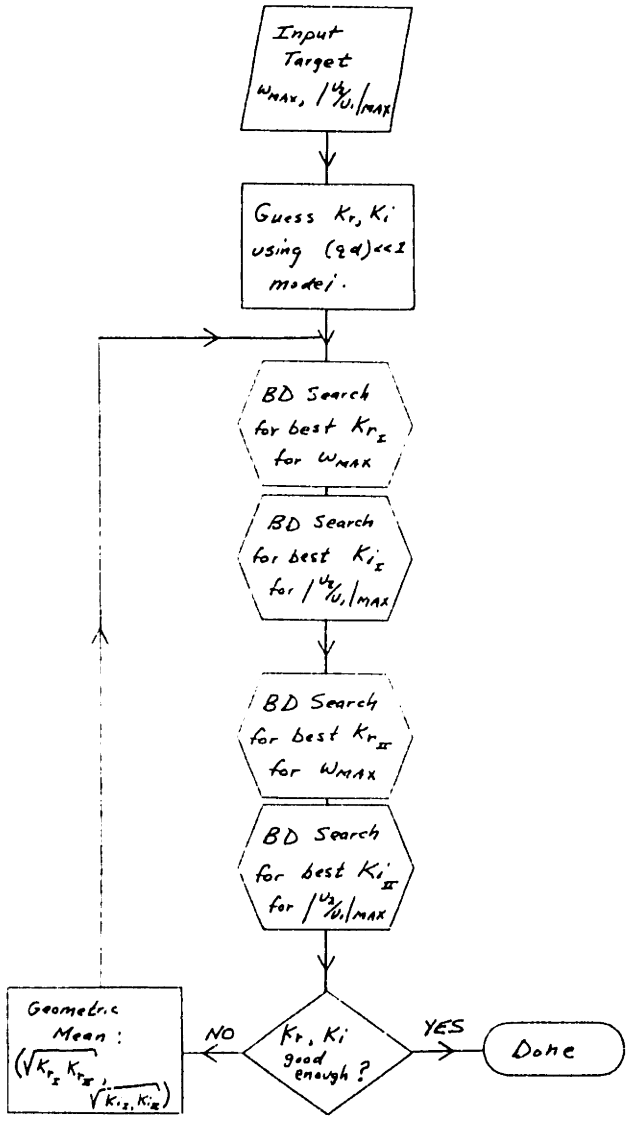

Sample Run

```
athenaX run

COMPRESS - Complex Compressibility Program

General parameters:
Mass ratio ?.5
Density ratio ?26
Sample Thickness (inches) ?1

Target values:
Frequency for |u2/u1| maximum ?160
Maximum |u2/u1| value ?2.2

START K = (6.985167,3.175076)
INTERIM K = (6.866055,4.103356)
INTERIM K = (5.523096,3.303356)
INTERIM K = (6.745447,4.031278)
INTERIM K = (6.326043,3.780099)
INTERIM K = (6.143250,3.677716)
INTERIM K = (6.213849,3.720735)
INTERIM K = (6.232725,3.724489)
INTERIM K = (6.223280,3.722612)
INTERIM K = (6.223280,3.722612)
FINAL BEST K = (6.223280,3.722612)
Target Freq_Max=160.000000, Actual Freq_Max=160.018372
Value=2.200000, Actual Value=2.200071
Fractional Error using K̃      = (0.122425,-0.147084)
athenaX
```

Chapter 7

Concluding Remarks

7.1 Consequences of Flexibility

Flexibility has been shown to have important consequences for the acoustical properties of porous materials. In some cases, assuming a flexible porous material to be limp or rigid introduces significant errors in, for example, the predicted absorption coefficient. The effect of flexibility, in many circumstances, has been shown to be related to a structural layer resonance. The structure sustains wave motion which causes losses due to its deformation (related to the imaginary part of the complex compressibility) and the viscous drag between the structure and fluid. In a number of different examples, including anisotropic materials and periodic structures, we have demonstrated how these effects can influence the sound absorption performance of a porous material. In addition, flexibility has been shown to alter the equilibrium properties of a porous material with mean flow. We have found that, if a shock wave is incident on a flexible porous layer, the momentum in the incident pulse can cause gross motion of the layer, resulting in large deformations (for example, an 80% deformation for an 1 atm shock). In addition, the dragging of the layer against a constraining surface, if present, has been shown to introduce dependence of the front reflection coefficient (defined in chapter 5) on the peak pressure of the incident shock. Both of these effects are a direct consequence of the mobility of the material; the first depends strongly on the flexibility of the material as well.

In chapter 2 we set the stage for most of the subsequent analyses by discussing the characteristic lengths and times of the acoustic problem of the flexible porous material, writing the equations of mass balance, momentum balance, and compressibility definitions, and deriving expressions for the propagation constants. For high frequencies these propagation constants were readily identified as one for a fluid wave and one for a structure wave. For low frequencies, the single important mode was due to comotion of the fluid and structure and therefore associated with an effective density and effective compressibility (see appendix A). In addition, we derived a power balance relation for the flexible porous material which explicitly identified two loss mechanisms for sound absorption: the losses due to the irreversible deformation of the structure (labeled $loss_k$ below) and those attributed to the viscous drag between the fluid and the structure ($loss_r$). These quantities, giving the power absorbed per unit area of the layer, are divided by the incident intensity and written as

$$loss_k = \frac{1}{\Pi_0} \int_{x=-d}^{0} \frac{1}{2} \omega K_i |p'|^2 \, dx \tag{7.1}$$

$$loss_r = \frac{1}{\Pi_0} \int_{x=-d}^{0} \frac{1}{2} Hr |u - u'|^2 \, dx \tag{7.2}$$

where Π_0 is the incident intensity. The above quantities were related to the normal incidence absorption coefficient α through

$$\alpha = loss_r + loss_k \tag{7.3}$$

The finite flexible porous layer backed by a rigid wall was then considered in chapter 3. We derived normal incidence and angle averaged absorption coefficients for the layer with and without an impervious skin covering the free surface. The above integrals 7.1, 7.2, and the ratio of structure to fluid velocity were calculated for a number of cases, then used to study the mechanisms of sound absorption in such a medium. The flexibility of the layer was found to increase the absorption coefficient at some frequencies. Particularly interesting was the observation that at some frequencies, corresponding to structural layer resonances, the absorption

coefficient was actually reduced due to the reduced relative motion between the fluid and structure. The absorption of sound in closed porous layers was shown to result mostly from irreversible deformations of the structure. Transmission matrices were then derived for a layer of flexible porous material for the two cases where the layer is, or is not, covered with an impervious skin on both boundaries.

In chapter 4 three departures from the basic model of chapters 2 and 3 – a porous layer with anisotropic flow resistance and structure factor, periodic structures consisting of porous layers separated by air gaps, and the porous medium in bulk with mean fluid flow – were considered. An anisotropic material, treated as isotropic in the laboratory because of its high flow resistance, was shown to exhibit very anisotropic behavior at some frequencies where structural resonances reduce the relative motion between the fluid and structure and therefore reduce the effective flow resistance. Another interesting consequence of flexibility was found in the periodic structure; the multiple layer attenuator was used as an example. Here the dips in the absorption coefficient due to structural layer resonances could coincide with peaks or dips due to fluid resonances in the air gaps; the absorption coefficient which resulted from this overlap could be made more or less smooth over frequency compared to the corresponding rigid case. Mean flow was shown to introduce a spatial gradient in the equilibrium porosity (and other field variables) of a flexible porous material, an effect which could have important consequences for the design of a porous baffle with a graded wave impedance.

To better understand the non-linear interaction of sound with flexible porous materials, the reflection of shock waves was studied in chapter 5. A quasi-linear theory was developed which reproduced the principal features in experimental results obtained previously by Ingard [14]. The theory assumed that the propagating pulses in the air and the structure were linear and modeled the gross, zeroth order motion of the porous layer by including its energy and momentum in the conservation equations; these equations compared the system just before and just after the reflection of the incident shock from the front surface of the layer. The substantial motion of the layer and its dragging against a constraining boundary (in this case the walls of the

shock tube) were found to introduce a dependence of the front reflection coefficient and maximal layer deformation on the peak pressure of the incident shock.

Lastly, in chapter 6, we addressed the question of measurement of the complex compressibility K, a key parameter used to describe the dynamics of a given flexible porous material. The standard long-wavelength assumption, used to determine K from an experimental measurement of the frequency dependent velocity transfer function across a sample, often introduces significant errors into the subsequent estimate of K. These errors were calculated for a number of cases. We then provided a computer algorithm which made the long-wavelength assumption unnecessary. A listing of the computer program based on the algorithm is provided in appendix E.

7.2 Future Work

The influences of mean flow on the equilibrium properties of a flexible porous material in bulk were derived in chapter 4 for the case when the equilibrium fluid density is assumed constant. Future studies should attempt to solve this problem without this assumption. Additionally, the corresponding problem of sound in the fluid should be studied, and the derivation of a transmission matrix for a flexible porous layer with mean flow should be attempted.

The quasi-linear theory of the reflection of shock waves presented in chapter 5 falls short of being able to provide a quantitative, complete prediction of the reflected shock waveform in terms of the incident shock waveform. Such predictability would require a numerical, computational model of the problem. The analysis is complicated by the fact that, in addition to the applicable differential equations being non-linear, the free surface boundary of the layer is in motion. Although the low frequency limit of the flexible porous medium used in chapter 5 may still be appropriate, the problem remains a difficult one.

Through all the chapters we have assumed that the porous medium consisted exclusively of open, interconnected pores; in some cases a semi-porous material could be modeled with minor additions to the theory. Sound absorption in closed cell ma-

terials, however, is an important and poorly understood phenomenon. Some progress might be achieved by treating the closed cell foam as consisting of a large number of adjacent, very thin closed porous layers – this model would predict significant absorption of sound – then studying more carefully the relative role of irreversible changes in the gas and the structure with the passage of the wave.

Appendix A

Complex Compressibility and Bulk Viscosity

If a plane sound wave propagates through a medium of density ρ and compressibility κ, which has bulk viscosity β, the propagation constant q can be taken as complex, giving for the pressure field in one-dimension

$$p(x,t) = p_0 e^{i(qx-\omega t)} = p_0 e^{-q_i x} e^{iq_r x} e^{-i\omega t} \tag{A.1}$$

where the $e^{-q_i x}$ factor accounts for the attenuation of the wave.

In order to derive an expression for the propagation constant q in this case, we write the mass balance relation

$$\frac{\partial \rho}{\partial t} + \rho \frac{\partial u}{\partial x} = 0 \tag{A.2}$$

and momentum balance

$$\rho \frac{\partial u}{\partial t} + \frac{\partial p}{\partial x} = \beta \frac{\partial^2 u}{\partial x^2} \tag{A.3}$$

and real compressibility

$$\kappa = \frac{1}{\rho}\left(\frac{\partial \rho}{\partial p}\right) \tag{A.4}$$

which lead to the amplitude equations

$$-i\kappa\rho\omega\, p(q,\omega) + iq\rho\, u(q,\omega) = 0 \tag{A.5}$$

$$-i\rho\omega\, u(q,\omega) + iq\, p(q,\omega) + \beta q^2\, u(q,\omega) = 0 \tag{A.6}$$

which give, to first order in β, the propagation constant

$$q_I^2 = k_0^2\left(1 + i\frac{k_0^2\beta}{\omega\rho}\right) \tag{A.7}$$

Alternatively, we can make the compressibility complex ($\tilde{\kappa} = \kappa_r + i\kappa_i$) and omit the bulk viscosity term in the momentum equation.

The resulting amplitude equations are

$$-i\kappa_r\rho\omega\, p(q,\omega) + \kappa_i\rho\omega\, p(q,\omega) + iq\rho\, u(q,\omega) = 0 \tag{A.8}$$

$$-i\rho\omega\, u(q,\omega) + iq\, p(q,\omega) = 0 \tag{A.9}$$

In terms of the real and imaginary parts of the complex compressibility, the propagation constant is

$$q_{II}^2 = k_0^2\left(1 + i\frac{\kappa_i}{\kappa_r}\right) \tag{A.10}$$

By requiring $q_I = q_{II}$, equations A.7 and A.10 give

$$\frac{\kappa_i}{\kappa_r} = \frac{k_0^2\beta}{\omega\rho} \tag{A.11}$$

which means, to first order in β, that the imaginary part of the compressibility κ_i corresponding to the bulk viscosity β is

$$\kappa_i = \frac{k_0^2\beta\kappa_r}{\omega\rho} = \frac{k_0^2\beta}{\omega\rho}\frac{1}{\rho c_0^2} = \frac{\beta}{\omega}\left(\frac{k_0}{\rho c}\right)^2 = \beta\omega\left(\frac{1}{\rho c^2}\right)^2 = \beta\omega\kappa_r^2 \tag{A.12}$$

Appendix B

The Rigid Porous Material

B.1 Absorption Coefficient for the Open Layer

The rigid porous layer is a useful limiting case of the flexible porous layer when the motion of the structure is negligible. The equations of motion are simplified because the velocity of the structure is zero, and the porosity of the medium is independent of position and time. The flexible model of the *open* porous layer predicts absorption coefficients consistent with the rigid layer when the frequency is sufficiently high so that the inertia of the structure prevents it from moving in response to the wave in the fluid; this occurs when $\omega \gg \frac{r}{H'\rho'}$. The flexible model of the *closed* porous layer does not have a useful rigid limit because of the boundary conditions; the fluid velocity in a rigid closed layer would be identically zero. It does have a meaningful high frequency limit, however, as discussed in chapter 3.

This makes the rigid-layer calculation an excellent diagnostic tool when working with the more complex flexible model. By setting the compressibilities κ' and K close to zero in the flexible case, one can readily compare the rigid limit to the true rigid model.

For a rigid porous material we define an average fluid velocity $\vec{u}$, a pressure p, and a compressibility κ. The linearized equations for conservation of mass and momentum and defined compressibility are

$$H\frac{\partial \rho}{\partial t} + H\rho \operatorname{div} \vec{u} = 0 \tag{B.1}$$

$$H\rho\frac{\partial \vec{u}}{\partial t} + H\rho G\frac{\partial \vec{u}}{\partial t} = -Hr\vec{u} - \operatorname{grad} p \tag{B.2}$$

$$\kappa = \frac{1}{\rho}\left(\frac{\partial \rho}{\partial p}\right) \tag{B.3}$$

For the case of a plane wave of frequency ω propagating in the rigid porous medium, equations B.1, B.2, and B.3 give the propagation constant

$$q = \sqrt{iH\tilde{r}\omega\kappa} \tag{B.4}$$

or

$$Q = \frac{q}{k_0} = \sqrt{\frac{iH\tilde{r}}{\rho\omega}} \tag{B.5}$$

where

$$\tilde{r} = r - i\omega\rho(1+G) \tag{B.6}$$

For the open porous layer with a free surface at $x = -d$ and a rigid wall at $x = 0$, we can then write for the normalized normal input admittance

$$\eta = \beta + i\sigma = \rho c\frac{u_x(x=-d)}{p(x=-d)} = \frac{-\rho c q}{H\tilde{r}}\tan qd \tag{B.7}$$

The absorption coefficients can then be found using 3.29 and 3.31.

B.2 Power Balance

In a manner analogous to the discussion in chapter 3, we can combine the equations B.1, B.2, and B.3 to obtain

$$\frac{\partial}{\partial t}(\mathcal{KE} + \mathcal{PE}) + \operatorname{div}\vec{\mathcal{I}} = -\mathcal{L} \tag{B.8}$$

where the kinetic energy density is

$$\mathcal{KE} = \frac{1}{2}H\rho|\vec{u}|^2 + \frac{1}{2}H\rho G|\vec{u}|^2 \tag{B.9}$$

the potential energy density is

$$\mathcal{PE} = \frac{1}{2}\kappa|p|^2 \tag{B.10}$$

and the intensity is given by

$$\vec{\mathcal{I}} = \frac{1}{2}Re(p\vec{u}^*) \tag{B.11}$$

and with

$$\mathcal{L} = Hr|\vec{u}|^2 \tag{B.12}$$

The quantity $\mathcal{L}$ on the right hand side of equation B.8 represents the sound absorption mechanism due to viscous drag between the fluid and structure.

For the case of normal incidence, equation B.8 can be time averaged and integrated over the thickness of the layer to give the power absorbed per unit area

$$\Pi_{abs} = \int_V \frac{1}{2}Hr|\vec{u}|^2 dV \tag{B.13}$$

If one divides by the incident intensity Π_{inc}, equation B.13 gives the normal incidence absorption coefficient

$$\alpha = \frac{\Pi_{abs}}{\Pi_{inc}} = \frac{1}{\Pi_{inc}}\int_V \frac{1}{2}Hr|\vec{u}|^2 dV \tag{B.14}$$

Appendix C

The Rigid Anisotropic Porous Layer

The assumption of rigidity makes analysis of the anisotropic porous layer much simpler. The predictions of such a rigid model are not only useful in describing the behavior of rigid porous materials; they also serve as an excellent diagnostic tool for checking the results for the flexible anisotropic porous material in the rigid limit.

With the $\hat{x}$ and $\hat{y}$ coordinate directions specified as in chapter 3, we define the flow resistance in the two directions as r_x and r_y and the structure factors as G_x and G_y. The average fluid velocities in the $\hat{x}$ and $\hat{y}$ directions are u_x and u_y.

Assuming a plane wave of angular frequency ω and propagation constant components q_x and q_y, the amplitude equation for mass balance is

$$i\omega\kappa\, p(\omega, q_x, q_y) = iq_x\, u_x(\omega, q_x, q_y) + iq_y\, u_y(\omega, q_x, q_y) \tag{C.1}$$

and the corresponding equations for momentum balance in the $\hat{x}$ and $\hat{y}$ directions are

$$H\tilde{r}_x\, u_x(\omega, q_x, q_y) = -iq_x\, p(\omega, q_x, q_y) \tag{C.2}$$

$$H\tilde{r}_y\, u_y(\omega, q_x, q_y) = -iq_y\, p(\omega, q_x, q_y) \tag{C.3}$$

where we have used the definitions

$$\tilde{r}_x \equiv r_x - i\omega(1+G_x)\rho \ , \ \tilde{r}_y \equiv r_y - i\omega(1+G_y)\rho \tag{C.4}$$

This leads to the dispersion relation

$$\frac{q_x^2}{H\tilde{r}_x} = i\omega\kappa - \frac{q_y^2}{H\tilde{r}_y} \tag{C.5}$$

and since the trace wavenumber is $q_y = k_0 \sin\phi$, we can write for the normalized $\hat{x}$ component of the wavevector in the porous layer

$$Q_x \equiv \frac{q_x}{k_0} = \sqrt{\frac{iH\tilde{r}_x}{\omega\rho} - \left(\frac{\tilde{r}_x}{\tilde{r}_y}\right)\sin^2\phi} \tag{C.6}$$

Comparing equations B.5 and C.6, we see that the effects of anisotropy are not important for normal incidence.

For the open layer we have for the normalized normal input admittance

$$\eta_x(x=-d) \equiv \frac{u_x(x=-d)}{p(x=-d)} = -\frac{\rho\omega Q_x}{\tilde{r}_x}\tan(Q_x k_0 d) \tag{C.7}$$

where d is the layer thickness. The absorption coefficient for a plane wave of angle of incidence ϕ is

$$\alpha(\phi,\eta_x) = \frac{4\beta\cos\phi}{(\beta+\cos\phi)^2+\sigma^2} \tag{C.8}$$

where $\eta_x = \beta + i\sigma$.

Appendix D

Low Frequency Effective Quantities

In the low frequency limit of the basic theory of the flexible porous material presented in chapters 2 and 3, we found that there was no relative motion of the fluid and the structure. Here we examine the consequences of this assumption.

If we take

$$\vec{u} - \vec{u}' = 0 \tag{D.1}$$

we can write the basic equations of momentum balance 2.17, 2.18 as

$$H\rho\frac{\partial\vec{u}}{\partial t} = -\text{grad}\, p \tag{D.2}$$

and

$$H'\rho'\frac{\partial\vec{u}'}{\partial t} = -\text{grad}\, p' \tag{D.3}$$

which can be summed and written as

$$(H\rho + H'\rho')\frac{\partial\vec{u}}{\partial t} = -\text{grad}\,(p + p') \tag{D.4}$$

The mass balance equations

$$\frac{\partial H\rho}{\partial t} + H\rho \,\mathrm{div}\, \vec{u} = 0 \tag{D.5}$$

and

$$\frac{\partial H'\rho'}{\partial t} + H'\rho' \,\mathrm{div}\, \vec{u} = 0 \tag{D.6}$$

which can be summed and written as

$$\frac{\partial(H\rho + H'\rho')}{\partial t} + (H\rho + H'\rho') \,\mathrm{div}\, \vec{u} = 0 \tag{D.7}$$

Defining $\tilde{p} \equiv p + p'$, $\tilde{\rho} \equiv H\rho + H'\rho'$, and

$$\tilde{\kappa} = \frac{1}{\tilde{\rho}} \frac{\partial \tilde{\rho}}{\partial \tilde{p}}, \tag{D.8}$$

we can combine equations D.4 and D.7 to obtain the wave equation

$$\nabla^2 \tilde{p} - \frac{1}{\tilde{c}^2} \frac{\partial^2 \tilde{p}}{\partial t^2} = 0 \tag{D.9}$$

where the effective wave speed is

$$\tilde{c} = \frac{1}{\sqrt{\tilde{\rho}\tilde{\kappa}}} \tag{D.10}$$

We focus our attention now on this effective compressibility $\tilde{\kappa}$. In particular we will try to express it in terms of defined compressibilities of chapter 2

$$\kappa = \frac{1}{\rho} \frac{\partial \rho}{\partial p}, \; \kappa' = \frac{1}{\rho'} \frac{\partial \rho'}{\partial p}, \; K = \frac{1}{H'} \frac{\partial H'}{\partial p'} \tag{D.11}$$

Since $\mathrm{div}\, \vec{u} = \mathrm{div}\, \vec{u}'$ we know, for a small fractional density change

$$\frac{\triangle(H\rho)}{H\rho} = \frac{\triangle(H'\rho')}{H'\rho'} \tag{D.12}$$

or

$$\frac{\triangle H}{H} + \frac{\triangle \rho}{\rho} = \frac{\triangle H'}{H'} + \frac{\triangle \rho'}{\rho'} \tag{D.13}$$

and using using the defined compressibilities in D.11 this leads to

$$\kappa \triangle p - (H'/H) K \triangle p' = K \triangle p' + \kappa' \triangle p' \tag{D.14}$$

We will take $\kappa' = 0$ since typically κ' is much smaller than the compressibility of air κ.

Equation D.14 tells us that the small pressure changes in the fluid and structure are related through

$$\triangle p' = \alpha \triangle p \tag{D.15}$$

where

$$\alpha \equiv \frac{H\kappa}{K} \tag{D.16}$$

This means that the partial derivative in equation 2.21 can be replaced by

$$\frac{\partial}{\partial \tilde{p}} \rightarrow \left(\frac{1}{1+\alpha}\right) \frac{\partial}{\partial p} \text{or} \left(\frac{\alpha}{1+\alpha}\right) \frac{\partial}{\partial p'} \tag{D.17}$$

which means equation 2.21 can be written as

$$\tilde{\kappa} = \frac{1}{H\rho + H'\rho'} \left[H \left(\frac{1}{1+\alpha}\right) \frac{\partial \rho}{\partial p} + \rho \left(\frac{\alpha}{1+\alpha}\right) \frac{\partial H}{\partial p'} + H' \left(\frac{1}{1+\alpha}\right) \frac{\partial \rho'}{\partial p} + \rho' \left(\frac{\alpha}{1+\alpha}\right) \frac{\partial H'}{\partial p'} \right] \tag{D.18}$$

or, using the defined compressibilities in equation D.11 and $\kappa' = 0$

$$\tilde{\kappa} = \frac{1}{H\rho + H'\rho'} \left[H \left(\frac{1}{1+\alpha}\right) (\kappa\rho) + \rho \left(\frac{\alpha}{1+\alpha}\right) (-H'K) + \rho' \left(\frac{\alpha}{1+\alpha}\right) (H'K) \right] \tag{D.19}$$

which can be simplified to give

$$\tilde{\kappa} = \frac{H\kappa K}{H\kappa + K} \tag{D.20}$$

or

$$\frac{1}{\tilde{\kappa}} = \frac{1}{H\kappa} + \frac{1}{K} \tag{D.21}$$

Appendix E

Exact Method Program

The *c++* program listed below takes as input the general material properties of a sample whose complex compressibility is to be measured by a shaker experiment as described in chapter 6. In addition, one inputs the frequency and height of the maximum of the velocity transfer function magnitude, measured across the layer. The program's search algorithm is described in chapter 6. The program returns the real and imaginary parts of the material's complex compressibility; a flowchart and sample run are shown in figure 6-6.

```
#include <stdio.h>
#include <Complex.h>
#include <math.h>

#define check_it() \
  chk = omega_m_check(); \
  if (chk == -1) goto start; \
  else if (chk == 1) goto done

#define check_it_Kreal() \
  chk = Kreal_m_check(); \
  if (chk == -1) goto start; \
  else if (chk == 1) goto done

#define check_it_Kimag() \
  chk = Kimag_m_check(); \
  if (chk == -1) goto start; \
  else if (chk == 1) goto done
```

```
void setup();
void input();
void guess();
void check_both();
void check_freq();
void check_value();
void search();
void omega_report();
void Kreal_report();
void Kimag_report();

int omega_m_check();
int Kreal_m_check();
int Kimag_m_check();

double value(double omega_arg, Complex K_arg);
double miss_omega(Complex K_arg_mo);
double miss_value(Complex K_arg_mv);

double omega_max(Complex Kw_arg);

double best_Kreal(double Krs, double Kis, double Ks);
double best_Kimag(double Kirs, double Kiis, double Kis);

int done, omega_done, pass, squeeze_flag, omega_restart, i;

double omega_step_start, omega_start, omega_best;
double mass_ratio, density_ratio, sample_thickness;
double max_freq, max_value, max_freq_check, max_value_check, c;
double K_step, omega_f1, omega_f2, omega_step;
double value_criteria, omega_crit;
double frequency, slope1, slope2, squeeze_factor, omega, omega_f3;
double error_zero, error_plus, error_minus;
double Kreal_f1, Kreal_f2, Kreal_f3;
double Kimag_f1, Kimag_f2, Kimag_f3;
double Kreal, Kreal_start, K_crit, Kreal_best;
double Kimag, Kimag_start, Kimag_best, K_step_start;

Complex K_guess, eye;
Complex qd1, qd2;
Complex K_plus, K_minus;
```

```
main()
{

  setup();

  input();

  guess();

  search();

}

double miss_omega(Complex K_arg_mo)
{
  double morv;

  morv = fabs(max_freq - omega_max(K_arg_mo));

  return morv;
}

double miss_value(Complex K_arg_mv)
{
  double mvrv;

  mvrv = fabs(max_value - value(omega_max(K_arg_mv), K_arg_mv));

  return mvrv;
}



double best_Kreal(double Krs, double Kis, double Ks)
{
  int N, chk;
  double fp, fo, fm;
  double fpp, fom, fmm;
  double fpm, fop, fmp;

Kreal_start = Krs;
Kimag_start = Kis;
K_step = Ks;

 start:
```

```
      Kreal = Kreal_start;

      fp = miss_omega(Complex(Kreal+K_step, Kimag_start));

      fo = miss_omega(Complex(Kreal, Kimag_start));
      fm = miss_omega(Complex(Kreal-K_step, Kimag_start));



      fpp = fp; fpm = fp;
      fom = fo; fop = fo;
      fmm = fm; fmp = fm;

      Kreal_f3 = fp;
      Kreal_f2 = fo;
      Kreal_f1 = fm;

  check_it_Kreal();

    for (N=1; N>0; N += 1)
      {
        Kreal = Kreal_start + (N * K_step);

        Kreal_f2 = fpp;
        Kreal_f1 = fop;
        Kreal_f3 = miss_omega(Complex(Kreal+K_step, Kimag_start));

        fpp = Kreal_f3;
        fop = Kreal_f2;
        fmp = Kreal_f1;

  check_it_Kreal();

/* patch below prevent Kreal<0 values */

        if ((Kreal_start - ((N+1) * K_step)) > 0.0)
          {


            Kreal = Kreal_start - (N * K_step);

            Kreal_f3 = fom;
            Kreal_f2 = fmm;
            Kreal_f1 =
```

```
            miss_omega(Complex(Kreal-K_step, Kimag_start));

          fpm = Kreal_f3;
          fom = Kreal_f2;
          fmm = Kreal_f1;

          check_it_Kreal();

        }

      if (N>250)
        printf("DANGER - HIGH N WARNING IN Kreal SEARCH\n");


    }

 done:

  return Kreal_best;

}

double best_Kimag(double Kirs, double Kiis, double Kis)
{
  int N, chk;
  double fp, fo, fm;
  double fpp, fom, fmm;
  double fpm, fop, fmp;

Kreal_start = Kirs;
Kimag_start = Kiis;
K_step = Kis;

 start:

    Kimag = Kimag_start;

    fp = miss_value(Complex(Kreal_start, Kimag+K_step));
    fo = miss_value(Complex(Kreal_start, Kimag));
    fm = miss_value(Complex(Kreal_start, Kimag-K_step));

    fpp = fp; fpm = fp;
    fom = fo; fop = fo;
    fmm = fm; fmp = fm;
```

```
      Kimag_f3 = fp;
      Kimag_f2 = fo;
      Kimag_f1 = fm;

  check_it_Kimag();

    for (N=1; N>0; N += 1)
      {
        Kimag = Kimag_start + (N * K_step);

        Kimag_f2 = fpp;
        Kimag_f1 = fop;
        Kimag_f3 = miss_value(Complex(Kreal_start, Kimag+K_step));

        fpp = Kimag_f3;
        fop = Kimag_f2;
        fmp = Kimag_f1;

  check_it_Kimag();

/* patch below prevents Kimag<0 values */

        if ((Kimag_start - ((N+1) * K_step)) > 0.0)
          {

          Kimag = Kimag_start - (N * K_step);



          Kimag_f3 = fom;
          Kimag_f2 = fmm;
          Kimag_f1 =
            miss_value(Complex(Kreal_start, Kimag-K_step));

          fpm = Kimag_f3;
          fom = Kimag_f2;
          fmm = Kimag_f1;

          check_it_Kimag();

          }

        if (N>250)
            printf("DANGER - HIGH N WARNING IN Kimag SEARCH\n");
```

```
      }

 done:

  return Kimag_best;

}



double omega_max(Complex Kw_arg)
{
  int N, chk;
  double fp, fo, fm;
  double fpp, fom, fmm;
  double fpm, fop, fmp;

omega_start = max_freq;
omega_step = omega_step_start;


 start:

      omega = omega_start;

      fp = value(omega+omega_step, Kw_arg);
      fo = value(omega, Kw_arg);
      fm = value(omega-omega_step, Kw_arg);

      fpp = fp; fpm = fp;
      fom = fo; fop = fo;
      fmm = fm; fmp = fm;

      omega_f3 = fp;
      omega_f2 = fo;
      omega_f1 = fm;

  check_it();


    for (N=1; N>0; N += 1)
      {
```

```
        omega = omega_start + (N * omega_step);

        omega_f2 = fpp;
        omega_f1 = fop;
        omega_f3 = value(omega + omega_step, Kw_arg);

        fpp = omega_f3;
        fop = omega_f2;
        fmp = omega_f1;

  check_it();


/* patch below prevents omega<0 values */

        if ((omega_start - ((N+1) * omega_step)) > 0.0)
          {


            omega = omega_start - (N * omega_step);

            omega_f3 = fom;
            omega_f2 = fmm;
            omega_f1 = value(omega - omega_step, Kw_arg);

            fpm = omega_f3;
            fom = omega_f2;
            fmm = omega_f1;

            check_it();

          }

        if (N>250)
          {printf("DANGER - HIGH N WARNING IN OMEGA SEARCH\n");
           printf("omega=%lf, omega_step=%lf\n",
                  omega, omega_step);}

      }

 done:

  return omega_best;

}
```

```
double value(double omega_arg, Complex K_arg)
{
  Complex qdz;
  double ans;


        qdz = omega_arg * (sample_thickness / c) *
        sqrt(density_ratio * K_arg);

  ans = sqrt(norm(1.0 /
                  (cos(qdz) - (mass_ratio * qdz * sin(qdz)))));

  return ans;

}



void setup()
{

  c = 34411.9;                /* Isentropic Sound speed */

  eye = Complex(0.0,1.0);

  printf("\n\nCOMPRESS - Complex Compressibility Program\n\n");

}

void input()
{

  printf("General parameters:\n");

  printf("Mass ratio ?");
  scanf("%lf", &mass_ratio);

  printf("Density ratio ?");
  scanf("%lf", &density_ratio);

  printf("Sample Thickness (inches) ?");
  scanf("%lf", &sample_thickness);
  sample_thickness = sample_thickness * 2.54;
```

```
  printf("\nTarget values:\n");

  printf("Frequency for |u2/u1| maximum ?");
  scanf("%lf", &max_freq);
  max_freq = max_freq * 2.0 * PI;

  printf("Maximum |u2/u1| value ?");
  scanf("%lf", &max_value);

/*
  printf("\nSearch parameters:\n");

  printf("Start Delta K step size ?");
  scanf("%lf", &K_step_start);

  printf("Start Fract. Omega step size (Frac of Omega start)?");
  scanf("%lf", &omega_step_start);
  omega_step_start *= max_freq;
*/

K_step_start = .2;
omega_step_start = .1 * max_freq;
omega_crit = .000001 * max_freq;
K_crit = .01;

  printf("\n\n");

}

void guess()
{

K_guess = Complex( (1.0 / (density_ratio * (.5 + mass_ratio) *
                           ((max_freq * sample_thickness) / c) *
                           ((max_freq * sample_thickness) / c))),
                   (1.0 / (density_ratio * (.5 + mass_ratio) *
                           ((max_freq * sample_thickness) / c) *
                           ((max_freq * sample_thickness) / c)) /
                             max_value) );

printf("START K = (%lf,%lf)\n", real(K_guess), imag(K_guess) );


}
```

```
int omega_m_check()
{
  double mp, mm;
  int rv;

  rv = 0;
/*
omega_report();
*/
  mp = omega_f3 - omega_f2;
  mm = omega_f2 - omega_f1;

  if ( (mm > 0.0) && (mp < 0.0) )
    { omega_start = omega;
      if (omega_step < omega_crit)
        {omega_best = omega;
         rv = 1;}
      else {omega_step = omega_step * .75;
            rv = -1;}
    }

  return rv;            /* rv = -1, restart
                                0, continue
                                1, done        */

}

int Kreal_m_check()
{
  double mp, mm;
  int rv;

  rv = 0;
/*
Kreal_report();
*/

  mp = Kreal_f3 - Kreal_f2;
  mm = Kreal_f2 - Kreal_f1;

  if ( (mm < 0.0) && (mp > 0.0) )
    { Kreal_start = Kreal;
      if (K_step < K_crit)
        {Kreal_best = Kreal;
         rv = 1;}
```

```
      else {K_step = K_step * .75;
            rv = -1;}
    }

  return rv;            /* rv = -1, restart
                                0, continue
                                1, done        */

}


int Kimag_m_check()
{
  double mp, mm;
  int rv;

  rv = 0;
/*
Kimag_report();
*/
  mp = Kimag_f3 - Kimag_f2;
  mm = Kimag_f2 - Kimag_f1;

  if ( (mm < 0.0) && (mp > 0.0) )
    { Kimag_start = Kimag;
      if (K_step < K_crit)
        {Kimag_best = Kimag;
         rv = 1;}
      else {K_step = K_step * .75;
            rv = -1;}
    }

  return rv;            /* rv = -1, restart
                                0, continue
                                1, done        */

}




void search()
{
```

```
omega_start = max_freq;

int all_over;
Complex K;
double xxx,yyy,j1,j2,j3,j4,j5,j6,ferr_real,ferr_imag;

xxx = 0.0;
yyy = 0.0;

j1 = best_Kreal(real(K_guess),imag(K_guess),K_step_start);
j2 = best_Kimag(j1,imag(K_guess),K_step_start);

    printf("\nINTERIM K = (%lf,%lf)\n", j1, j2);

all_over = 0;

for (;all_over == 0;)

  {

    j3 = best_Kreal(j1,j2,K_step_start);
    j4 = best_Kimag(j3,j2,K_step_start);

    printf("\nINTERIM K = (%lf,%lf)\n", j3, j4);


    j1 = j3;
    j2 = j4;

    j5 = best_Kreal(j1,j2,K_step_start);
    j6 = best_Kimag(j5,j2,K_step_start);

    printf("\nINTERIM K = (%lf,%lf)\n", j5, j6);

    if ((fabs(j1-j5)<.005) && (fabs(j2-j6)<.005))
      all_over = 1;

    j1 = j5;
    j2 = j6;

/* Special inf loop avoider patch below */


        j1 = sqrt( j3 * j5 );
```

```
        j2 = sqrt( j4 * j6 );


  }

printf("\nFINAL BEST K = (%lf,%lf)\n", j5, j6);

printf("\nTarget Freq_Max=%lf, Actual Freq_Max=%lf\n",
       (max_freq / (2.0 * PI)),
       ((omega_max(Complex(j5,j6))/(2.0*PI))));

printf("\nValue=%lf, Actual Value=%lf\n",
       max_value,
       value((omega_max(Complex(j5,j6))),Complex(j5,j6)) );


ferr_real = (real(K_guess) - j5)/j5;
ferr_imag = (imag(K_guess) - j6)/j6;

printf("\nFractional Error using K_guess = (%lf,%lf)\n\n",
ferr_real,ferr_imag);

}

void omega_report()
{

  printf("om1=%lf, om2=%lf, om3=%lf,\nf1=%lf, f2=%lf, f3=%lf\n\n",
         omega - omega_step, omega, omega + omega_step,
         omega_f1, omega_f2, omega_f3);


}

void Kreal_report()
{

  printf("kr1=%lf, kr2=%lf, kr3=%lf,
 \nf1=%lf, f2=%lf, f3=%lf\n\n",
         Kreal - K_step, Kreal, Kreal + K_step,
         Kreal_f1, Kreal_f2, Kreal_f3);


}
```

```
void Kimag_report()
{

  printf("ki1=%lf, ki2=%lf, ki3=%lf,
 \nf1=%lf, f2=%lf, f3=%lf\n\n",
         Kimag - K_step, Kimag, Kimag + K_step,
         Kimag_f1, Kimag_f2, Kimag_f3);


}
```

Bibliography

[1] Lord Rayleigh. *Theory of Sound*, volume 2. MacMillian and Co. First Ed., 1973.

[2] A.F. Monna. Absorption of sound by porous walls. *Physica V*, 3:129–142, 1938.

[3] Michael Rettinger. The theory of sound absorption of porous materials, flexible and nonflexible. *J. Acoust. Soc. Am.*, 8:53–59, 1936.

[4] P.M. Morse and R.H. Bolt. Sound waves in rooms. *Rev. Mod. Phys.*, 16:69, 1944.

[5] R.A. Scott. The absorption of sound in a homogeneous medium. *Proc. Phys. Soc.*, 58:165–183, 1946.

[6] C. Zwikker and C.W. Kosten. *Sound Absorbing Materials.* Elsevier Publishing Company, Inc., 1949.

[7] L.L. Beranek. Acoustical properties of homogeneous, isotropic rigid tiles and flexible blankets. *J. Acoust. Soc. Am.*, 19:556–568, 1947.

[8] M.A. Biot. Theory of propagation of elastic waves in a fluid-saturated porous solid. i. low frequency range. *J. Acoust. Soc. Am.*, 28:168–178, 1956.

[9] M.A. Biot. Theory of propagation of elastic waves in a fluid-saturated porous solid. ii. higher frequency range. *J. Acoust. Soc. Am.*, 28:179–191, 1956.

[10] K. Attenborough. The influence of microstructure on propagation in porous fibrous absorbents. *J. Sound Vib.*, 16:419–442, 1971.

[11] J.H.B. Zarek. Sound absorption in flexible porous materials. *J. Sound Vib.*, 61:205–234, 1978.

[12] R.F. Lambert. Surface admittance of highly porous foams with finite stiffness. *J. Acoust. Soc. Am.*, 81:1293–1298, 1988.

[13] K.U. Ingard. Locally and nonlocally reacting porous layers; a comparison of acoustical properties. *ASME Trans., Journal of Engineering for Industry*, 103:39–44, 1982.

[14] K.U. Ingard. Repetitively pulsed electric laser acoustic studies. Technical report, Massachusetts Institute of Technology, Department of Aeronautics and Astronautics, 1983.

[15] K.U. Ingard. Lecture notes - noise control engineering. Massachusetts Institute of Technology, Department of Aeronautics and Astronautics, 1981.

[16] L. Brillouin. *Wave Propagation in Periodic Structures.* McGraw-Hill Book Co., Inc., 1946.

[17] K.U. Ingard. Lecture notes - noise control engineering. Massachusetts Institute of Technology, Department of Aeronautics and Astronautics, 1981.